Grant F49620-95-1-0139



# EURASIAN SURFACE WAVE PHENOMENOLOGY AND INVERSION FOR CRUSTAL AND UPPER MANTLE STRUCTURES

Anatoli L. Levshin
Michael H. Ritzwoller

University of Colorado
Department of Physics
Campus Box 583
Boulder, CO 80309-0583



10 February 1997

Final Report



Approved for public release; distribution unlimited

Directorate of Life and Environmental Sciences

Air Force Office of Scientific Research/NM
BOLLING AIR FORCE BASE, DC 20332-0001

# REPORT DOCUMENTATION PAGE

Form Approved
OMB No. 0704-0188



| 1. AGENCY USE ONLY (Leave blank) | 2. REPORT DATE | 3. REPORT TYPE AND DATES COVERED |
|---|---|---|
| | 10 February 1997 | Final Report |

**4. TITLE AND SUBTITLE**
Eurasian surface wave phenomenology and inversion for crustal and upper mantle structures.

**5. FUNDING NUMBERS**
F4920-94-1-0139

**6. AUTHOR(S)**
Anatoli Levshin
Michael H. Ritzwoller

**7. PERFORMING ORGANIZATION NAME(S) AND ADDRESS(ES)**
University of Colorado
Department of Physics
Campus Box 583
Boulder, CO 80309-0583

**8. PERFORMING ORGANIZATION REPORT NUMBER**
4702 - 02/10/97

**9. SPONSORING/MONITORING AGENCY NAME(S) AND ADDRESS(ES)**
AFOSR/NM
110 Duncan Ave., Suite B155
Bolling AFB, DC 20332-0001
Dr. Stanley K. Dickinson

**10. SPONSORING/MONITORING AGENCY REPORT NUMBER**

**11. SUPPLEMENTARY NOTES**

**12a. DISTRIBUTION/AVAILABILITY STATEMENT**
Distribution Unlimited

**12b. DISTRIBUTION CODE**

**13. ABSTRACT** *(Maximum 200 words)* Earthquake seismogramms recorded by several global and regional networks between 1988 and late-1995 were used to measure the group velocity dispersion of fundamental Rayleigh and Love waves crossing Eurasia. More than 9,000 three-component long period seismograms following more than 600 events with Ms greater than 4.5 were processed. This data set was reduced by 'clustering' observations along similar paths into measurements along the 'unique path,' and rejecting outliers. The resulting curves were used to construct group velocity maps from 20 s period to 200 s period for Rayleigh waves and up to 150s period for Love waves. These maps have better resolution and are more reliable than globally estimateddispersion maps or such maps computed from current global models of the crust and mantle. In particular, they contain new information about large sedimentary features, lower crustal and upper mantle structures, Moho topography. These maps guide the identification and extraction of surface waveforms which emanate from small seismic events. They should be added to the 'Knowledge Base' used to monitor clandestine nuclear tests. More accurate and detailed crustal and upper mantle models derived from these maps are very important for improvement of location/depth estimation in the strategic areas of Eurasia characterized by complex geology (such as the Middle East, Central Asia, and the Far East).

| 14. SUBJECT TERMS | | 15. NUMBER OF PAGES |
|---|---|---|
| Surface Waves | Tomography | 87 |
| Eurasia | Lithospheric Structure | 16. PRICE CODE |

| 17. SECURITY CLASSIFICATION OF REPORT | 18. SECURITY CLASSIFICATION OF THIS PAGE | 19. SECURITY CLASSIFICATION OF ABSTRACT | 20. LIMITATION OF ABSTRACT |
|---|---|---|---|
| Unclassified | Unclassified | Unclassified | None |

# Table of Content

# Abstract

This report presents the results of a study of the dispersion characteristics of broadband fundamental surface waves propagating across Eurasia. Frequency - Time ANalysis (FTAN) is used to estimate group velocities, phase velocities, and wave packet amplitudes for both Rayleigh and Love waves. This is an interactive group velocity - period filtering method designed to identify the fundamental dispersion ridge and extract it from sources of noise such as other types of waves (Rayleigh/Love, overtones, body waves) and scattering coda. We present group velocity maps from 20 s to 200 s period for Rayleigh waves and from 20 s to 150 s for Love waves. Broadband waveform data from about 600 events from 1988 - 1995 recorded at 83 individual stations from the GDSN, IRIS/GSN, GEOSCOPE, CDSN, MEDNET, KNET, and KAZNET networks across Eurasia have produced about 9,000 paths for which individual dispersion curves have been estimated. Dispersion curves from similar paths are clustered to reduce redundancy, identify outliers for rejection, and assign uncertainty estimates. On average, measurement uncertainty based upon repeatability is about 0.015 km/s and is not a strong function of frequency. The tomographic method of Yanovskaya and Ditmar is used to estimate group velocity maps separately for each period and wave type (Rayleigh or Love) utilizing a penalty function that is a linear combination of misfit and a measure of 'smoothness' that is related to the spatial gradient of the estimated map. Since this penalty function ignores Laplacian smoothness, we apply a posteriori spatial smoothing filters based on the resolution at each period and wave type. Resolution is estimated from 'checker-board' tests and we show that resolutions for most of Eurasia range from 5 - 7.5 degrees, but degrade at periods above about 100 s. We discuss problems expected to result from theoretical approximations, in particular off-great-circle propagation, azimuthal anisotropy, and systematic event mislocations near subducting slabs, and argue that these effects should not alter the maps strongly beyond the reported resolution estimates either qualitatively or quantitatively. The estimated maps produce a variance reduction relative to PREM of more than 90% for Rayleigh waves below 60 s period reducing to about 70% between 80 - 200 s period. For Love waves, variance reductions are similar being above 90% for most periods below 100 s and falling to 70% at 150 s. Variance reductions for the hybrid

model CRUST-5.1/S16B30 are lower but are still impressive except at periods particularly sensitive to crustal thicknesses and for long period Love waves, presumably because of polarization anisotropy. Many known geological and tectonic structures are observed in the group velocity maps. Of particular note are the signatures of sedimentary basins, continental flood basalts, crustal thickness, back-arc spreading, down-going slabs, and continental roots. Comparison of the estimated group velocity maps with those predicted by CRUST-5.1/S16B30 is qualitatively very good. Explicit comparisons are carried out at several periods related to a few structural features, including sedimentary basins, crustal thicknesses, and back-arc spreading.

# 1. Introduction

This report presents the results of a study of the dispersion characteristics of broadband (15 - 200 s) Rayleigh and Love waves propagating across Eurasia. These results are presented as group velocity maps which represent the local group velocity of a Rayleigh or a Love wave at each period. There are two main motivations for this study. First, accurate high resolution group velocity maps are useful in monitoring clandestine nuclear tests. These maps guide the identification and extraction of surface waveforms which emanate from small seismic events. The estimation of surface wave magnitude, $M_s$, is thereby facilitated for use as part of, for example, the $M_s : m_b$ method of discriminating underground explosions from naturally occurring earthquakes (e.g., Lieberman and Pomeroy, 1969; Dahlmann and Israelson, 1977; Stevens and Day, 1985; Taylor, 1996). Second, the group velocity maps that result from this study provide new constraints on the shear velocity structure of the crust and uppermost mantle underlying Eurasia. These maps should have better resolution and be more reliable than globally estimated dispersion maps or such maps computed from current global models of the crust and mantle. They should also help calibrate future generations of global dispersion maps and seismic models and provide valuable, transportable data to be used in future inversions for the velocity structure of Eurasia. More accurate crustal and upper mantle models are very important for improvement of location/depth estimation capabilities in strategically important geographical area of Eurasia characterized by complex geology ( the Middle East, Central Asia, and the Far East).

The study of surface wave dispersion was begun independently by Love (1911) and Golitzin (1912). Surface wave dispersion studies applied to understanding the structure of the Earth date from the 1920's and 1930's with the early works or Gutenberg (1924, 1926), Jeffreys (1928, 1935), Stoneley (1926, 1928), Byerly (1930), Gutenberg and Richter (1936) and others. The 'modern era' of surface wave dispersion research probably began with the studies of Press (1956) and Press *et al.* (1956), and was ushered in by the the text Ewing *et al.* (1957). The flurry of surface wave studies that took place in late 1950's and continued throughout the 1960's defined 'classical dispersion analysis', but is too voluminous to list. However, Ewing *et al.* (1957) presents a review that is relatively complete

into the late 1950's, Oliver (1962) presents a review from the early 1960's, Dziewonski (1971) and Knopoff (1972) present useful reviews from the early 1970's which were subsequently updated a decade later (Knopoff, 1983). In the 1980's, surface waveform fitting became popular and Nolet *et al.* (1987) and Snieder (1993) present reviews. However, classical dispersion studies based on both single-station and multi-station or multi-event methods, continue in common practice today. Most current dispersion studies are little different from those in the 1960's other than computers are far better, instrumentation has been vastly improved, and there is now much more complete path coverage across most regions of interest. Together these improvements allow tomographic methods to be applied to surface wave dispersion measurements to produce maps of surface wave dispersion over broad areas.

We present the results of a classical single-station dispersion study and the subsequent estimation of dispersion maps using standard tomographic methods. The study is distinguished by its broadbandedness, the relatively high resolution of the resulting group velocity maps, and by it geographical scale. We present surface wave maps across Eurasia between 20 and 200 s period. Measurements are regularly obtained down to 10 s and up to 250 s period, but the reliability of the group velocity maps across large regions of the continent degrades sharply below 20s and above about 175 s for Rayleigh waves and 125 s for Love waves. Surface wave maps at and below 30 s period are particularly important since they provide significant constraints on crustal thickness by helping to resolve Moho depth from the average shear velocity of the crust (e.g., Das and Nolet, 1995). Although there have been numerous studies of surface wave dispersion that have produced measurements of group and/or phase velocities between 10 - 40 s period, these studies have typically been confined to areas of about 15 degrees in lateral extent or less. We are not aware of any study to date that has provided detailed dispersion maps below 30 s period over an area as large as Eurasia. We argue below that we determine the sign and approximate location of group velocity features between 5 - 7.5 degrees in spatial extent at most periods across most of the continent.

The scale of this study is somewhat unusual in surface wave studies. Most surface wave studies are performed either regionally (average path lengths $\Delta < 1{,}500$ km) or globally

($\Delta$ > 10,000 km). There have been a very large number of regional surface wave studies in Eurasia. Some of these from last 20 years, segregated coarsely by geographical region, include those in the following lists. In Europe there are the largest number of studies, they include: Nolet (1977), Calcagnile and Panza (1978, 1979, 1980, 1990), Mueller and Sprecher (1978), Calcagnile *et al.* (1979, 1985), Levshin and Berteussen (1979), Panza *et al.* (1980), Neuenhofer *et al.* (1981), Mantovani *et al.* (1985), Mindevalli and Mitchell (1989), Dost (1990), Yanovskaya *et al.* (1990), Snieder (1993b), Stange and Friederich (1993), Vaccari and Panza (1993), Pedersen *et al.* (1994), and Lomax and Snieder (1995). In the Middle East, Central Asia and China there are the studies of Chen and Molnar (1975), Knopoff and Fouda (1975), Bird and Toksoz (1977), Chun and Yoshii (1977), Pines *et al.*, (1980), Knopoff and Chang (1981), Wier (1982), Romanowicz (1982), Feng *et al.* (1983), Jobert *et al.* (1985), Brandon and Romanowicz (1986), Lyon-Caen (1986), Bourjot and Romanowicz (1992), Levshin *et al.* (1992), Wu and Levshin (1994), Levshin *et al.* (1994), Levshin and Ritzwoller (1995), Curtis and Woodhouse (1996), Ritzwoller *et al.* (1996b), Zhang (1996), Griot *et al.* (1997). In Northern Asia surface wave studies are fewer in number, but include Lander *et al.* (1982), Kozhevnikov and Barmin (1989), Zeng *et al.* (189) Kozhevnikov *et al.* (1992). Dispersion studies performed on a global scale almost always involve waveform fitting. Some of the more recent of these include the studies of Zhang and Tanimoto (1993), Su *et al.* (1994), Laske (1995), Trampert and Woodhouse (1995, 1996), Laske and Masters (1996), Li and Romanowicz (1996), Masters *et al.* (1996), and Ekstrom *et al.* (1996). A review can be found in Ritzwoller and Lavely (1995).

The present study is a continental-scale study, performed at a length-scale intermediate between regional and global surface wave studies. The improvements in resolution and bandwidth over global-scale studies result from the mixture of measurements obtained from surface waves which propagate both regionally ($\Delta$ <3,000 km) and continent-wide ($\Delta$ >6,000 km). Regionally propagating surface waves provide many of the measurements at the short period end of the spectrum and improve resolution appreciably. Their use alone, however, would provide rather patchy path coverage, would result in very strong sensitivity to errors caused by event mislocation, and would not yield many measurements at periods longer than

about 60 s. Utilizing measurements from both the regional and continental scales allows us to combine the best characteristics of regional and global studies and provides a data set that is strongly and differentially sensitive to both crustal and upper mantle structures. Other studies of Eurasia on a continental scale include those of Patton (1980), Feng and Teng (1983a), Lerner-Lam (1983), Levshin *et al.* (1996), and Curtis and Snieder (1997). There are, however, advantages to the regional and global scale studies. Resolution can be locally better in the regional studies and global studies are generally more reliable at long periods beyond about 175 s for Rayleigh waves and 125 s for Love waves.

Another aspect of this study which is perhaps somewhat unusual is that it is a group velocity rather than a phase velocity study. We have performed a group velocity study for three reasons. First, estimates of group velocities are much less sensitive to source effects than phase velocities (e.g., Knopoff and Schwab, 1968) since they derive from measurements of the wave packet envelope rather than the constituent phases. This is particularly true for shorter periods and longer ranges. This has allowed us to use small events for which no moment tensor has been estimated. Second, as Figure 1 shows, group velocity sensitivity kernels are compressed nearer to the surface than the related phase velocity kernels, which should help resolve crustal from mantle structures. Finally, it is group velocity rather than phase velocity that is needed to extract surface waveforms for seismic discrimination. It should be noted that the group velocity maps that are presented here are intrinsically different from group velocity maps derived from the frequency derivative of phase velocity maps or approximate relationships between phase and group velocity. As described in Section 2, the group velocities estimated in this study involve measurements made on the group envelope rather than the phases that constitute the envelope. Hence, the group velocities presented here place constraints on the velocity structure of Eurasia independent of phase information. We will present the phase velocity maps that are estimated from the phases that constitute the wave packet envelope in a later contribution.

Although some recent surface wave studies have produced phase velocity maps that display azimuthal anisotropy (e.g., Tanimoto and Anderson, 1986; Nishimura and Forsyth, 1988; Montagner and Tanimoto, 1990, 1991; Trampert and Woodhouse, 1996; Griot *et al.*,

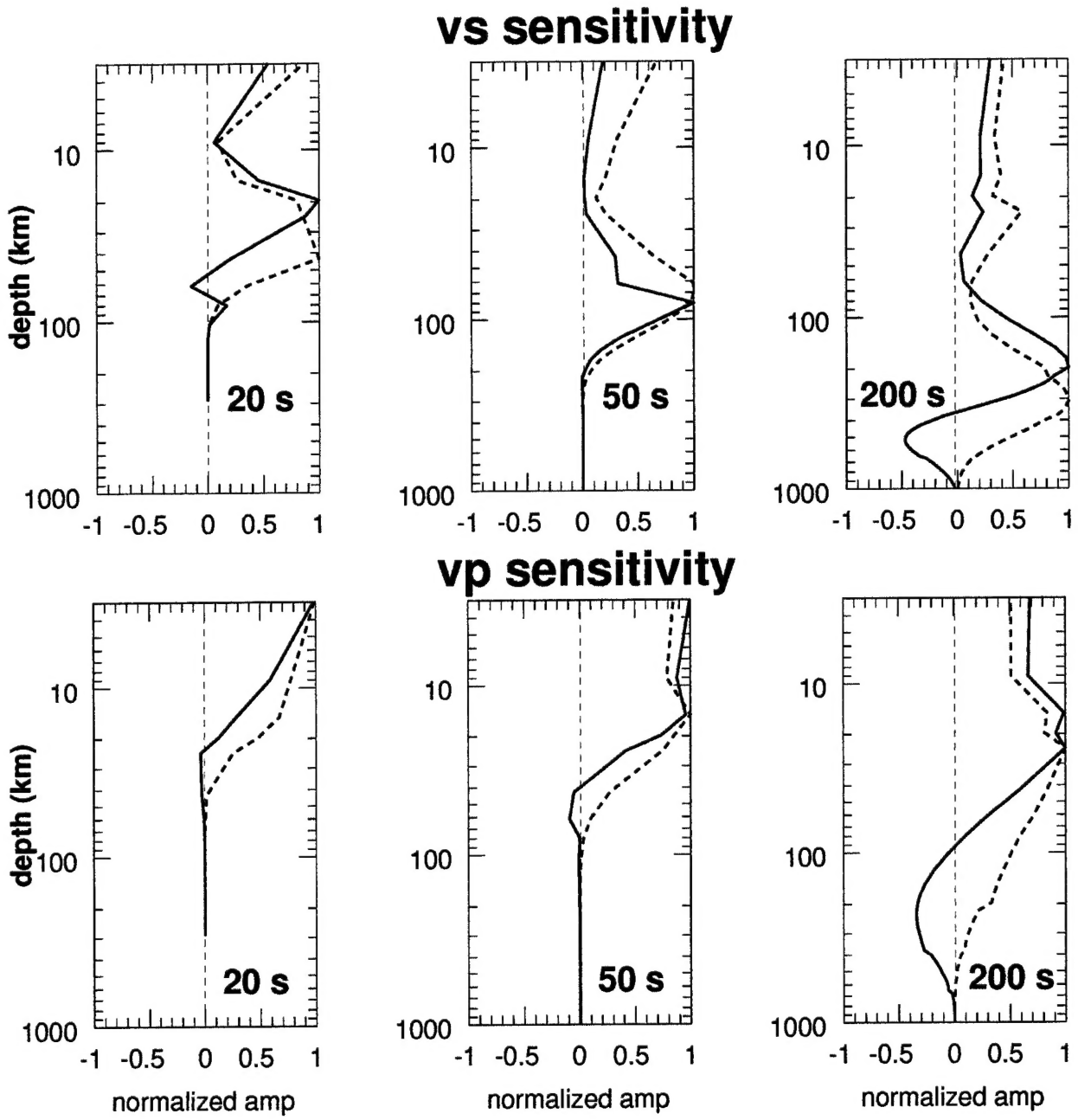


**Figure 1.** Rayleigh wave phase (bold dash lines) velocity and group (bold solid lines) velocity sensitivity kernels to shear velocity and compressional velocity at three periods: 20s, 50s, and 200s. These kernels are computed for PREM.

1997), our maps do not demonstrate this feature. However, our maps do display polarization anisotropy (transverse isotropy, horizontal fast axis). Polarization anisotropy is expressed as a specific differential perturbation to the Rayleigh and Love wave velocities at each spatial point (Montagner and Nataf, 1986). In general, relative to the best fitting isotropic model, polarization anisotropy manifests itself by speeding up the Love wave and slowing down the Rayleigh wave. The estimated maps presented here contain this information and, therefore, should not be seen as isotropic but rather as transversely isotropic. In many locations, no realistic isotropic model can be found that simultaneously fits both the Rayleigh and Love waves, especially at periods above about 100 s.

There are several key assumptions or approximations on which this study rests. We assume that the effects of the following phenomena on the estimated group velocity maps are small compared to the size of the heterogeneity observed in each map and that their accumulated impact does not greatly change the character of the estimated maps either quantitatively or qualitatively:

- the deviation of ray paths from the great-circles linking the sources to the receivers,
- azimuthal anisotropy,
- mislocations of earthquake epicenters, and
- source phase.

We refer to errors in these assumptions generically as 'theoretical errors'. The effects of the first three of these theoretical errors on the estimated group velocity maps are the subject of Section 4.2. The final phenomenon, the effect of source phase on group travel times and the estimated group velocity maps, is the subject of Levshin *et al.* (1997).

The outline of the report is as follows. Section 2 presents a discussion of the data used in the study and the method of measurement used to produce the estimated group velocity curves. Section 3 discusses the tomographic method used to translate the measured group velocity curves into group velocity maps as each period and for each wave type (Rayleigh or Love). Section 4 presents a discussion of uncertainties expected in the estimated group velocity maps. This discussion breaks into two parts. Section 4.1 discusses uncertainties

unrelated to theoretical errors which result mainly from the distribution of wave paths in number and azimuth. These types of uncertainties are summarized in an analysis of resolution and bias. Section 4.2 presents a discussion of uncertainties that result directly from theoretical errors. A sampling of the estimated group velocity maps is presented in Section 5 and they are discussed in Section 6. In particular, the discussion concentrates on identifying the types of geological and tectonic features in the crust and uppermost mantle that are distinguishable in the estimated group velocity maps. It is these features that will be constrained by the use of the estimated group velocity maps in inversions for the shear velocity structure of the crust and mantle under Eurasia such as the study of Ritzwoller *et al.* (1996a). The estimated maps are compared with group velocity maps predicted from the hybrid model composed of the crustal model CRUST-5.1 of Mooney *et al.* (1996) together with the mantle model S16B30 (Masters *et al.*, 1996).

## 2. Data and Measurement

Eurasia is an ideal site to perform surface wave tomography. Broad band station coverage has been very good across most of the continent for several years now, Eurasia is nearly surrounded by nearby plate boundaries, and it is the only continent that possesses significant, intra-continental seismicity (Fig. 2). Thus, surface wave path density and azimuthal distribution over most of the continent are good and many relatively short paths (<4,000 km) are available for analysis, at least below about 40 s period. These factors in combination control resolution and bias which is the subject of Section 3.

The goal of the measurement phase of this research is to obtain accurate estimates of surface wave characteristics (group and phase velocity, amplitude, and polarization in some cases) for each source-receiver pair and to estimate the uncertainty in these measurements. The most significant issues that must be addressed include the accrual of high quality waveform data, the identification and extraction of unwanted signals, the measurement of the dispersion characteristics of the signals of interest, the rejection of bad measurements, and the estimation of measurement uncertainties.

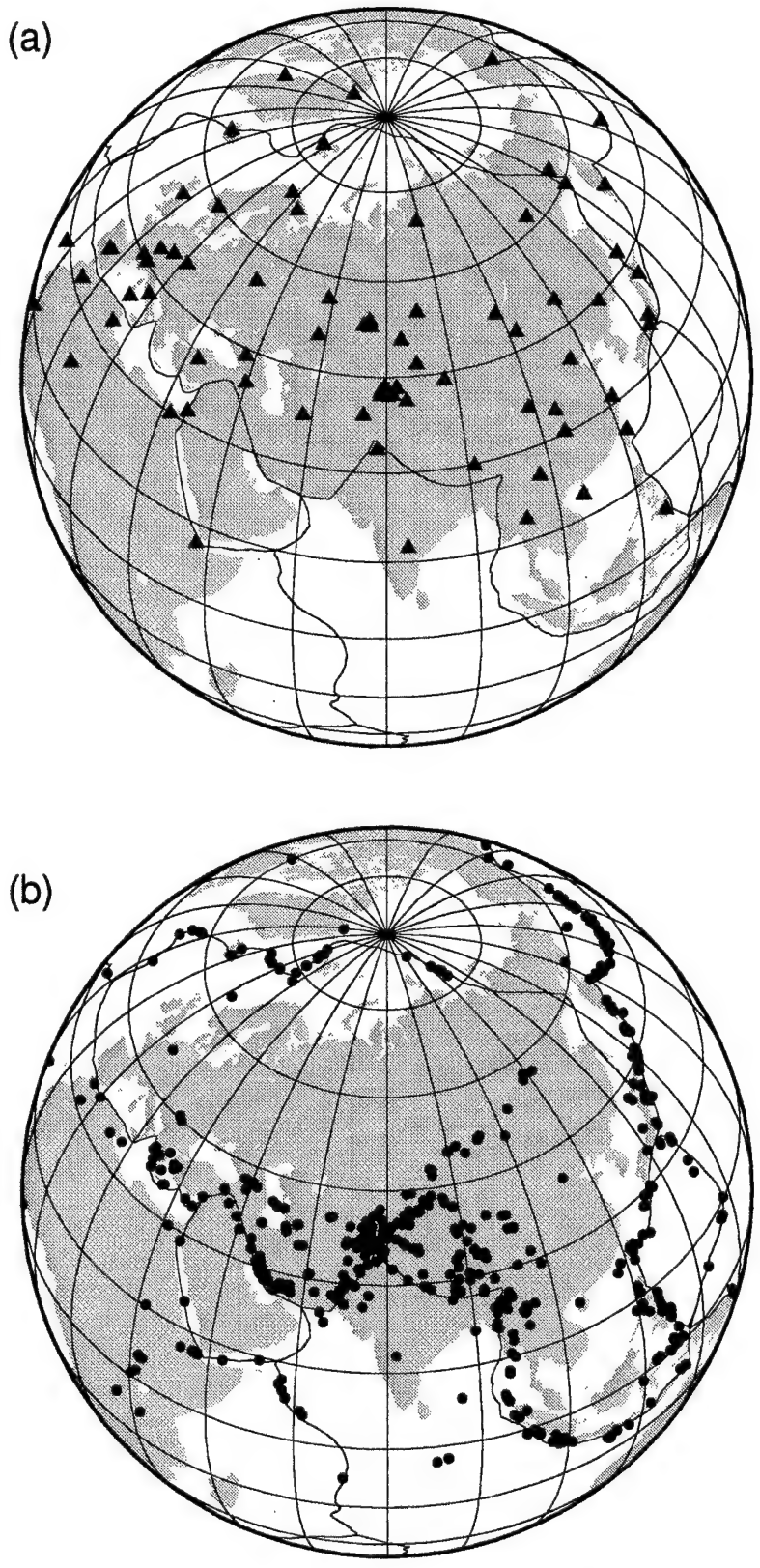


**Figure 2.** Station and event location. The locations of the stations used in this study are marked with triangles in (a) and event locations are marked with circles in (b).

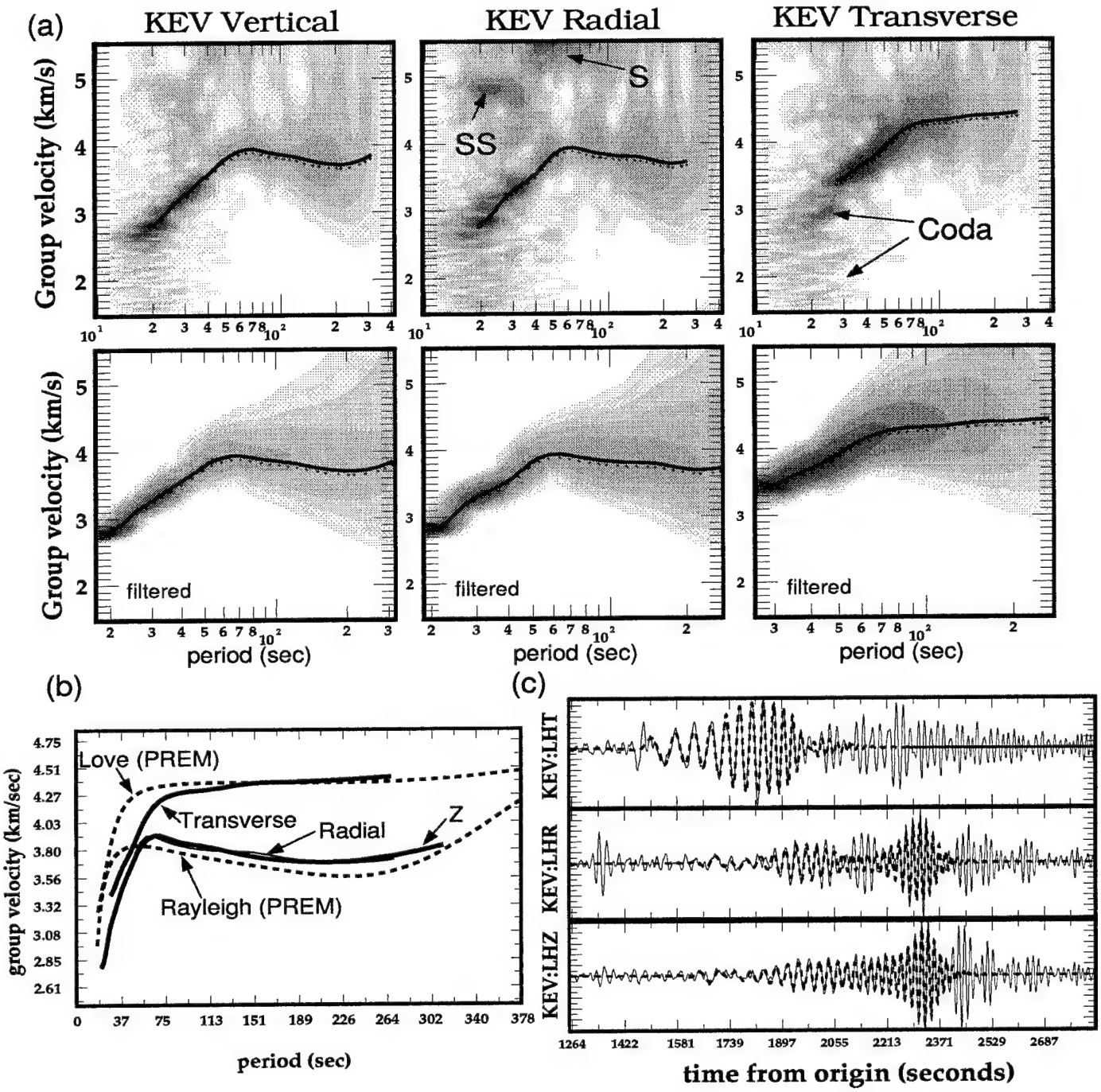


**Figure 3.** FTAN. Example of a frequency-time analysis for the vertical, radial, and transverse components recorded at the GSN station at Kevo, Finland for an event in the Kuril Islands (10/9/94, M=7.0, Δ= 58.5°). (a) The analyst-defined filter removes potentially interfering signals such as body waves, other surface waves, overtones, and coda. Group velocity curves are estimated automatically on the filtered images. (b) Rayleigh and Love group velocity measurements (solid lines) are compared with predicted from PREM (dashed lines). (c) Comparison of the raw (thin solid) with the filtered (bold dashed) waveforms reveals the effect of the filtering displayed in (a).

Data quality from both global (e.g., GSN, GEOSCOPE) and regional (e.g., CDSN, KNET, KAZNET, MEDNET) networks is very good. The main problem to be faced is that Eurasia is structurally complicated. This not only makes interpretation in terms of structural models difficult, it also complicates the identification of the aspects of the waveforms on which measurement methods should be applied. Our aim is to extract the nearly directly arriving surface waves, that can be interpreted deterministically, from the potentially interfering multipaths and coda, which are more stochastic in nature.

The basic characteristics of the current measurement procedure are based on a long history of development of surface wave analysis (e.g., Dziewonski *et al.* 1969; Landisman *et al.*, 1969; Levshin *et al.*, 1972, 1989, 1992, 1994; Cara, 1973; Herrin and Goforth, 1977; Feng and Teng, 1983b; Russell *et al.*, 1988; Ritzwoller *et al.*, 1995), and are described in detail by Levshin *et al.* (1992), which refers to the method as Frequency-Time ANalysis (FTAN). FTAN is exemplified in Figure 3. Group velocity - period diagrams for the vertical, radial, and transverse components are constructed and graphically displayed. An analyst manually traces the apparent group velocity curve for the Rayleigh wave (on the vertical and radial components) and the Love wave (on the transverse component) to define time-variable filters which are applied around the selected curve in order to separate the desired signal from the 'noise'; in particular, surface wave coda, overtones and body waves. This results in filtered group velocity - period diagrams on which contamination from interfering signals should be reduced. Group time, phase time, amplitude, and polarization measurements are automatically obtained on the filtered images. Group velocity and phase velocity are computed from the distance between the receiver and the CMT location (Dziewonski *et al.*, 1981) when it exists, and the PDE location otherwise. The analyst tailors the bandwidth of each measurement to the individual seismogram and assigns a qualitative grade to each measurement (A-F).

The success of this method depends on the analyst accurately identifying the fundamental dispersion ridge, separating the 'direct arrival' from surface wave coda at periods below about 30 s, inspecting interpolation near spectral holes, and truncating the measurements appropriately at short and long periods as the signals weaken. This interaction limits the

speed of the method, and, therefore, the volume of data that can be processed. However, it is necessary to insure that the measurements possess the desired quality and the method has been streamlined sufficiently to allow rapid progress to be made.

To date, FTAN has been applied to waveform data from approximately 600 events in and around Eurasia which occurred from the beginning of 1988 through mid-1995 (Fig. 2). Waveforms from most of the events which took place around Eurasia during this time period with $M_s \geq 5.0$ were acquired and processed. However, in regions of particularly high seismic activity (e.g., Kurile Islands region, Taiwan, Honshu, Philippines) a higher magnitude threshold of at least $M_s = 5.5$ was used. Particular attention was devoted to optimizing resolution in Central Asia, and events with $M_s$ as low as 4.0 were processed in this region since KNET was installed in late 1991. Waveform data were obtained from seven networks (CDSN, GDSN, GEOSCOPE (Romanowicz *et al.*, 1984), GSN, KAZNET (Kim *et al.*, 1995), KNET (Pavlis *et al.*, 1994; Vernon, 1994), MEDNET) comprising 83 individual broadband stations. The application of FTAN to these waveform data has yielded more than 9,000 measured Rayleigh wave dispersion curves and more than 7,600 Love wave dispersion curves. The total number of curves as a function of period and wave type (Rayleigh/Love) is shown as the bold lines in Figure 4.

By design, the resulting data set exhibits considerable redundancy, which allows for consistency tests, outlier rejection, and the estimation of measurement uncertainty. These tests are performed as part of what we call a 'cluster analysis'. Measurements whose path-endpoints lie within 2% of the path length are grouped to produce a 'cluster' of dispersion curves. This cluster defines a 'unique path'. Frequently these clusters are composed of a large earthquake and its after-shocks recorded at a single station, but in some cases nearby stations (e.g., stations in KNET and KAZNET; MAJO/INU) allow clustering from a single earthquake. All dispersion curves that are not part of some cluster individually define a unique path.

An example of a cluster of dispersion curves is shown in Figure 5a for a set of five events in the Philippines recorded at Eskdalemuir, Scotland (ESK). Outliers are identified in two ways. First, a measurement is accepted only if it falls within a fairly broad group velocity corridor.

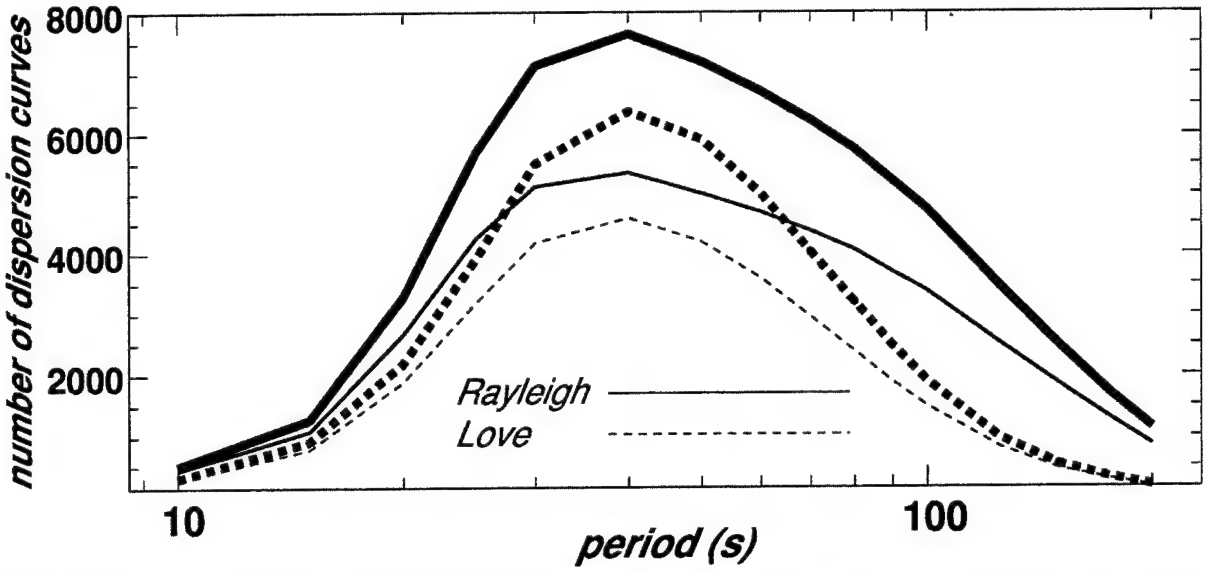


**Figure 4.** The number of dispersion measurements before (bold lines) and after (thin lines) the cluster analysis. Rayleigh waves are solid lines and Love waves are dotted lines. The analysis reduces the size of the data set by combining redundant measurements and discarding outliers.

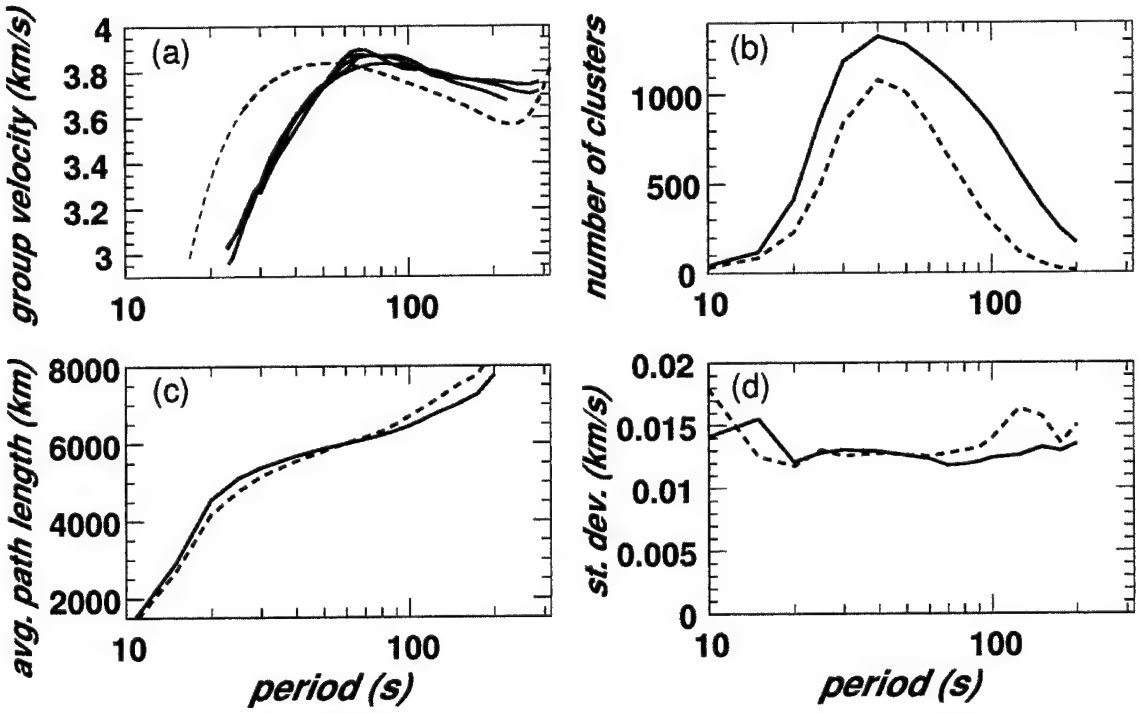


**Figure 5.** Cluster analysis. (a) Example of a cluster of measured group velocity curves. Estimated Rayleigh wave group velocity curves from a set of five events in the Philippnes measured at ESK, Scotland are compared with one another (solid lines) and prediction from PREM (dashed line). (b) The total number of clusters in the data set plotted as a function of period and wave type (Rayleigh; solid line, Love: dashed line.) (c) The average path length in km versus period (Rayleigh: solid line, Love: dashed line). (d) The average of the standard deviation of the group velocity curves composing the clusters.

Second, measurements that form part of a cluster are compared and visually inspected if there is significant disagreement. An analyst then interactively chooses which measurements to discard, if any. Higher graded measurements from larger events are given precedence in the selection process. After outlier rejection, the average velocity and standard deviation of the cluster are assigned to the path. The number of clusters as a function of period is shown in Figure 5b and the number of unique paths is displayed in Figure 4 as the thin line. About one-third of the original measured dispersion curves at intermediate periods form part of some cluster. The average path length as a function of period is presented in Figure 5c. The standard deviation of the dispersion curves within each cluster averaged over all clusters is plotted as a function of period and wave type in Figure 5d. We interpret this standard deviation as the average measurement uncertainty which we then associate with all dispersion curves that are not part of a cluster. Thus, if a dispersion curve has resulted from a cluster of measured curves, the uncertainty attributed to that curve arises from the variation among the individual curves composing the cluster. If the curve is for a ray that is not part of a cluster, the average of the standard deviation of the measurements taken over all clusters is used to define the measurement uncertainty.

The estimates of measurement uncertainty presented in Figure 5d are estimates of repeatability. Systematic theoretical errors, such as those caused by event mislocations or lateral ray refractions, are not incorporated in these estimates. Later discussions of the fit of the estimated group velocity maps to the measured dispersion curves will require more accurate absolute uncertainties and we will take this issue up again at that time (Section 5). The effects of both measurement uncertainty and theoretical errors on the estimated group velocity maps will be discussed in Section 4.

## 3. Surface Wave Tomography

This report presents the first part of an inversion for crustal and uppermost mantle structure beneath Eurasia. This inversion is broken into two stages: (1) the estimation of broadband group velocity maps at a variety of periods for both Rayleigh and Love waves and (2) the inversion of these maps for a structural model. We call the estimation of group

velocity maps 'surface wave tomography' and this first stage of the inversion is as far as this report extends. We describe the nature of surface wave tomography in this section, and present a sampling of the estimated group velocity maps in the subsequent sections of the report.

We have employed the algorithm of Ditmar and Yanovskaya (1987) and Yanovskaya and Ditmar (1990) to construct the group velocity maps (see also Levshin *et al.*, 1989; Ch. 6) using the group velocity curves that emerge from the cluster analysis applied to measurements made with the frequency-time analysis (FTAN). The method of Yanovskaya and Ditmar is a generalization to two dimensions of the classical one dimensional method of Backus and Gilbert (e.g., Backus and Gilbert, 1968, 1970). There are several features that commend this method. First, it does not require any *a priori* parameterization or truncation of any expansion since the basis functions for the model are superpositions of the kernels of the group travel time integrals. Perhaps more importantly, the method has been well tested and provides a well understood foundation for our work. The major disadvantage of the method as it is currently used is that it does not include explicit penalties on model size or the second spatial derivative of the model.

For each frequency and wave type, group velocity is a local function of position, $U(\theta, \phi)$, which we decompose into some reference value (frequently, the average across the studied region), $U_0$, and a location dependent perturbation: $U(\theta, \phi) = U_0 + \delta U(\theta, \phi)$. The most significant assumptions of this method are the following. (1) The method seeks a smooth perturbation in group velocity, $\delta U(\theta, \phi)$, relative to a homogeneous model, $U_0$, such that $U(\theta, \phi)$ fits the $N$ observed group velocity travel times, $t_i^{obs} (i = 1, .., N)$, in a weighted least-squares sense. To do this the method attempts to minimize the following penalty function at each period and wave type:

$$\sum_{i=1}^{N} [w_i (t_i^{obs} - t_i^{pred})]^2 + \lambda \int_S |\nabla U(\theta, \phi)|^2 dA, \tag{1}$$

where

$$t_i^{pred} = \int_{p_i} U^{-1}(\theta, \phi) ds. \tag{2}$$

Here, $p_i$ represents the $i$-th wave path, $w_i$ is the weight associated with the $i$th path through

the group velocity map $U(\theta, \phi)$, $t_i^{pred}$ is the predicted group travel time along the $i$-th path, and $S$ is the region under study. Choosing different values of the trade-off parameter, $\lambda$, changes the trade-off between the fit to the data and the 'smoothness' of the resulting group velocity map. 'Smooth' here is defined in terms of the spatial gradient of the model. The inversion takes place independently for each period and wave type. (2) Relative group velocity variations are assumed to be small in amplitude for each period and wave type: $\delta U(\theta, \phi)/U_0 << 1$. This is the justification for a linearized inversion procedure. (3) In equation (2), we currently assume that each wave path $p_i$ is along the great-circle linking the source and receiver and no group time perturbation is introduced by a source phase shift.

Data weights result from three sub-weights. The weight for measurement $i$ is:

$$w_i = \sqrt{m}\frac{g_i}{\sigma_i}, \tag{3}$$

where $m$ is the number of raw measurements that compose the cluster that produced this measurement, $\sigma_i$ is the uncertainty determined from the cluster analysis for measurement $i$, and $g_i$ is a weight which depends on the qualitative grade (A - F) assigned to the measurement by the analyst. As discussed in Section 2, if a measurement has resulted from a cluster, the uncertainty, $\sigma_i$, is the standard deviation of the dispersion curves composing the cluster. If a measurement has not resulted from a cluster, the average of the standard deviations from all clusters is taken as the uncertainty. The weight $g_i$, based on the qualitative grade assigned to the measurement by the analyst, is defined as follows. The normative grade is A and receives a weight of 1.0. Grades of B, C, D, E, and F are given weights of 0.75, 0.4, 0.2, 0.0, and 0.0, respectively. Thus, no measurement receiving a grade less than D is used. The grades of the measurements composing a cluster are averaged to produce a cluster grade which is then subjected to the same weighting criteria. For ungraded measurements, $g_i = 0.5$.

The damping parameter $\lambda$ in equation (1) is chosen by analyzing misfit and the visual smoothness of the resulting group velocity maps. Figure 6 illustrates the trade-off curve between misfit and $\lambda$ for the 40 s Rayleigh wave. Misfit is presented, first, as variance reduction relative to the average value across a given map:

$$\text{Variance Reduction} = 1 - \frac{\sum_i (U_i^{obs} - U_i^{pred}(\lambda))^2}{\sum_i (U_i^{obs} - U_0)^2}, \tag{4}$$

where $i$ is the unique path index, $U_i^{pred}(\lambda)$ is the predicted group velocity for path $i$ through the group velocity map constructed with the damping parameter set to $\lambda$, $U_i^{obs}$ is the measured group velocity for path $i$, and $U_0$ is the reference group velocity. In Figure 6, $U_0$ is the average group velocity across the map. Misfit is also presented as the rms velocity residual:

$$\text{RMS Velocity Misfit} = \left( \sum_i (U_i^{obs} - U_i^{pred}(\lambda))^2 \right)^{1/2}. \quad (5)$$

Three points on the misfit curves are marked with an x: one overdamped, one slightly underdamped, and one severely underdamped. Group velocity maps for each of these dampings are shown in Figure 7. We typically choose $\lambda$ to produce a slightly underdamped model. Because the penalty function does not include a second-spatial gradient term, we smooth each map a posteriori by applying a Gaussian spatial-smoothing filter with a carefully chosen width. The width chosen depends both on wave type and period and derives from the resolution analyses discussed in Section 4. This smoothing is designed to be an anti-aliasing filter and we apply it such that the full width at $e^{-1}$ of the maximum height of the filter is half the estimated resolution (Fig. 12). For example, for a 40 s Rayleigh wave the Gaussian filter's full width is 2.5 degrees at the $e^{-1}$ point. The effect of this filter is also shown in Figure 7 as the 'smoothed' map. It reduces artifacts while only slightly degrading overall fit to the data (Fig. 6). Figure 8 presents one dimensional plots of these two dimensional Gaussian filters for several resolutions.

## 4. Uncertainties in the Estimated Group Velocity Maps: Resolution and Bias

Uncertainties in the estimated group velocity maps result from several sources of two general types. The first type of uncertainty results from measurement errors and the vagaries of path distribution. Of these, the more severe are the effects of path distribution. Path distribution, both density of wave paths and azimuthal distribution, controls resolution. We perform in Section 4.1 a set of classical checker-board tests to estimate the resolution of and bias in the estimated group velocity maps. As discussed in Section 3, these estimates of resolution are used in the construction of a posteriori smoothing filters which are applied

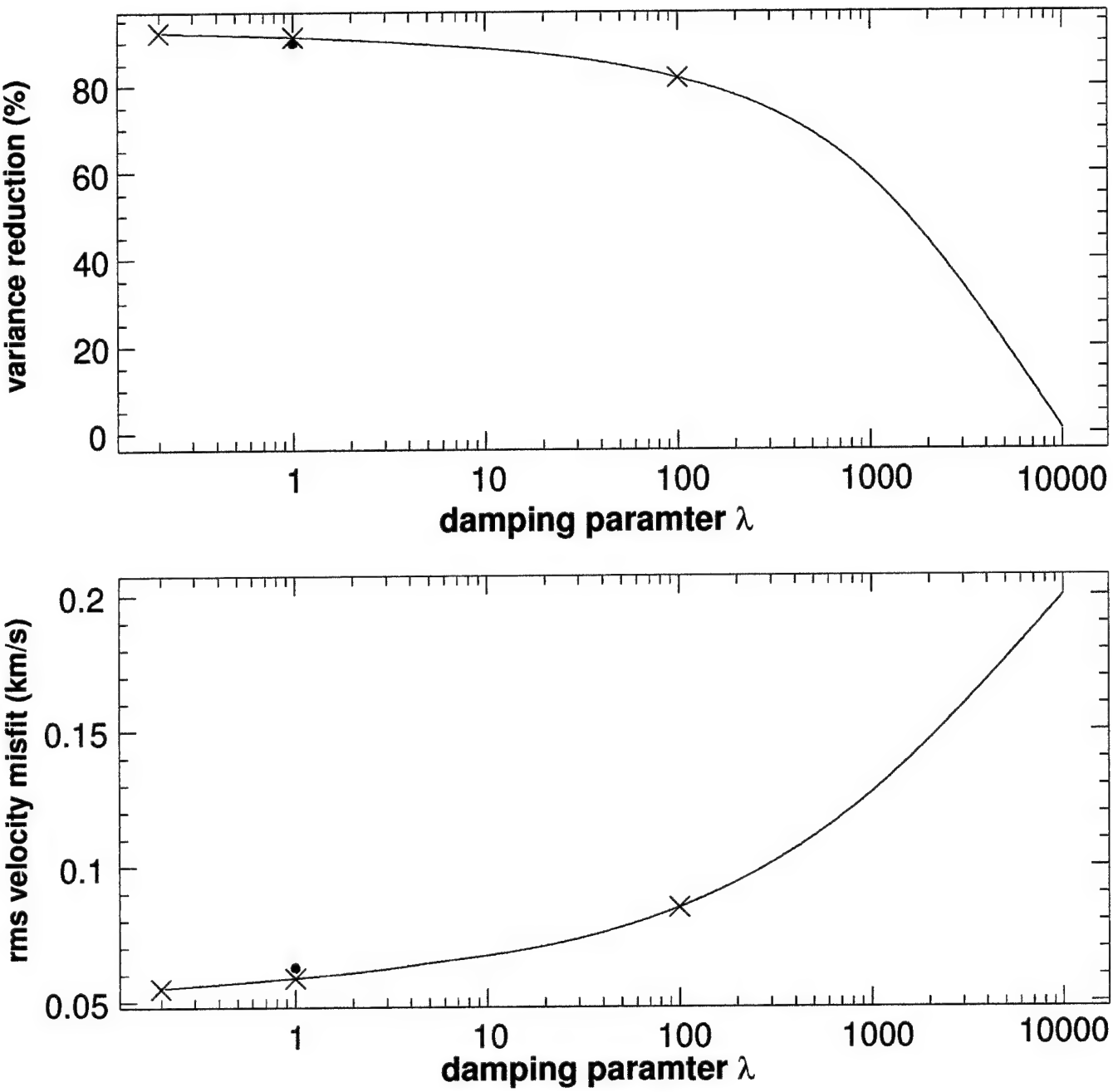


**Figure 6.** Two measures of misfit as a function of the damping parameter $\lambda$ in equation (1) for the 40 s Rayleigh wave. Three values of the damping parameter are highlighted as crosses on the trade-off curves: one severely underdamped ($\lambda \approx 0.2$), one slightly underdamped ($\lambda \approx 1$), and one highly overdamped ($\lambda \approx 100$). The group velocity maps constructed with these three values of $\lambda$ are shown in Figure 7. The application of the a posteriori smoothing filter to the group velocity map from the slightly underdamped inversion degrades fit to the data by a small amount, as is indicated with the closed circle.
(Top) Variance reduction relative to the average group velocity across the slightly underdamped map. (Bottom) Rms velocity difference between the observed group velocities and those predicted from the group velocity maps.

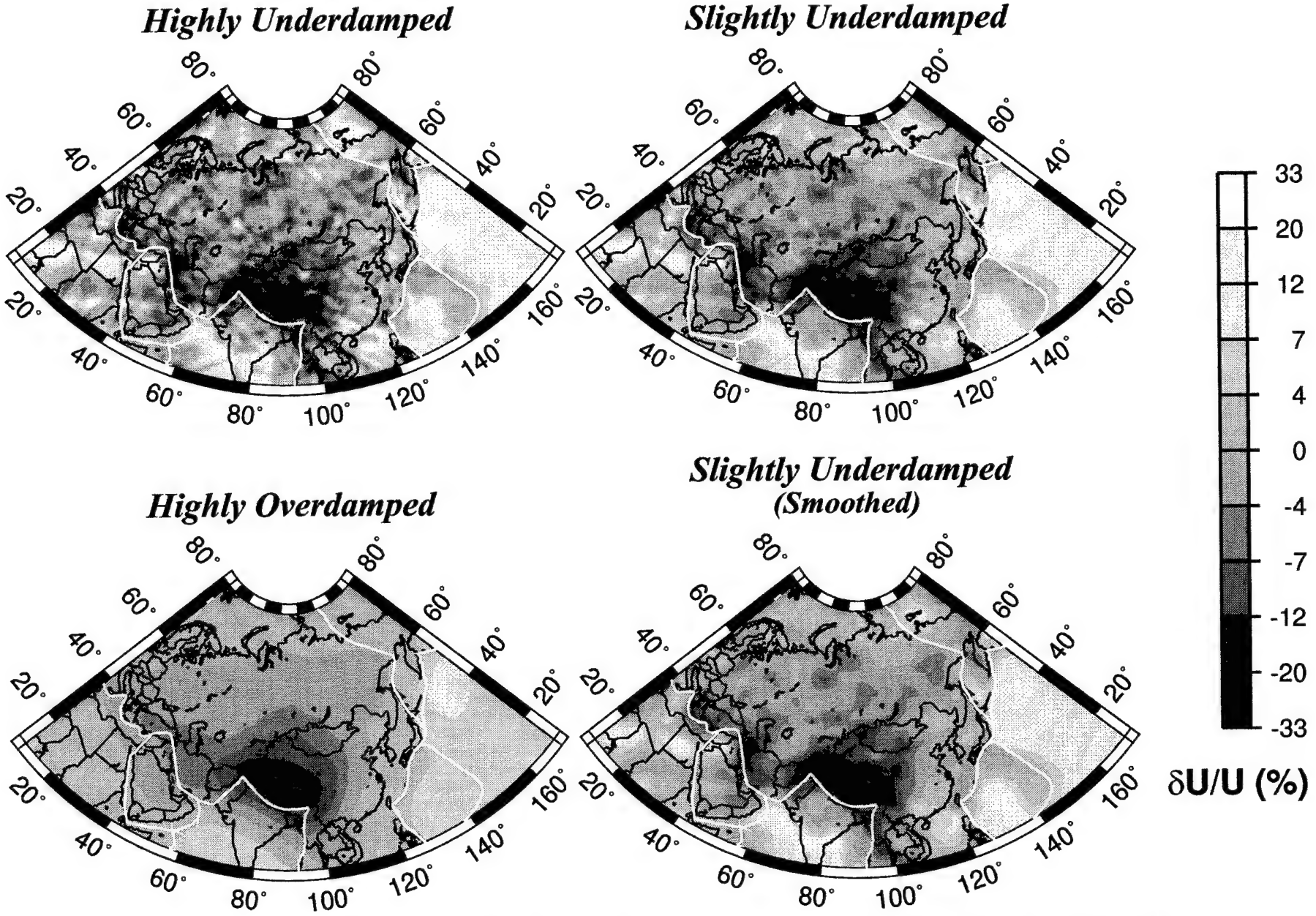


**Figure 7.** Group velocity maps constructed with the three damping parameters which are indicated with crosses in Figure 6: (top left) highly underdamped ($\lambda \sim 0.2$), (top right) slightly underdamped ($\lambda \sim 1$), and (bottom left) highly overdamped ($\lambda \sim 100$). The application of the a posteriori smoothing filter (full-width at the $1/e$ point of 2.5°) to the map at top right produces the smoothed map at bottom right.

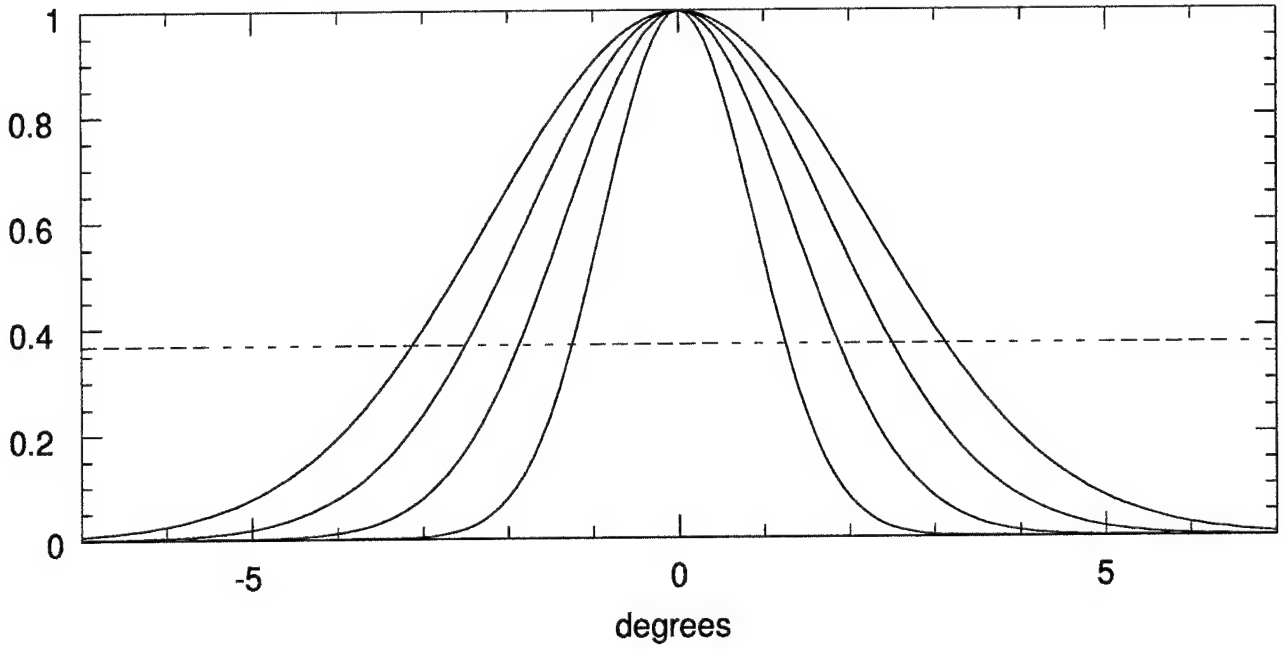


**Figure 8.** Plots of several one-dimensional slices of the two-dimensional Gauss smoothing filters with full-widths as the 1/e points of 2.5, 3.75, 5, and 6.25 degrees. The horizontal dashed line denotes 1/e .

to each of the estimated group velocity maps. The second type of uncertainty involves errors in assumptions, approximations, and input parameters which are not estimated in the inversion. Together we refer to these as 'theoretical errors'. The principal theoretical errors that will negatively affect the estimated group velocity maps include event mislocation, the existence of azimuthal anisotropy, wave path refractions from the great-circle linking source and receiver, and source group time shift. A discussion of the effects of the first three of these issues is the subject of Section 4.2 below. Levshin *et al.* (1997) discusses the nature and significance of source group time shift on tomographic studies. The estimates of both types of uncertainties need to be kept in mind when interpreting the group velocity maps presented in Section 5. This interpretation is the subject of Section 6.

## 4.1 Uncertainties Unrelated to Theoretical Errors

Ignoring theoretical errors, at each geographical point and period the resolution of the data set discussed in Section 2 will depend on the density of unique paths, the azimuthal distribution of these paths, and their average path length. Examples of the path coverage are shown in Figures 9a and 9b where we plot the path density, defined as the number of paths that intersect each square two degree cell ($\sim$50,000 km$^2$). The path density across much of Eurasia is high, but falls off rapidly near the periphery of the continent, particularly in India, in North Africa, and in the oceanic regions other than the marginal seas of the Western Pacific and much of the Philippine Sea. Path density is highest, particularly at periods below about 60 s, in Central Asia due to the presence of KNET and KAZNET. We will discuss the importance of azimuthal distribution and path length to resolution and bias later in this section.

To estimate resolution we perform a 'checker-board' test. The left column of Figure 10a displays three checker-board input models. Each model is divided into cells of equal area, each cell possessing a velocity perturbation of $\pm$10% of the average across each map. Travel time perturbations are accumulated along great circle paths linking source and receiver. Since no noise is added to the synthetic travel times, the estimated resolution is largely independent of the amplitude of the velocity perturbation chosen ($\pm$10%). The number and

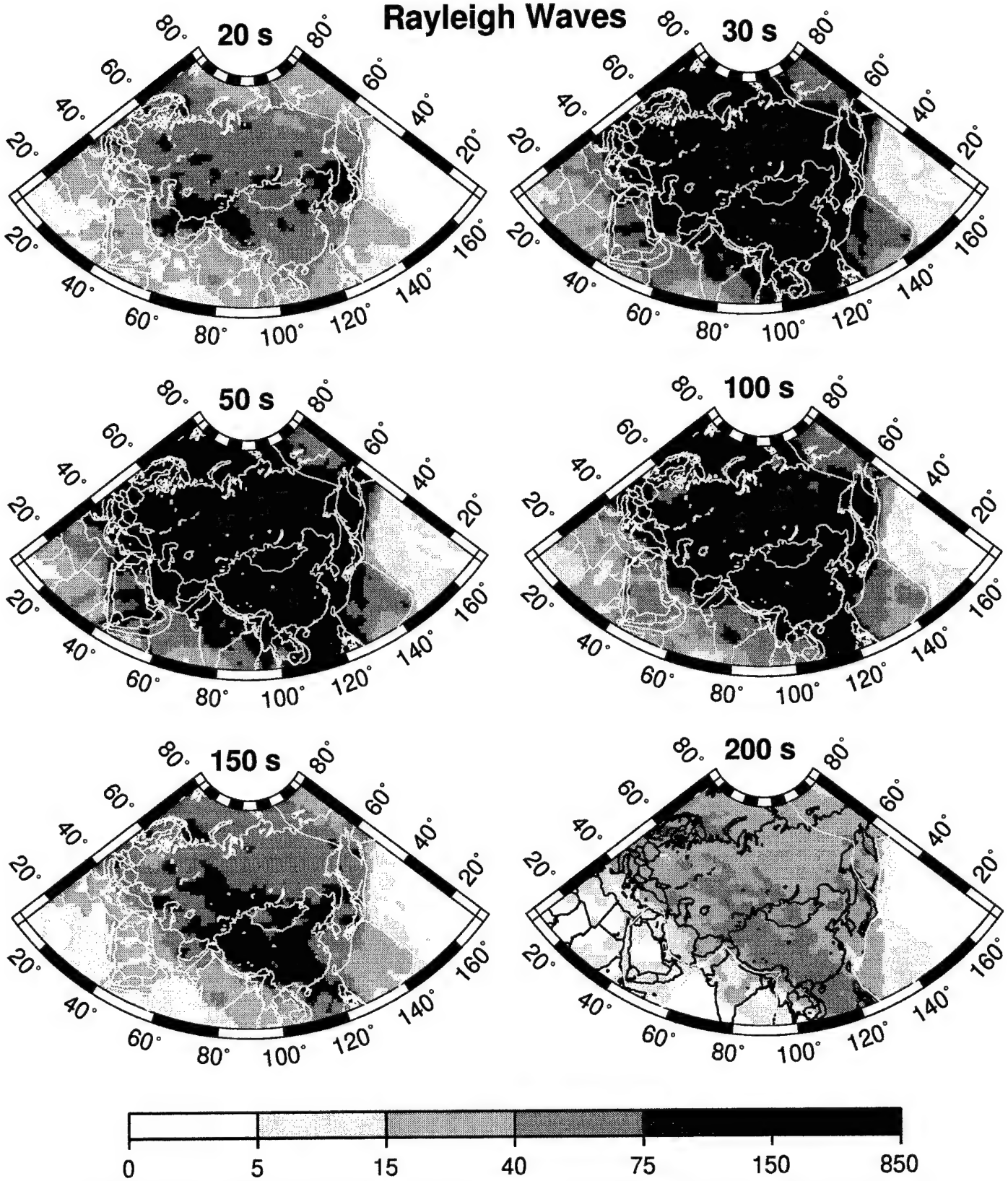


**Figure 9a.** Path density for Rayleigh waves at the six indicated periods. Path density is defined as the number of rays intersecting a 2 degree square cell (~ 50,000 sq. km). Regions of group velocity maps with densities below about 15 rays per cell should be suspect.

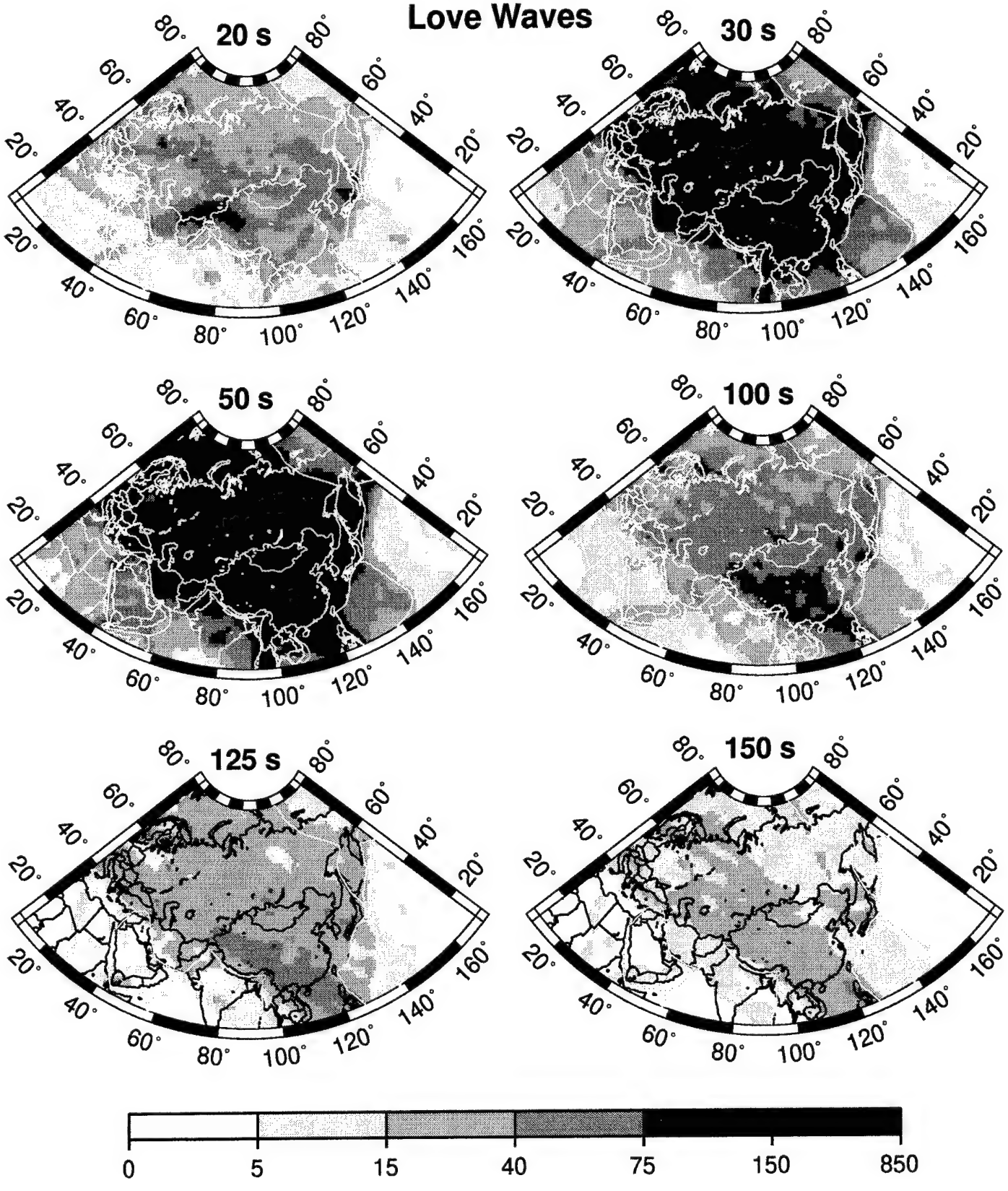


**Figure 9b.** The same as Figure 9b, but for Love waves at the indicated periods.

distribution of unique paths differ with period and wave type. We can estimate resolution as a function of wave type and period by computing synthetic travel times through the checker-board model for exactly the unique paths that have emerged from the cluster analysis and then inverting these synthetic data using the same weighting and damping used in the group velocity tomography described in Section 4.

The estimated maps are displayed in the right column of Figure 10a. The paths used in Figure 10 are those for the 40 s Rayleigh wave and the cell sizes are 3, 5, and 7.5 degrees. Although a few regions appear to be resolved at 3 degrees, most cells are not resolved until they are increased in size to 5 degrees. By the time squares are increased in size to 7.5 degrees, nearly all of the cells that can be resolved by the data set are resolved. The regions which possess very poor path coverage in Figure 9, such as those around the periphery of the continent, display very poor resolutions.

Plots such as those in Figure 10a are rather difficult to interpret and digest in large numbers. The key question is whether or not a given cell has been resolved in the inversion. What is desired principally is a yes or no answer. To simplify interpretation, we assign a 'Resolution Index', $\mathcal{R}_i$, to each cell:

$$\mathcal{R}_i = \frac{v_{\max}}{v_{\text{input}}} \qquad \text{(in percent)}. \tag{6}$$

Here $v_{\max}$ is the estimated velocity whose absolute value is maximum in the cell and $v_{\text{input}}$ is the input velocity in the same cell. Perfect resolution would result in $\mathcal{R}_i = 100\%$, poor resolution results in $\mathcal{R}_i \leq 30\%$. The resolution index can be less than zero if the sign of $v_{\max}$ is opposite from the input value, $v_{\text{input}}$, of the cell or greater than 100% if the estimated magnitude within is higher than the input value. We consider a cell fairly well resolved if $\mathcal{R}_i > 50\%$. In Figure 10b, we plot the resolution index for each of the three checker-boards in Figure 10a, again with the unique paths for the 40 s Rayleigh wave. Each cell is assigned one of three shades of grey in answer to the question: 'Is this cell resolved?'. The answer is 'yes' if $\mathcal{R}_i > 50\%$ and then the cell is shaded light grey. The regions with poorer resolutions are indicated by the darker cells. The average resolution emerges as about 5 degrees for a 40 s Rayleigh wave across most of Eurasia, although North Central Siberia is not resolved at 5 degrees. It should be noted that this is a fairly liberal test of resolution.

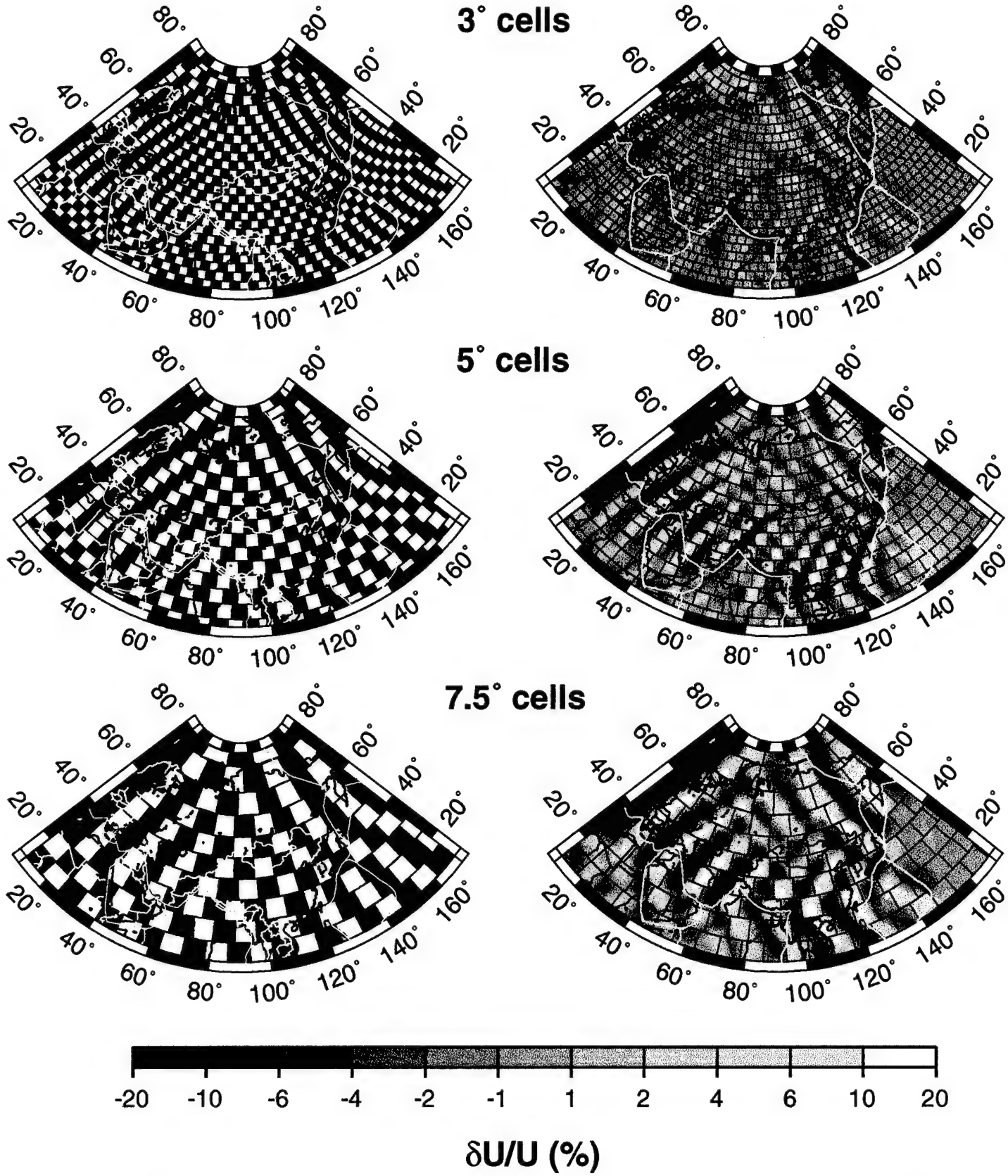


**Figure 10a.** Checker-board test for the 40 s Rayleigh wave with cells of three different sizes: (top) 3°, (middle) 5°, (bottom) 7.5°. There are regions in which 3° cells are resolved, but if cells are smaller than 5° most are not well resolved. Resolutions of 5° are observed across most of Eurasia, with the notable exception of North Central Siberia, where cells are not resolved below about 7.5° in size.

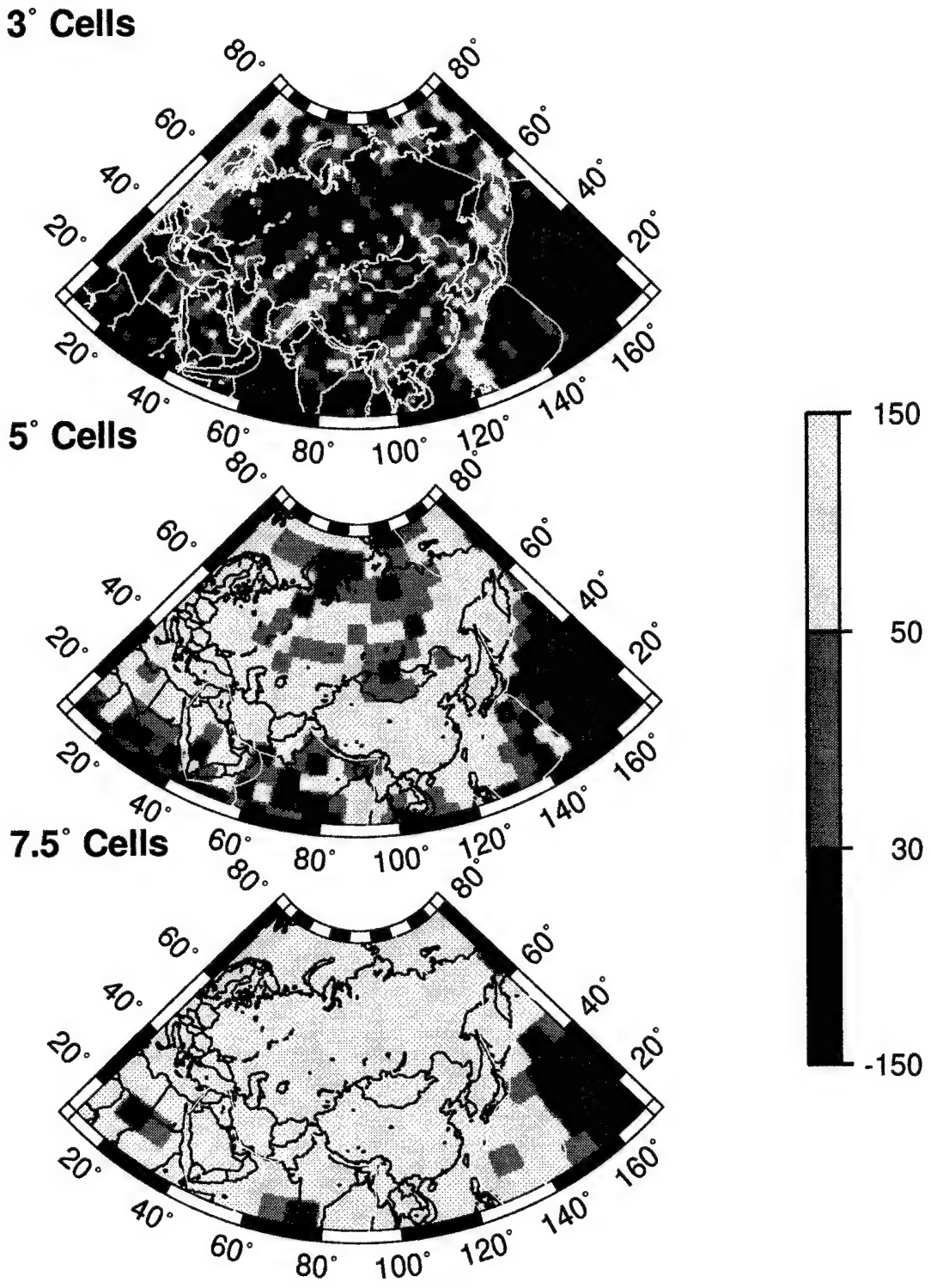


**Figure 10b.** Plots of the resolution index ($\Re$, eqn. (6)) for the 40 s Rayleigh wave with the same cell sizes as in Fig. 10a. Light grey cells are considered resolved, increasingly darker cells denote poorer resolution. The same sort of information is included in these figures as in Fig. 10a, but in this form it is more readily and quickly interpreted.

Figures 11a - 11d present a set of maps of the resolution index for both Rayleigh and Love waves at a variety of periods. The tests differ from one another in the cell sizes presented and the number and distribution of the paths that characterize the data set at each period and wave type. Each row of these figures presents two resolution index maps, one (the left) in which most of Eurasia is resolved but some regions are not quite resolved and the other (right) in which Eurasia is nearly fully resolved. The cell sizes defining these two figures differ from period to period and between wave types. However, a recurring problem emerges: North Central Siberia tends to be the most poorly resolved region of Eurasia independent of period and wave type. Figure 12 presents a summary of the minimum cell size for which most of Eurasia is resolved.

Bias is not as easily estimated with synthetic experiments such as those presented here. The synthetic experiments discussed above show that the amplitude of the estimated velocity variations will be somewhat smaller, on average, than the input value. This results largely from the damping in the inversion. This small amplitude bias is not as interesting as bias in geographical location of velocity features. Figure 13 displays a resolution analysis in which the input model comprises two square 7.5 degree cells with nonzero structural values (10%), one in a well resolved region of Central Asia and the other in a poorly resolved area of North Central Siberia. The rest of the model outside of these blocks is everywhere zero. The ray paths used, again, are the unique paths for the 40 s Rayleigh wave. In the checker-board test, we estimated a resolution of about 5 degrees in Central Asia and 7.5 degrees in North Central Siberia. Consistent with this test, the estimated Central Asian cell is well resolved and unshifted. The Siberian cell, however, is spread out and shifted to the south by about one-half of a cell size. This half-cell bias is below the 5 degree resolution we report for the 40 s Rayleigh wave in Figure 12. It should be remembered, however, that errors in the estimated group velocity maps may include shifting at a significant fraction of the reported resolution level in some regions.

The bias and degraded resolution characterizing North Central Siberia are not due to a shortage of ray paths in this area, as Figure 9a demonstrates. Path density throughout this region is high, although certainly not as high as in Central Asia. Furthermore, as Figure 14

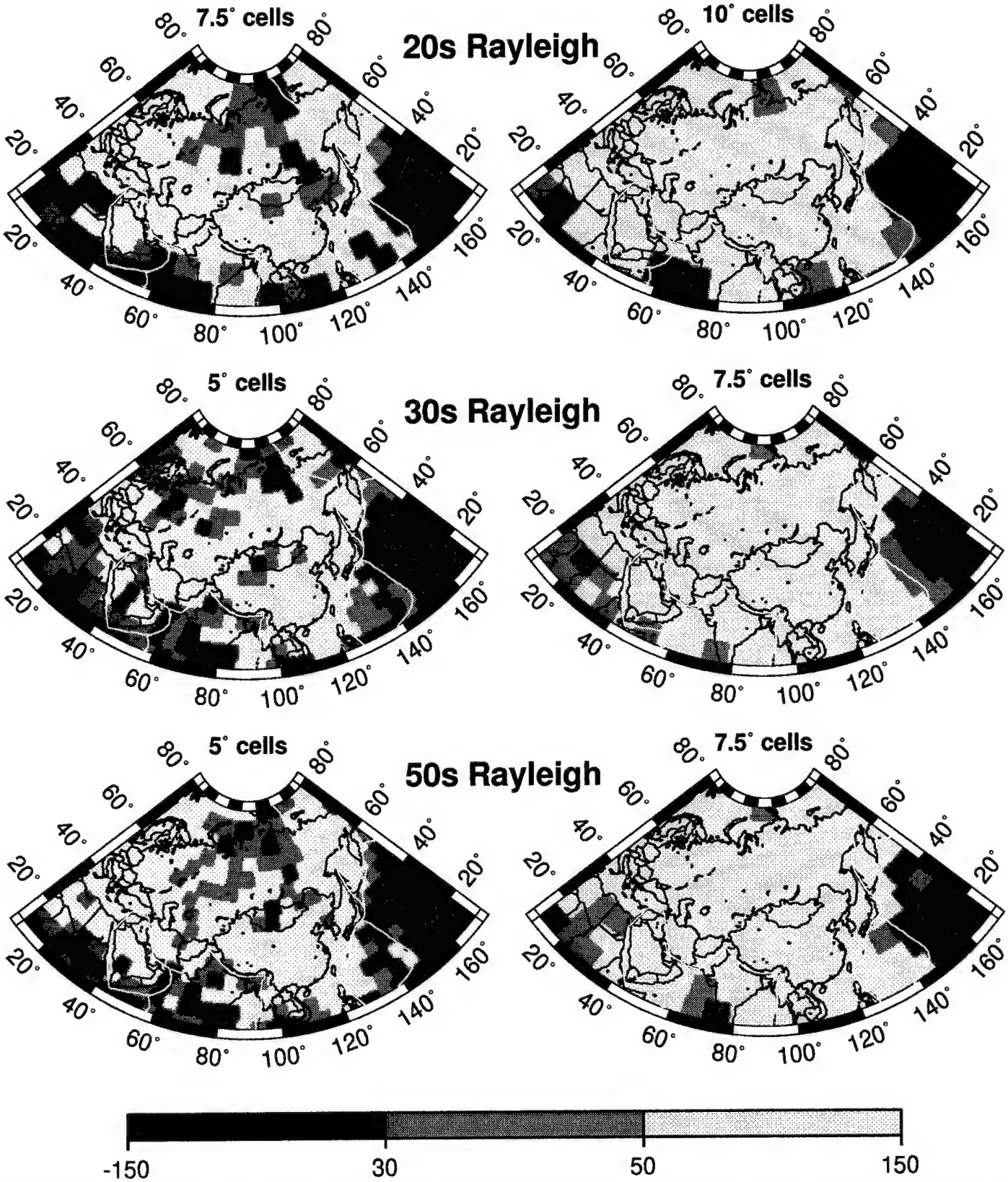


**Figure 11a.** Resolution index ($\Re$ , eqn (6)) plotted for intermediate period Rayleigh waves at the indicated periods and with specified cell sizes. Three grey-scale values are presented, the lightest indicates good resolution, increasingly dark cells reveal poorer resolutions.

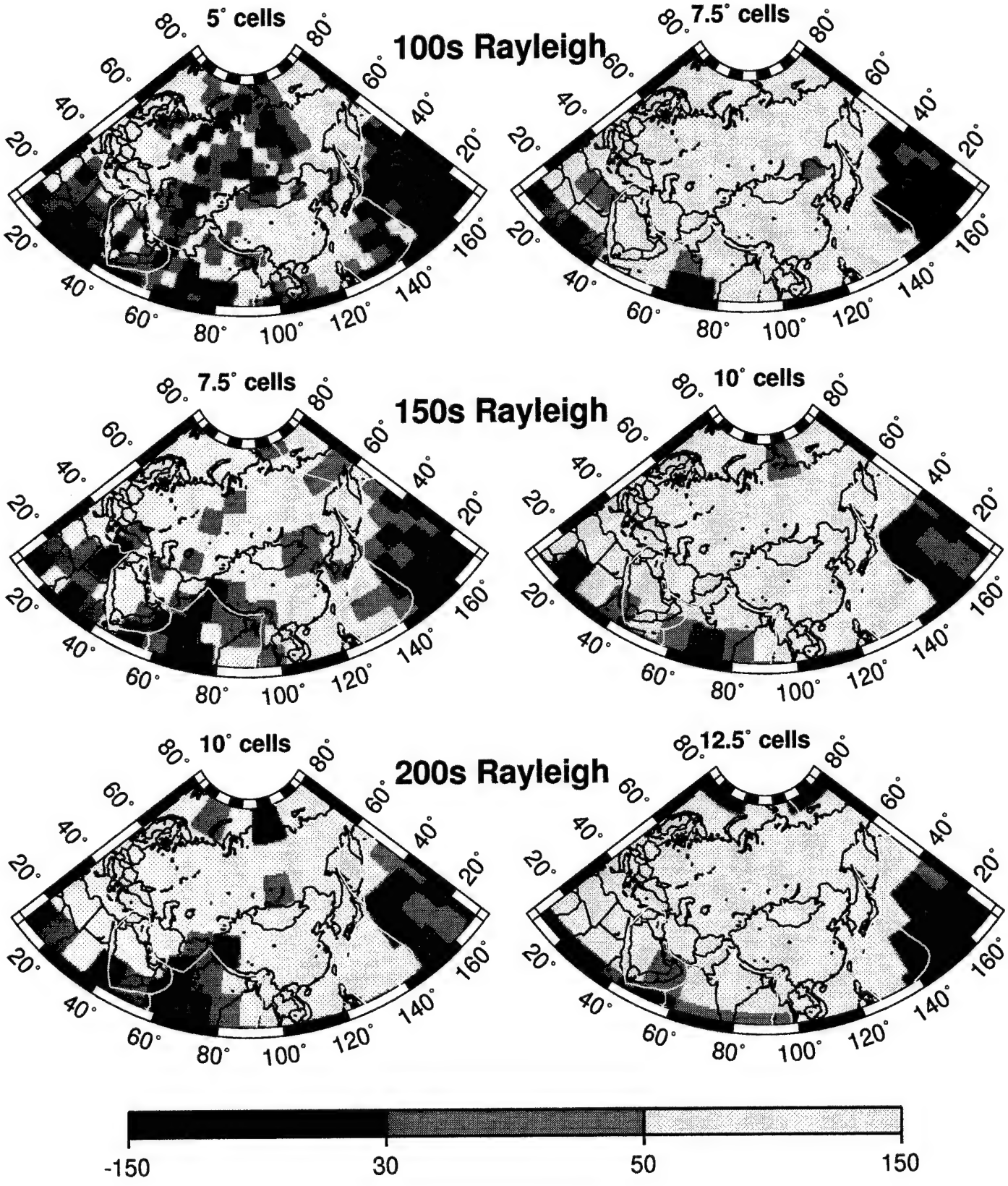


**Figure 11b.** Same as Figure 11a, but for long period Rayleigh waves at the indicated periods.

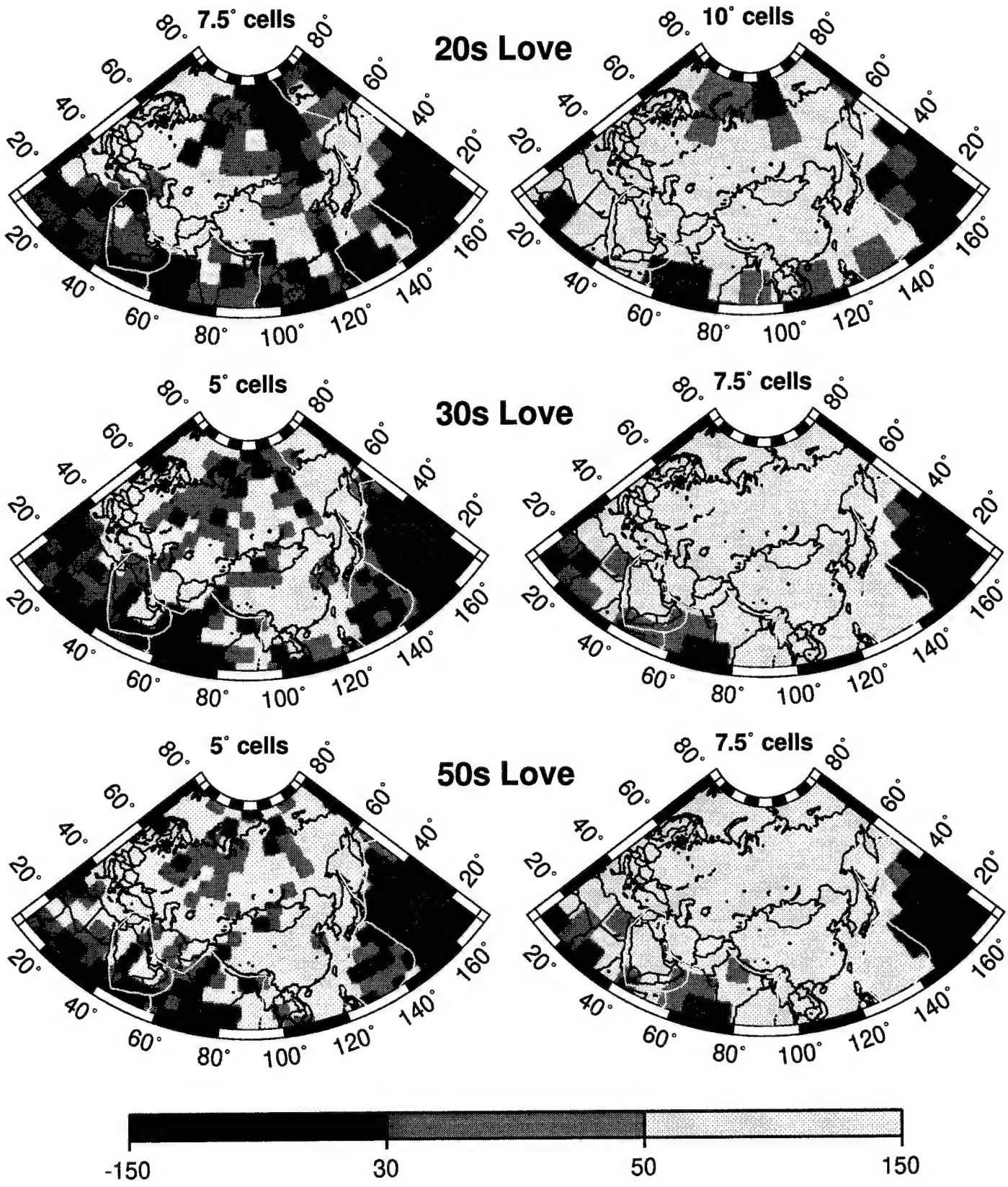


**Figure 11c.** Same as a Figure 11a, but for intermediate period Love waves at the indicated periods.

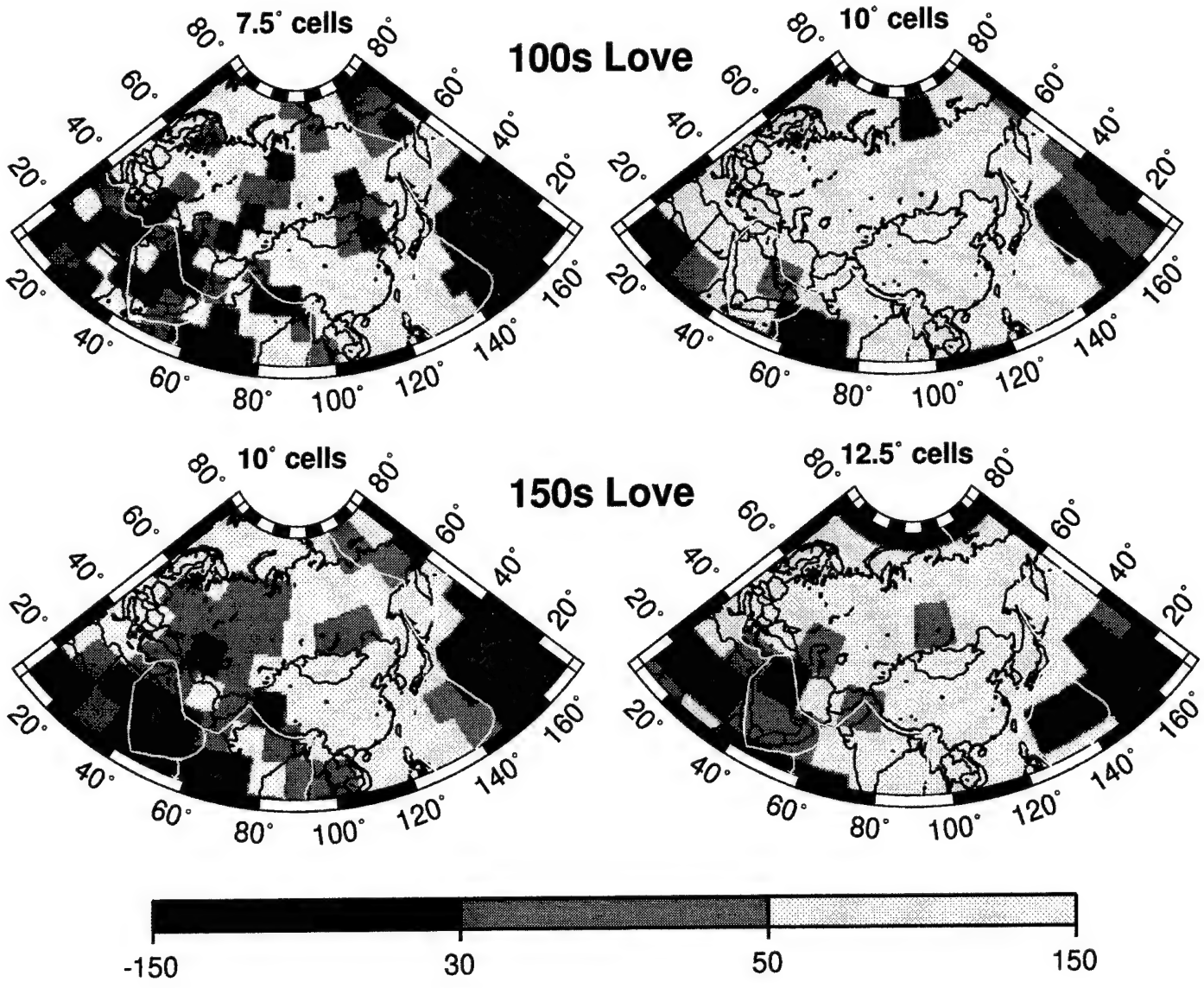


**Figure 11d.** Same as Figure 11a, but for the long period Love waves at the indicated periods.

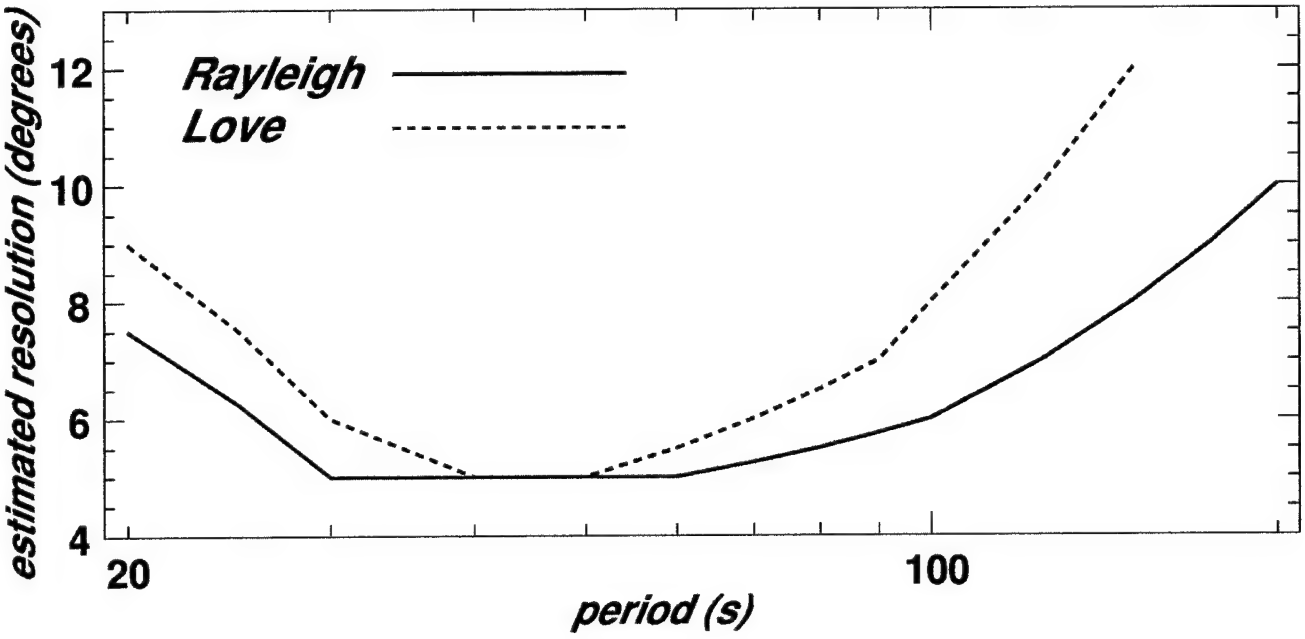


**Figure 12.** Estimated average resolution across the Eurasian continent. The value of resolution is chosen such that most of the continent appears to be resolved in 'Resolution index' plots, such as those shown in Figure 11. Some regions of the continent will display better or worse resolution.

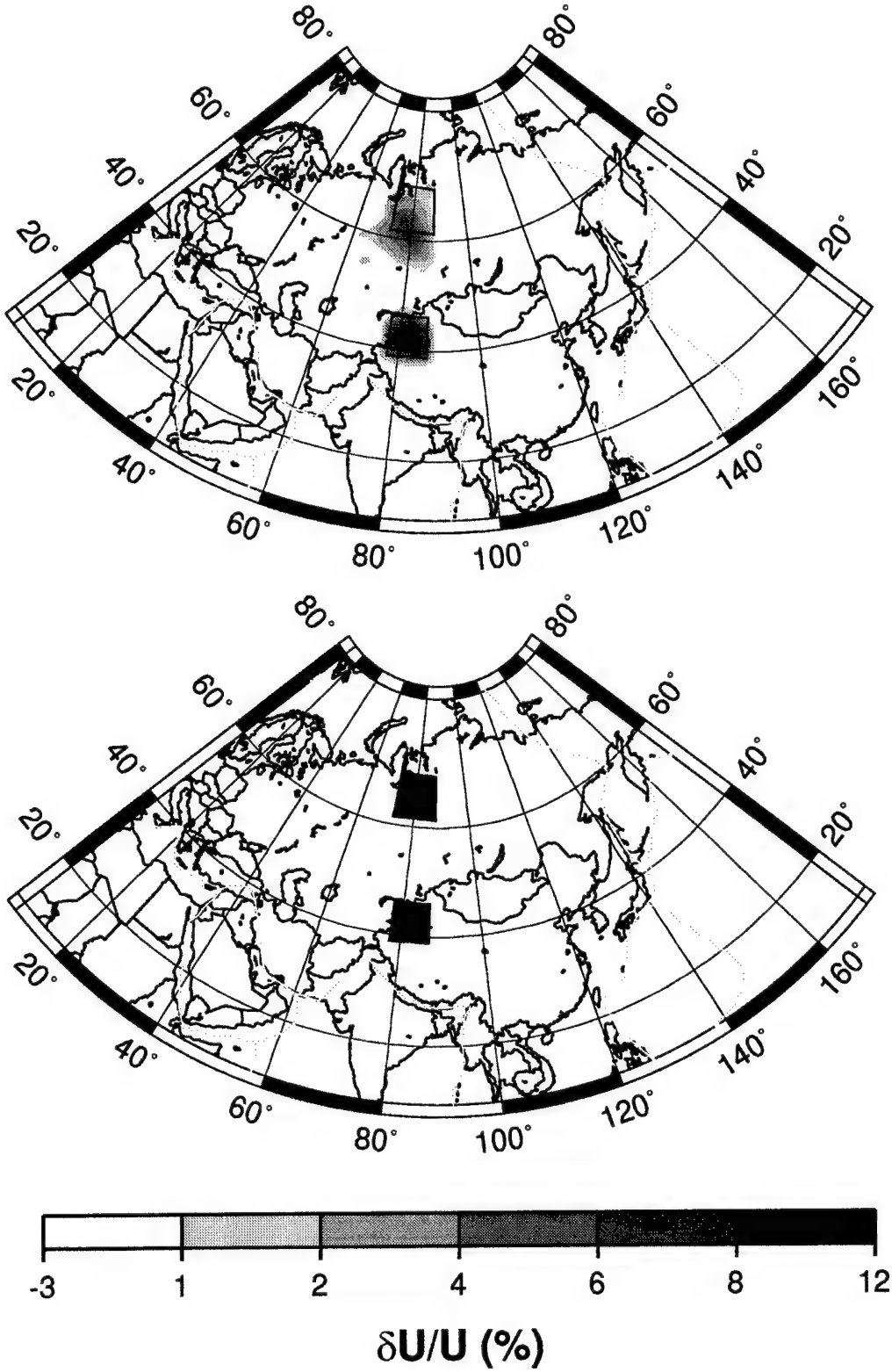


**Figure 13.** Bias analysis in which there are only two non-zero 7.5° square input cells, one in Central Asia (a region of very good resolution) and one in North Central Siberia (a region with poor resolution). Synthetic data used are the same as in Figure 7 for the 40 s Rayleigh wave. (Top) The estimated tomographic map is shown which demonstrates the southern shift of the North Central Siberian cell (by about one-half the cell width) and the high fidelity of the Central Asian cell. (Bottom) The input locations and shapes of the cells are shown. Both input cells have a velocity variation of 10%. The rest of the continent is homogeneous with no velocity variation.

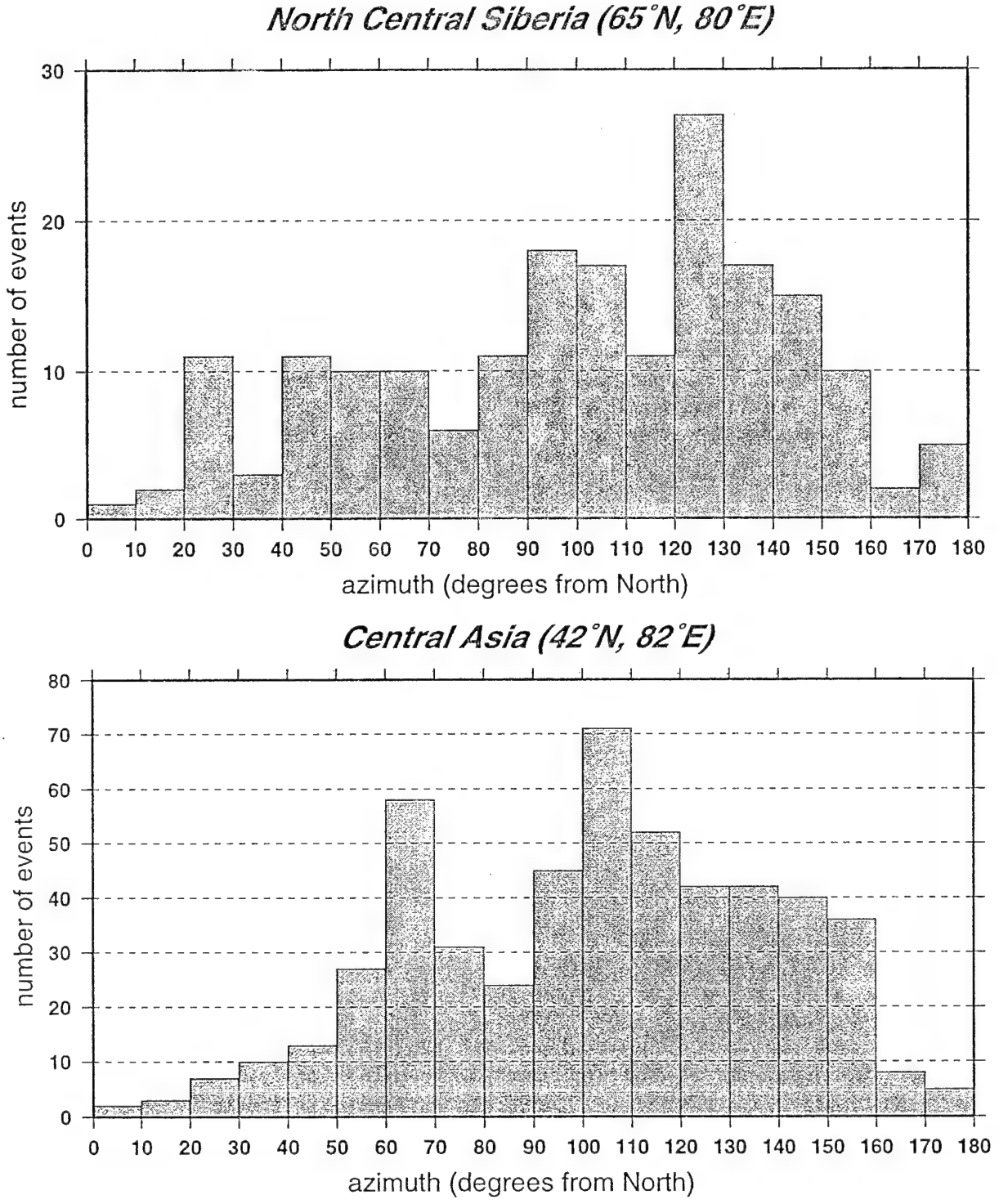


**Figure 14.** Histograms displaying the azimuthal distribution of the unique paths that pierce the two cells shown in Figure 13, (top) North Central Siberia and (bottom) Central Asia. Both regions demonstrate a shortage of nearly meridional (north-south) paths. Azimuthal distribution alone cannot account for the difference in resolution between these two regions.

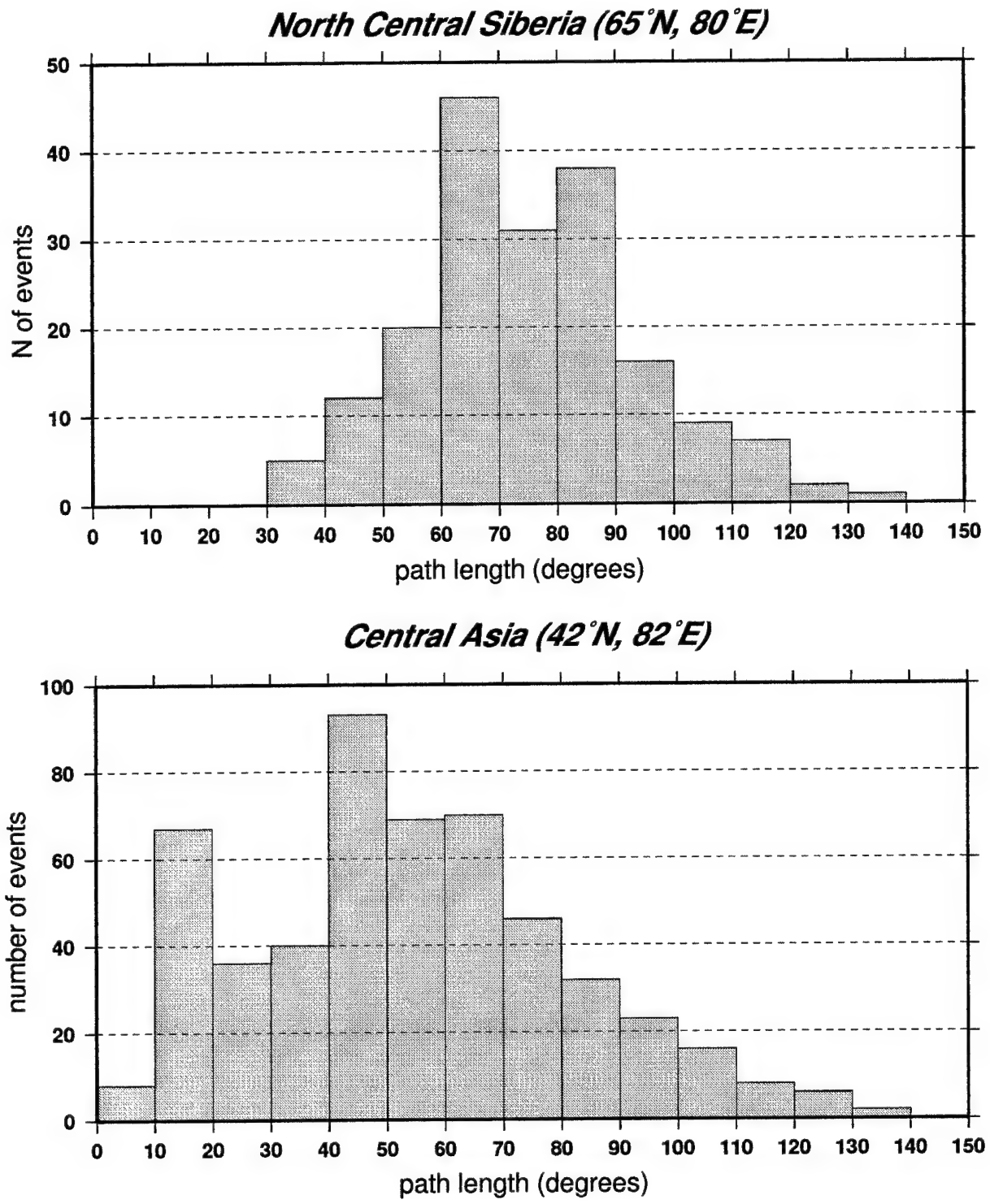


**Figure 15.** Histograms displaying the length distribution of the unique paths that pierce the two cells shown in Figure 13, (top) North Central Siberia and (bottom) Central Asia. (A degree is approximately 111 km.) The reduced resolution in North Central Siberia results from the lack of short paths combined with the absence of nearly meridional paths (Figure 14).

shows, the azimuthal distribution of paths piercing the Central Asian and Siberian cells is about the same. Both regions display a shortage of nearly meridional paths. What differs between these two regions is the existence of large numbers of relatively short paths in Central Asia, as Figure 15 shows. These short paths allow relatively small cells to be resolved even without an even azimuthal distribution. However, in the absence of regional seismicity and good seismic station coverage in North Central Siberia, the shortage of nearly north-south paths manifests itself as a degradation in resolution. The future addition of more nearly north-south paths originating from events in Central Asia and propagating to Canadian National and U.S. National Network stations should help improve resolution throughout much of Northern Eurasia. This will be the subject of future research.

## 4.2 Uncertainties Caused by Theoretical Errors

Other sources of bias can result from 'theoretical errors'. We discuss the following here: off-great-circle propagation, azimuthal anisotropy, and event mislocation.

A comparison between the locations of known structural boundaries and features apparent in the group velocity maps indicates that tomographic features may be shifted by as much as 3 - 5 degrees in geologically complicated regions, such as much of Central Asia, and that these shifts may be due to off-great-circle propagation. These shifts typically lie below the resolutions that we report here and errors in the estimated group velocity maps may include shifting due to off-gret-circle propagation at a significant fraction of the reported resolution level in some regions. A more careful simulation of the effects of off-great-circle propagation will be the subject of future research.

The estimated group velocity maps are directionally independent and, therefore, contain no information about azimuthal anisotropy. They should be viewed as azimuthal averages of group velocity at every point. A legitimate concern might be whether existing azimuthal anisotropy biases this average significantly. Over most of the continent, azimuthal coverage is sufficient to insure that bias caused by reasonable levels of azimuthal anisotropy is well below the estimated uncertainties in the original measurements. Simulations indicate that

bias should be below about 0.01 km/s for realistic models of anisotropy across the continent.

The multiplicity of sources helps mitigate against bias caused by source mislocation. Synthetic experiments show that if mislocations are random, their effect on the estimated group velocity maps is negligible. However, mislocations in certain source regions, in particular those adjacent to subducting slabs, may be systematic. Systematic errors in epicenter estimates of 10 km or more in extended regions may have an appreciable effect on the estimated group velocity maps.

Figure 16 presents examples from a synthetic experiment in which the locations of about 15 events in the Kurile Islands and in the Hindu Kush were shifted systematically and exactly parallel to one another by 10 km. Mislocations of the events in the Far East may be larger than this, but the fact that all events are parallelly shifted maximizes the effect of the mislocations on the estimated group velocity maps. We shifted the 'true' locations of the Kurile events to the southeast and the Hindu Kush events to the south relative to the erroneous locations used in the inversion. Figure 16 presents the tomographic simulation for the 20 s, 50 s, and 150 s Rayleigh waves for the Kuriles events and for the 20 s Rayleigh wave for the Hindu Kush events. All of the wave paths used in the inversion with real data at each period are used and the same weighting and damping are applied. In each inversion, only the events located in the specified regions are shifted; all other event locations are assumed known perfectly. Structure is laterally homogeneous so that the only 'signal' in the synthetic data should come from the event mislocations in the specified region.

The travel time signal due to a 10 km shift is only about 2 - 4 s. If a 3 s signal were distributed evenly along a 6,000 km path, the resulting velocity perturbation would be only about 0.1% of the average group velocity. However, as Figure 16 shows, in a tomographic inversion the effect of event mislocations is very small outside of the source region and the erroneous signal is compressed into a small region which amplifies the bias. The amplitude of the bias is approximately independent of period, with an absolute value maximizing between 0.5 - 0.8%. The size of this bias scales directly with the length of the mislocation. Biases of this size are not a problem at periods below about 100 s where the velocity anomalies are large, but become a concern at long periods where the amplitudes of velocity heterogeneity

are lower. In source regions away from the margins of the continent, such as the Hindu Kush, there are many paths crossing the region which do not originate in the source region. This diminishes the size of the bias. Figure 16 shows that the bias caused by the 10 km perturbation to the Hindu Kush events is less than half that caused by the Kurile events.

From these synthetic experiments we conclude that the largest source of bias is caused by systematic source mislocations. Bias from this effect will be most significant for source regions adjacent to descending slabs near the periphery of the area of study. The regions of greatest concern are near the Pacific Plate Boundary and, perhaps, the Eastern Mediterranean.

## 5. Group Velocity Maps

Using the tomographic method described in Section 3, we construct group velocity maps, which are smoothed using the results of the resolution analysis described in Section 4, for Rayleigh waves at the following periods: 20, 25, 30, 35, 40, 50, 60, 70, 80, 90, 100, 125, 150, 175, 200 s. The same periods are inverted for Love waves, except Love wave group velocity maps do not extend past 150 s period. The average group velocity curves across the studied region (latitude bounds: $10^o$N, $80^o$N; longitude bounds: $10^o$E, $170^o$E) for Rayleigh and Love waves are plotted in Figure 17. A sampling of the estimated group velocity maps is presented in Figures 18a - 18f. These maps represent lateral variations relative to the map average shown in Figure 17. Group velocity curves at few geographical locations which have been constructed by combining all of the estimated group velocity maps are shown in Figure 19. These maps are segregated roughly by tectonic or geologic type into three categories: sedimentary basins, continental plateaus or mountain ranges, and continental shields.

Our confidence in the longest period maps is not as high as in the shorter period maps; in particular, at 200 s for Rayleigh waves and at 125 s and 150 s for Love waves. There are two key reasons. First, accurate long period measurements can only be obtained from large earthquakes ($M_s \gtrsim 6.0$), and the distribution of these events around Eurasia is not uniform and their numbers are not large. On average over the period of study (1988 - 1995), only

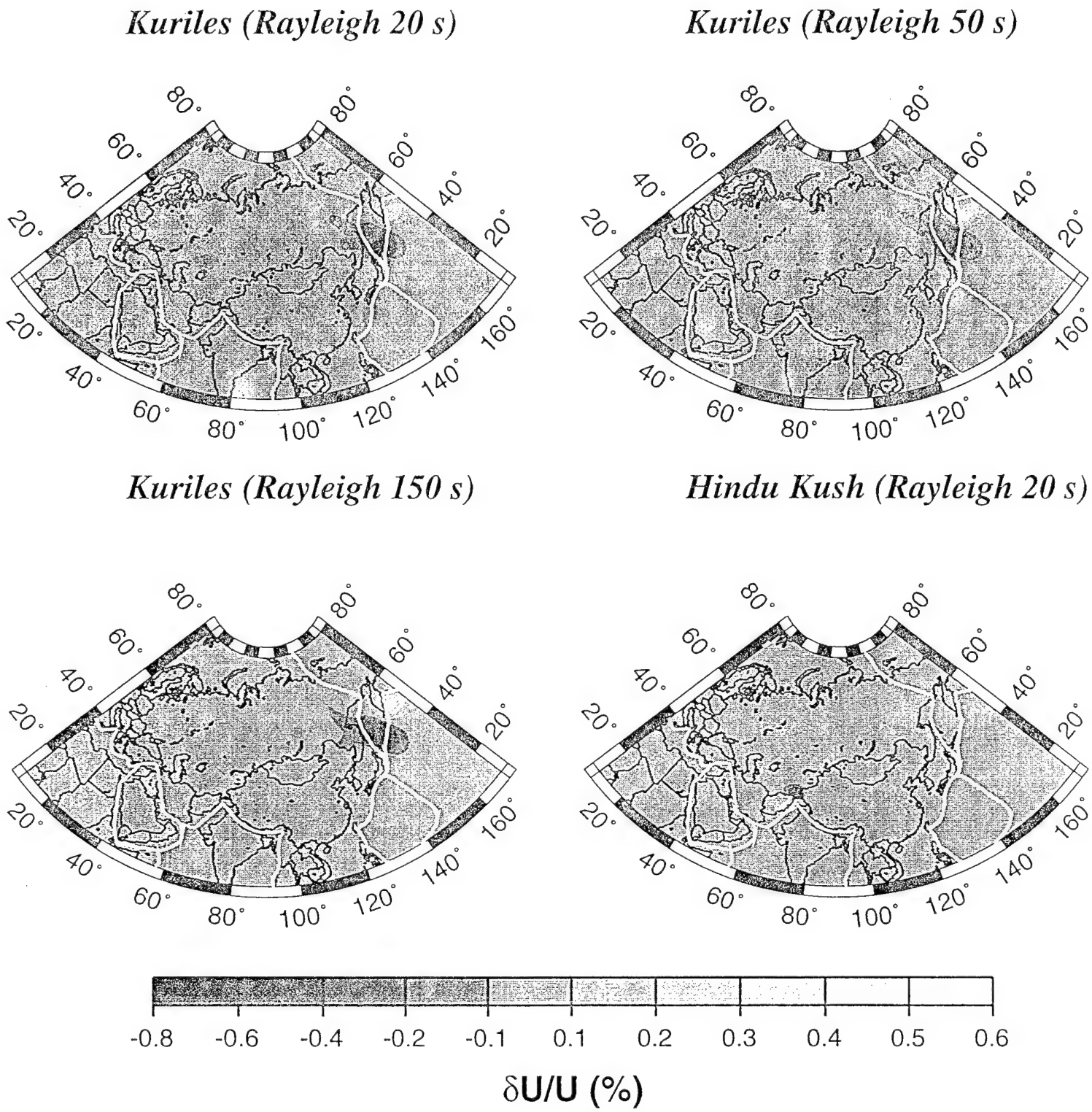


**Figure 16.** Mislocation bias. Results of a synthetic experiment in which approximately 15 events in two source regions (the Kurile Islands and the Hindu Kush) are shifted in the same direction by 10 km to determine the effect of systematic errors in source locations on the tomographic images. All events in the Kuriles are mislocated to the northwest and in the Hindu Kush to the north. Three Rayleigh wave periods (20 s, 50 s, 150 s) are shown for the Kurile Islands events and one period (20 s) for the Hindu Kush events. Bias is displayed in percent relative to the average group velocity across the map.

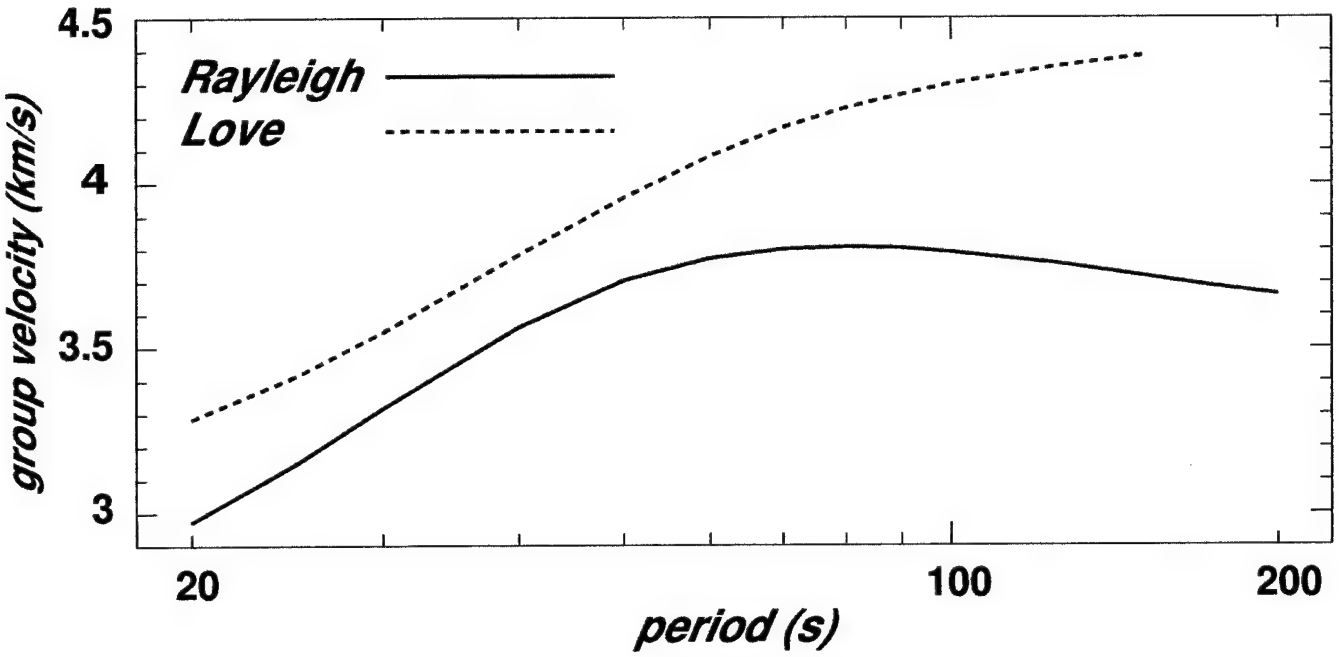


**Figure 17.** Average group velocity curve across the entire region of study (latitude: 10°N - 80°N, longitude:10°E - 170°E).

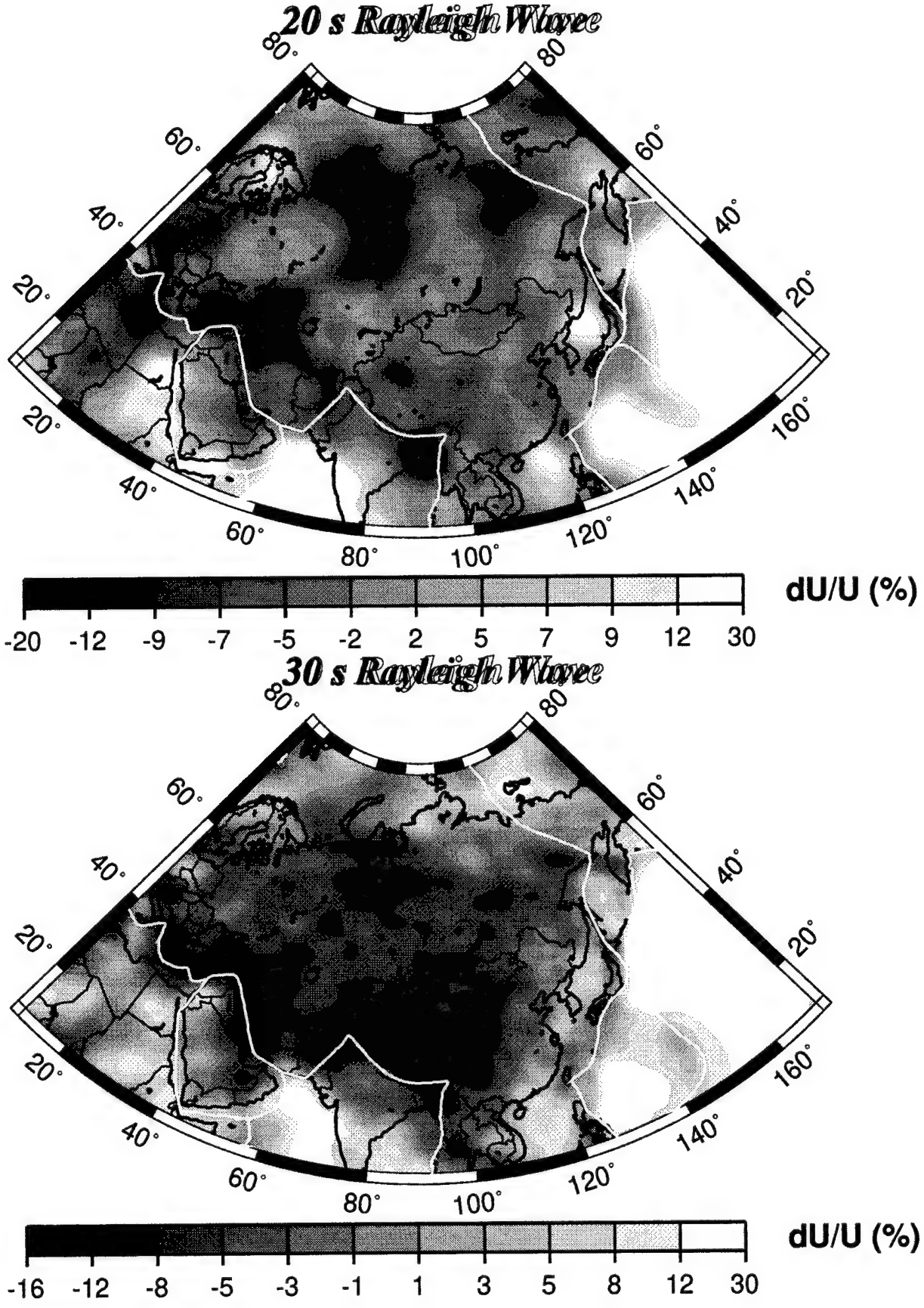


**Figure 18a.** Estimated group velocity maps across Eurasia for the 20 s and 30 s Rayleigh waves.

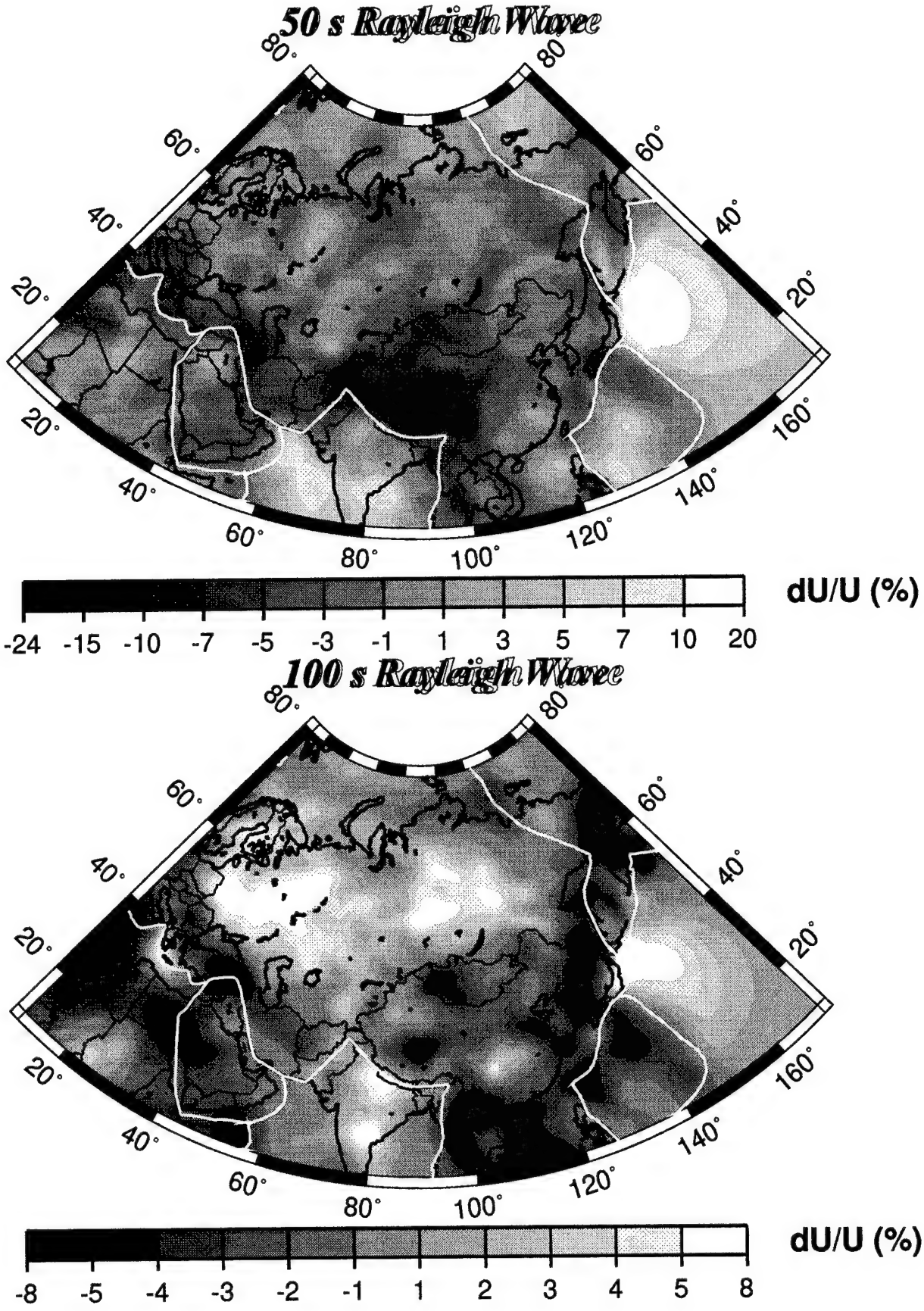


**Figure 18b.** Same as Figure 18a, except for the 50 s and 100 s Rayleigh waves

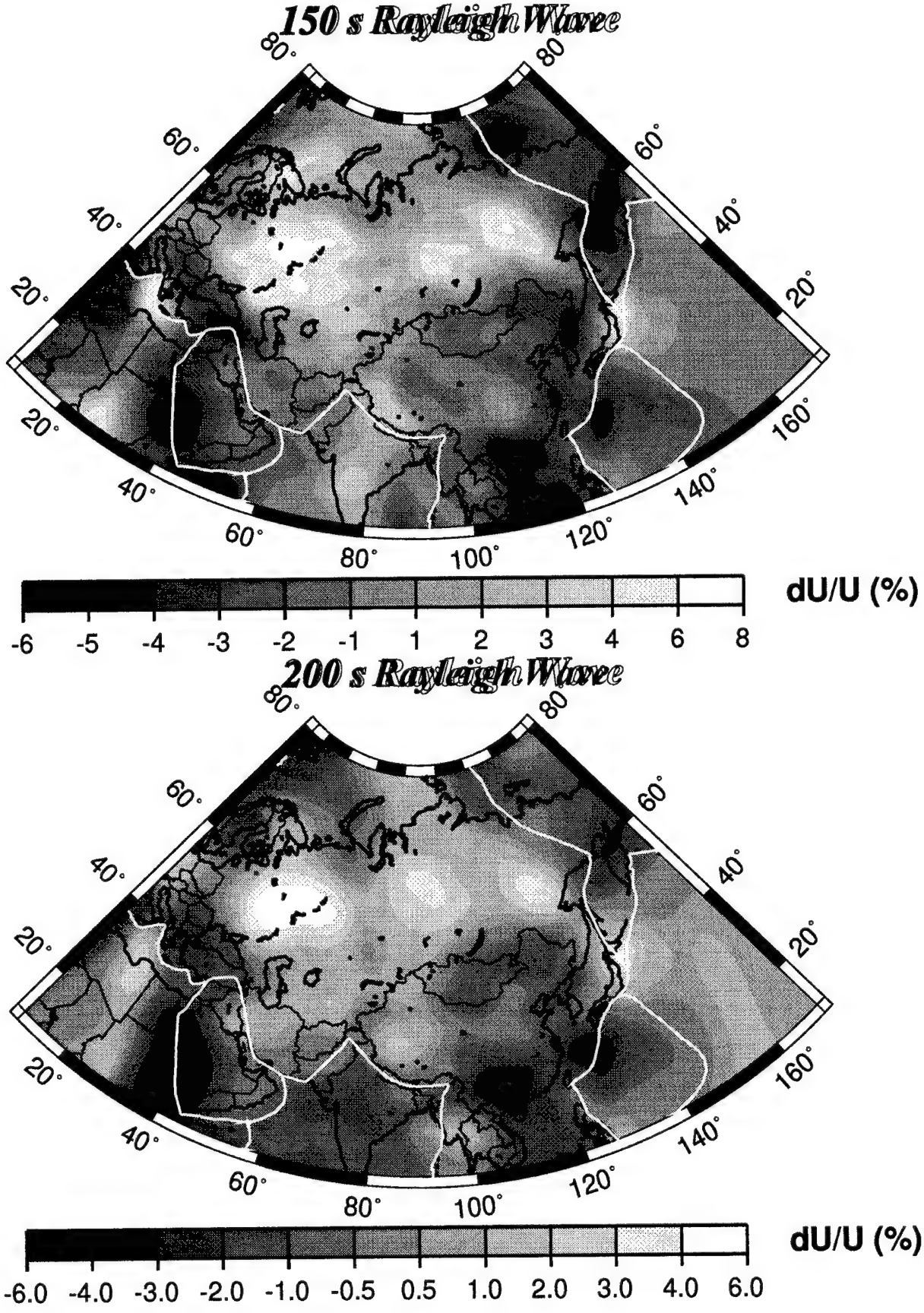


**Figure 18c.** Same as Figure 18a, except for the 150 s and 200 s Rayleigh wave

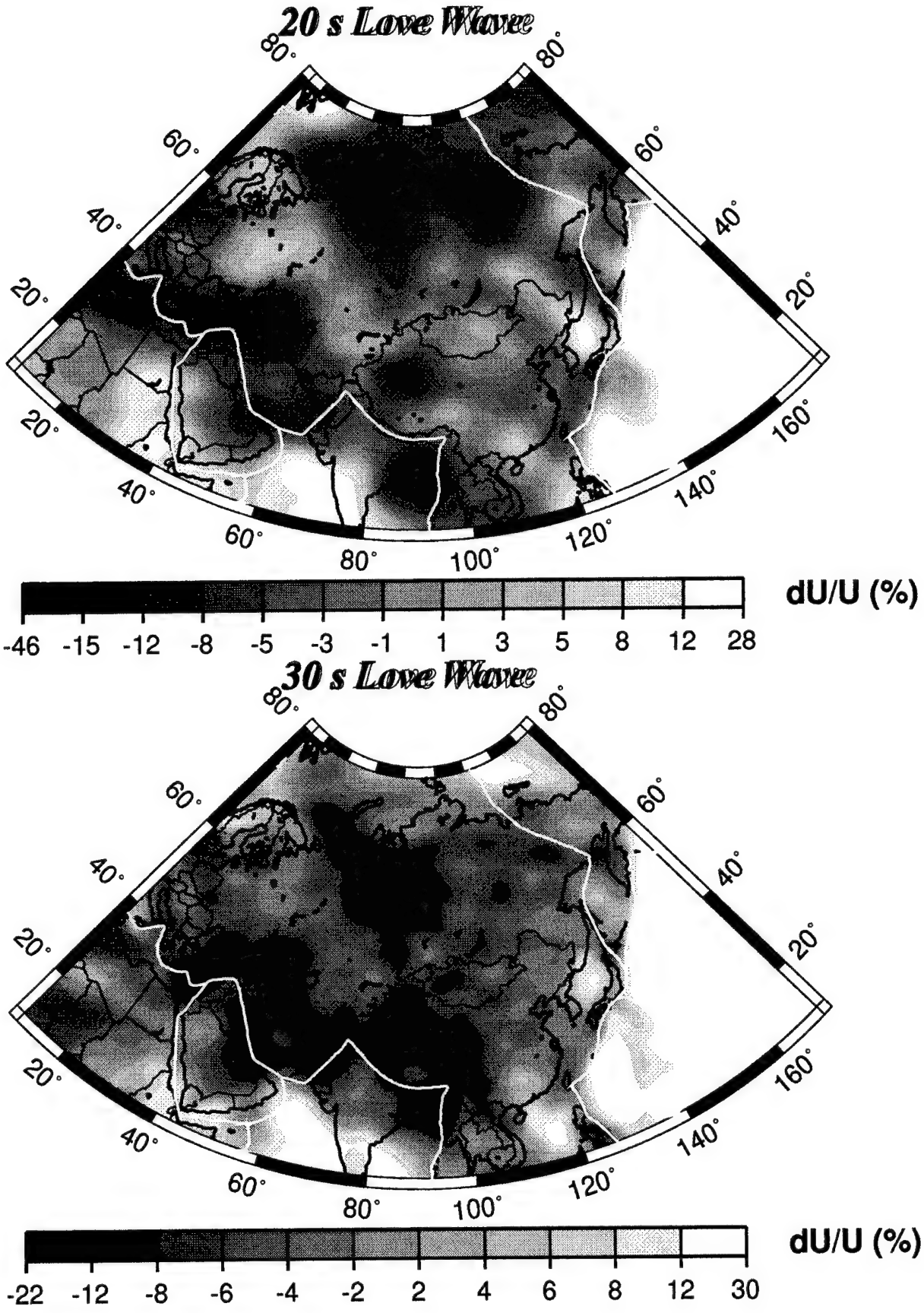


**Figure 18d.** Same as Figure 18a, except for the 20 s and 30 s Love waves.

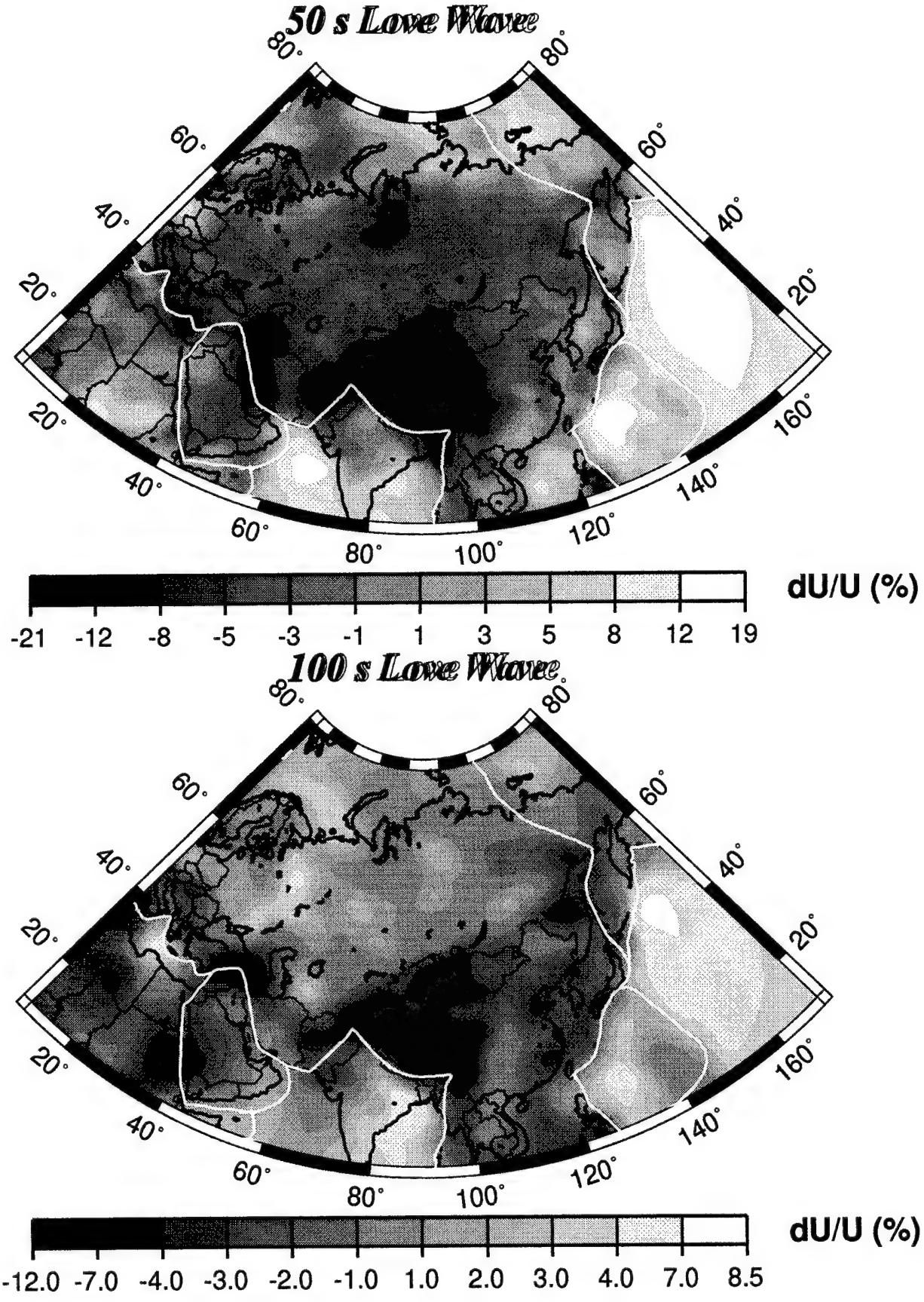


**Figure 18e.** Same as Figure 18a, except for the 50 s and 100 s Love waves.

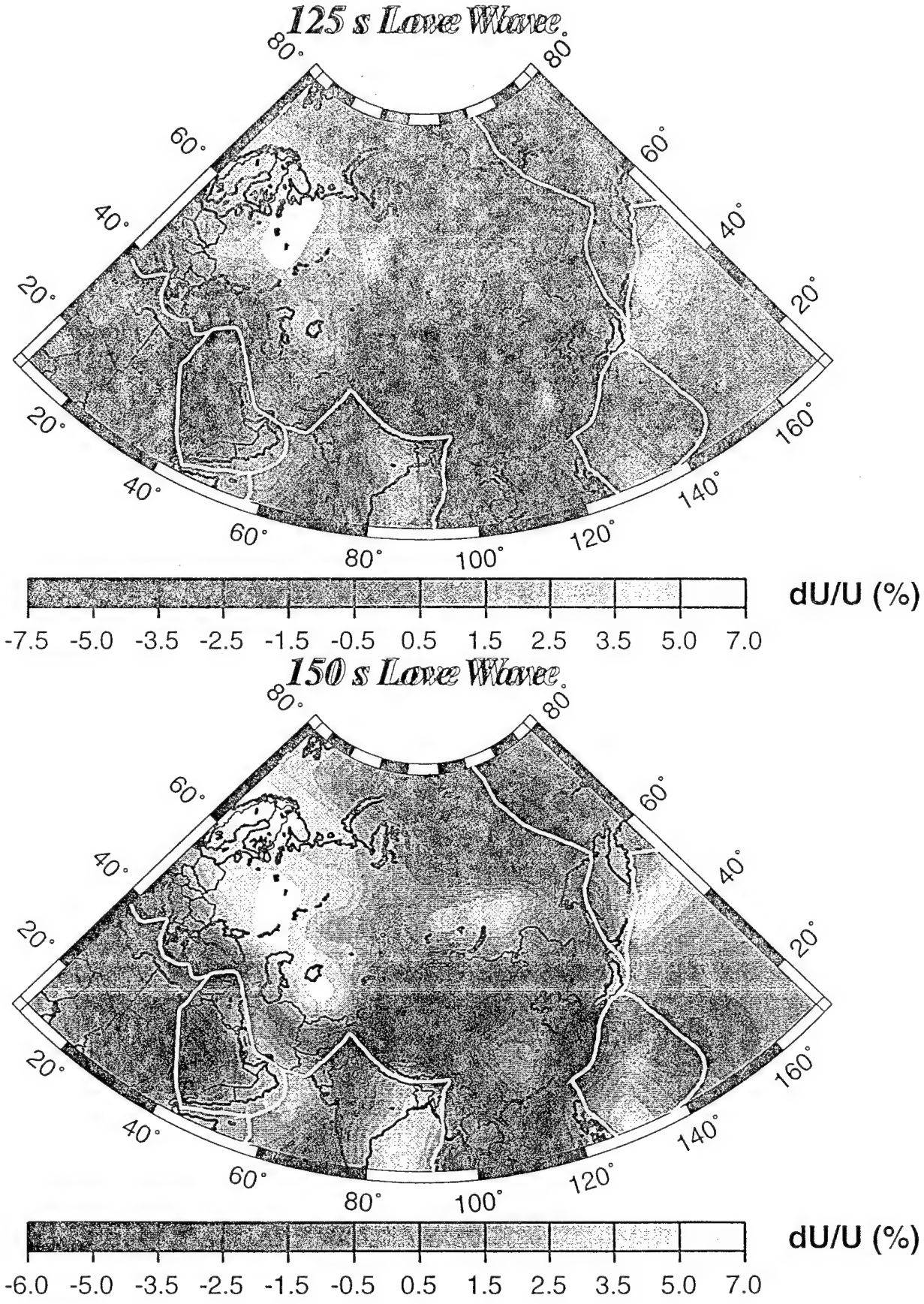


**Figure 18f.** Same as Figure 18a, except for the 125 s and 150 s Love waves.

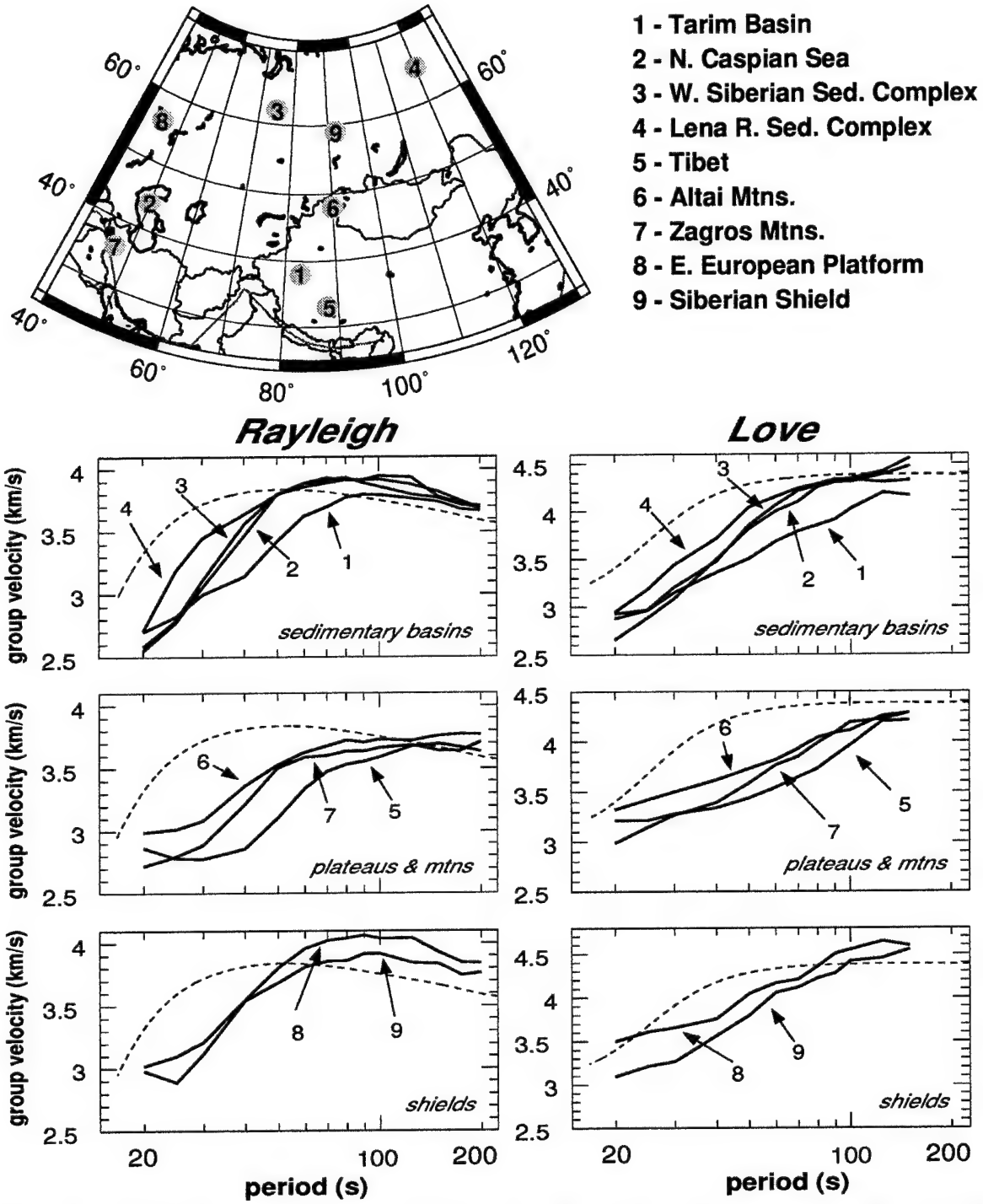


**Figure 19.** Group velocity curves constructed by combining values at the locations specified in the map at top from the estimated group velocity maps. The left column presents Rayleigh waves and the right Love waves. The curves are segregated by structural setting into three groups: sedimentary basins (1, 2, 3, 4), mountain ranges and continental plateaus (5, 6 , 7), and shields (8, 9). The group velocity for PREM is shown as the dash line on each graph. The jerkiness in the curves results from small inconsistencies between the group velocity maps at different periods. The observed curves are much smoother (e. g. Figure 3).

about 7 events per year with $M_s \geq 6.5$ occurred in the studied region. These events constitute less than 10% of our entire data set, which means that significant regions of Eurasia are not well covered at long periods, as the path coverage maps in Figure 9 demonstrate. Global scale studies that utilize both major and minor arc wave packets demonstrate more uniform coverage across the continent (e.g., Trampert and Woodhouse, 1995, 1996; Ekstrom *et al.*, 1996) and should do a better job at these very long periods. Second, certain theoretical errors result in larger relative effects at long periods. An example is event mislocation, as shown in Figure 16. Levshin *et al.* (1997) discuss the effect of ignoring source group time shift. In summary, the advantages of continental-scale studies over global studies break down at periods beyond about 175 s for Rayleigh waves and about 100 s for Love waves.

Figure 20 shows the improvement in fit to the measured dispersion curves delivered by the estimated group velocity maps, expressed as the variance reduction relative to the average group velocity across each map (eqn. (4)) and rms group velocity misfit (eqn. (5)). Variance reductions are more than 80% between 25 and 70 s period for both Rayleigh and Love waves. Variance reductions in excess of 80% continue for Love waves out to about 100 s period, but decrease at longer periods since waves become increasing sensitive to the upper mantle which possesses smaller amplitudes of velocity variations than the crust. Since lateral variations in the group velocity maps have smaller amplitudes at longer periods, there is less signal to fit and, therefore, there is less reduction in variance. This degradation in variance reduction begins at shorter periods for Rayleigh waves since they sample deeper than Love waves at every period. Consistent with this is the fact that at the short period end of the spectrum, absolute misfit is the greatest even though variance reduction continues to be high. Below about 30 s period, the decrease in variance reduction is probably due to off-great-circle propagation caused by sedimentary basins. The onset of this degradation in variance reduction is at longer periods for Love waves since they sample more shallowly than Rayleigh waves at every period. For example, the 30 s Love wave is more strongly sensitive to sedimentary features than the 30 s Rayleigh wave. Above 30 s period the absolute misfit is remarkably flat for both Rayleigh and Love waves, ranging between about 0.05 - 0.07 km/s.

Measurement uncertainties are also flat in this period range and average about 0.015

km/s, as Figure 5d shows. Thus, misfits on average are about at the 3 - 4$\sigma$ level relative to the uncertainties reported in Figure 5d, and there appears to be significant signal remaining to be fit in the raw measurements. Recall, however, that the measurement uncertainties reported in Figure 5d are estimates of the repeatability of the measurements either across a regional array or for events in the same region. This uncertainty in velocity results principally from difficulties in measuring the time of the arriving wave packet accurately, so we call it $\sigma_t$. These estimates do not accurately account for theoretical errors, such as those discussed in Section 4. For example, they do not include uncertainties resulting from difficulties in measuring range, caused by event mislocation, which we call $\sigma_x$. Measured velocity uncertainties are at least some combination of $\sigma_t$ and $\sigma_x$. If there is on average a 30 km error in event location, then using the average distance at each period in Figure 5c would yield erroneous group velocity estimates that decrease from about 0.02 km/s at the short period end to about 0.015 km/s at long periods for both Rayleigh and Love waves. Assuming the independence and, thus, taking the rms of $\sigma_t$ and $\sigma_x$ yields a more realistic absolute measurement uncertainty of at least 0.025 km/s. Therefore, the rms misfits shown in Figure 20 are nearer to the $2\sigma$ level above about 40 s period. We believe that signals of this magnitude can result from the remaining theoretical errors, mostly off-great-circle propagation at the short period end of the spectrum and the source group time shift at longer periods.

## 6. Discussion

Figure 21 compares the group velocities averaged across our estimated group velocity maps in the region of study (10N - 80N, 10E - 170E) with the group velocity from PREM (Dziewonski and Anderson, 1980) and the average group velocity in the studied region taken across the group velocity maps constructed from the model composed of CRUST-5.1 in the crust (Mooney *et al.*, 1996) and S16B30 (Masters *et al.*, 1996) in the mantle. Not surprisingly, PREM does a pretty bad job of fitting even average group velocities under largely continental regions, particularly below about 80 s period. The laterally inhomogeneous model (CRUST-5.1/S16B30) predicts average group velocities much better with two exceptions. First, for Rayleigh waves between 40 - 80 s period, group velocities predicted by CRUST-5.1/S16B30

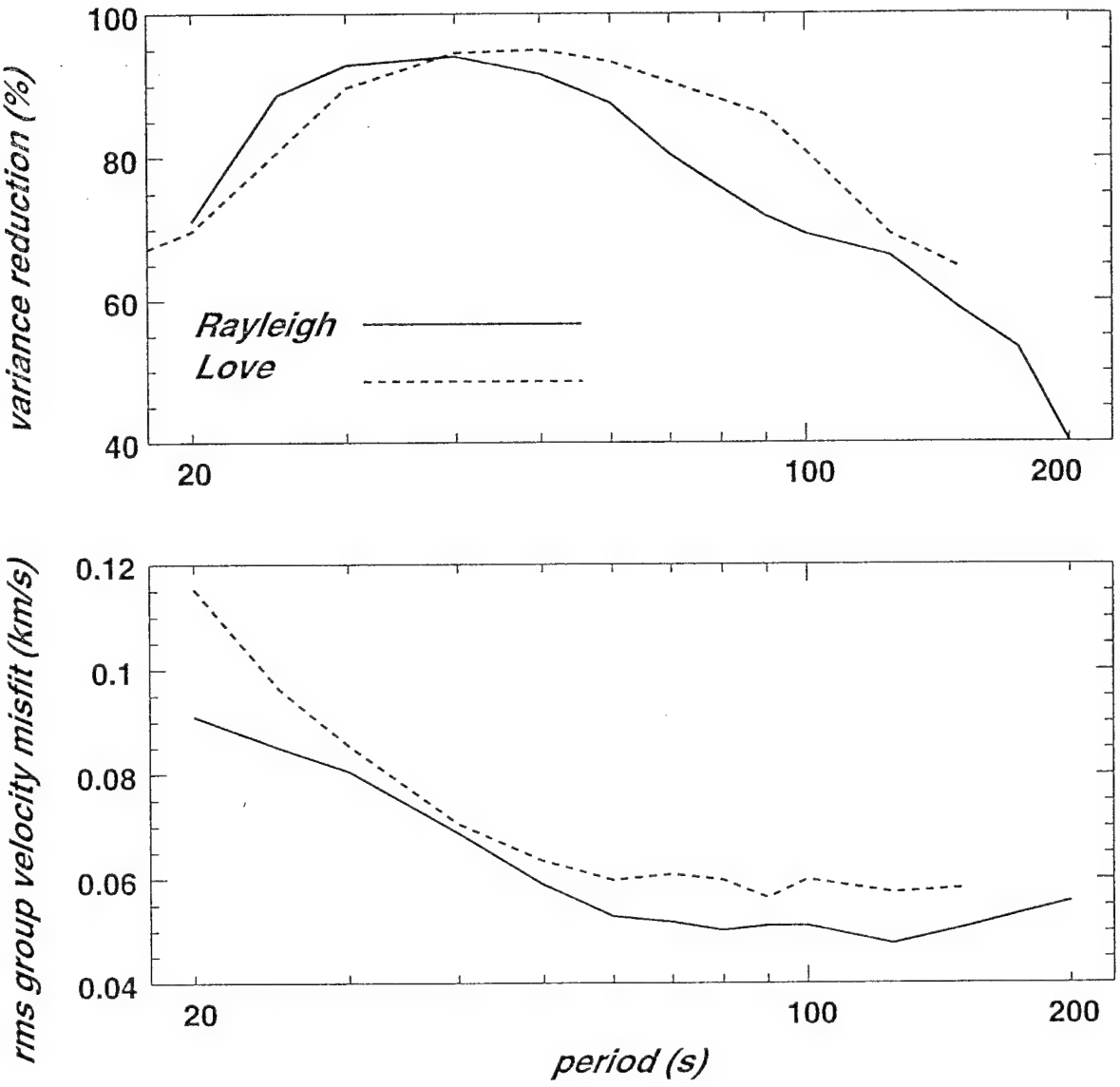


**Figure 20.** Two measures of misfit to our group velocity measurements for Rayleigh (solid lines) and Love (dashed lines) waves of our estimated group velocity maps. (Top) Misfit is represented as variance reduction relative to the average across each map [eq. (4)]. (Bottom) Misfit is the RMS group velocity misfit [eq. (5)].

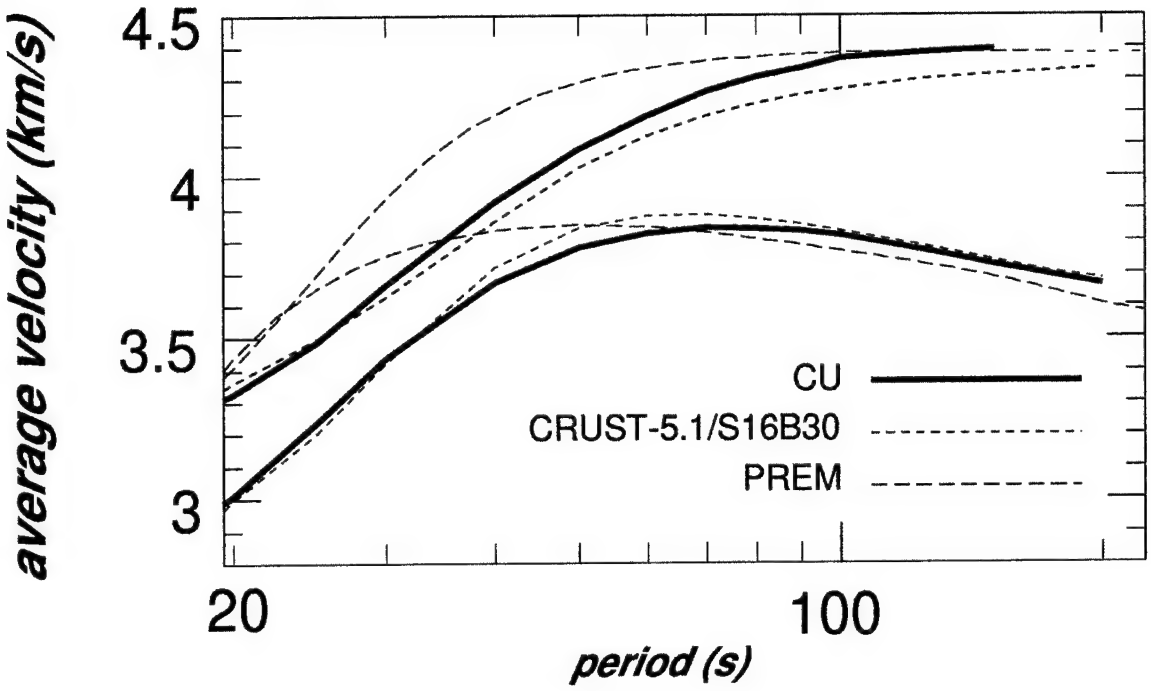


**Figure 21.** Average group velocity across the studied region (latitude: 10°N - 80°N, longitude: 10°E - 170°E) for our estimated group velocity maps (CU: solid lines), PREM (PREM: long dashed lines), and the group velocity maps predicted by a model composed of the crustal model CRUST-5.1 and the mantle model S16B30 (CRUST-5.1/S16B30: short dashed lines).

are on average too high. This is largely due to the fact that CRUST-5.1 tends to underestimate crustal thickness in structurally deformed areas. More significantly, group velocities predicted by CRUST-5.1/S16B30 are too low for long period Love waves. This principally results from the fact that CRUST-5.1/S16B30 is an isotropic model and the observed curves show clear signs of polarization anisotropy (transverse isotropy). CRUST-5.1/S16B30 does a better job of fitting long period Rayleigh waves than Love waves. It would be difficult for any isotropic model to fit both types of waves well.

Throughout the report we have discussed a number of influences which tend to corrupt the resulting group velocity maps. These include, in addition to problems associated with path coverage, problems caused by theoretical assumptions; e.g., event mislocation, azimuthal anisotropy, off-great-circle propagation, and source group time shift. These effects are all expected to be at levels significantly below the observed amplitude variations in the group velocity maps and within the resolutions reported here, with the possible exception of at long periods in source regions near the periphery of the maps. With this in mind, it is worthwhile pointing out some of the features that emerge in the group velocity maps, such as those in Figures 18a - 18e, that appear to have clear structural causes. In this interpretation, it is important to keep in mind path coverage and resolution (Figs. 9 and 11).

Interpretation is based on plots of group velocity sensitivity kernels such as those shown in Figure 1. Figure 1 is computed for PREM, and continent-ocean variations in crustal thickness, in particular, change the details of surface wave sensitivities appreciably. Several rules-of-thumb generally hold, however. As mentioned in Section 1, group velocity sensitivity kernels are more complicated than phase velocity sensitivity kernels (e.g., they change sign) and are compressed nearer to the surface at each period. At a given period, Love waves sample more shallowly than Rayleigh waves and sensitivities for both types of waves compress toward the surface as period decreases. Consequently, everything else being equal, the best probe of sedimentary basins should be the shortest period Love waves, which in this report is at 20 s. Rayleigh waves between 30 - 75 s are strongly sensitive to crustal thickness and the 50 s Rayleigh wave map, to a fair approximation, can be seen as inversely related to Moho depth. That is, for a 50 s Rayleigh wave, low velocities result largely from thickened

crust. Love wave sensitivity to crustal thickness maximizes nearer to 100 s period. At longer periods, the sensitivity of waves to crustal velocities and thicknesses diminish. The uppermost mantle (80 - 150 km) is well represented in the 100 s Rayleigh wave map. The 150 - 200 s Rayleigh waves provide deeper sampling of the upper mantle sublithosphere.

## 6.1 Crustal Structures

Group velocity maps, whose depth sensitivities are more compressed toward the surface at each period than phase velocity sensitivities, make excellent probes of crustal structure at periods below 100 s. Since Love wave group velocity sensitivities are nearly trapped within the continental crust at periods below about 30 s, broadband measurements (< 30s - > 100s) of Rayleigh and Love wave group velocities can help to resolve crustal from mantle structures.

### 6.1a Sedimentary Basins

Because of continuing rapid uplift across much of the Near East and Central Asia due to the collisions between the Eurasian Plate with the Arabian and Indian Plates, accumulations of relatively young sediments across Eurasia are considerably greater than on any other continent. The 20 s group velocity maps display low velocity anomalies associated with most of the known sedimentary basins across Eurasia. This is particularly true for the Love wave. Low velocity anomalies are associated with the Tarim Basin, the Ganges Fan and Delta, the Persian Gulf, the Tadzhyk Depression, the southern Indus River, the Caspian Sea and the Pri-Caspian Depression to the north of the sea, the Black Sea, the Eastern Mediterranean Sea, the Western Siberian sedimentary complex, the Pri-Verkhoyansky Foredeep along the Lena River and its tributary the Vilyuy River in Eastern Siberia, and the Barents Sea Shelf.

Figure 22a shows a closer view of the 20 s Love wave map across Central Asia and compares it with the prediction from the model CRUST-5.1/S16B30. CRUST-5.1 is a model defined on a 5 degree grid, and the blocky nature of the predicted group velocity maps results from the grid defining the model. There is a very good correlation between these two maps.

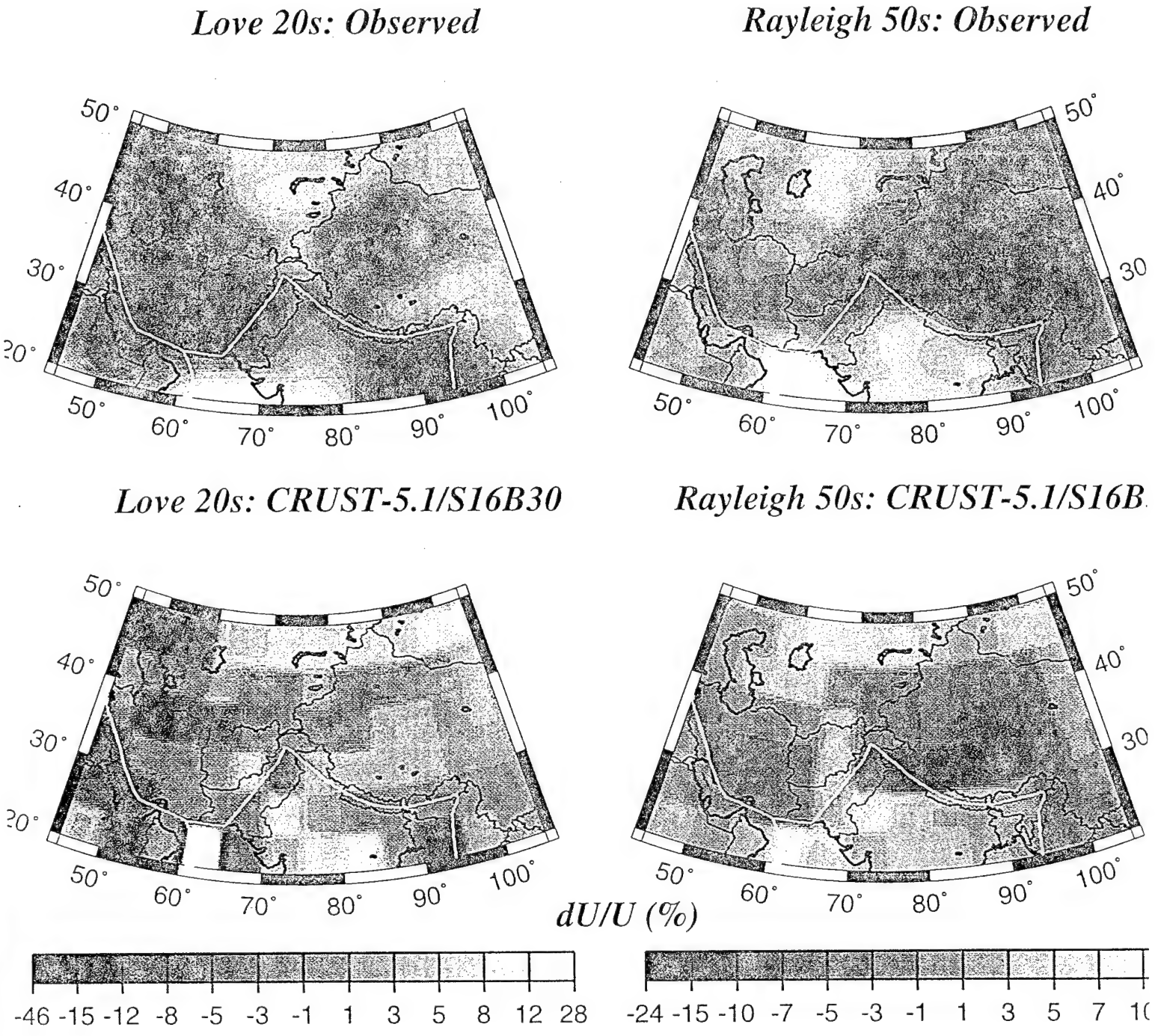


**Figure 22a.** Blow-ups in Central Asia of our group velocity maps at 20 s for Love waves and 50 s for Rayleigh waves compared with the same group velocity maps predicted by a model composed of the crustal model CRUST-5.1 and the mantle model S16B30.

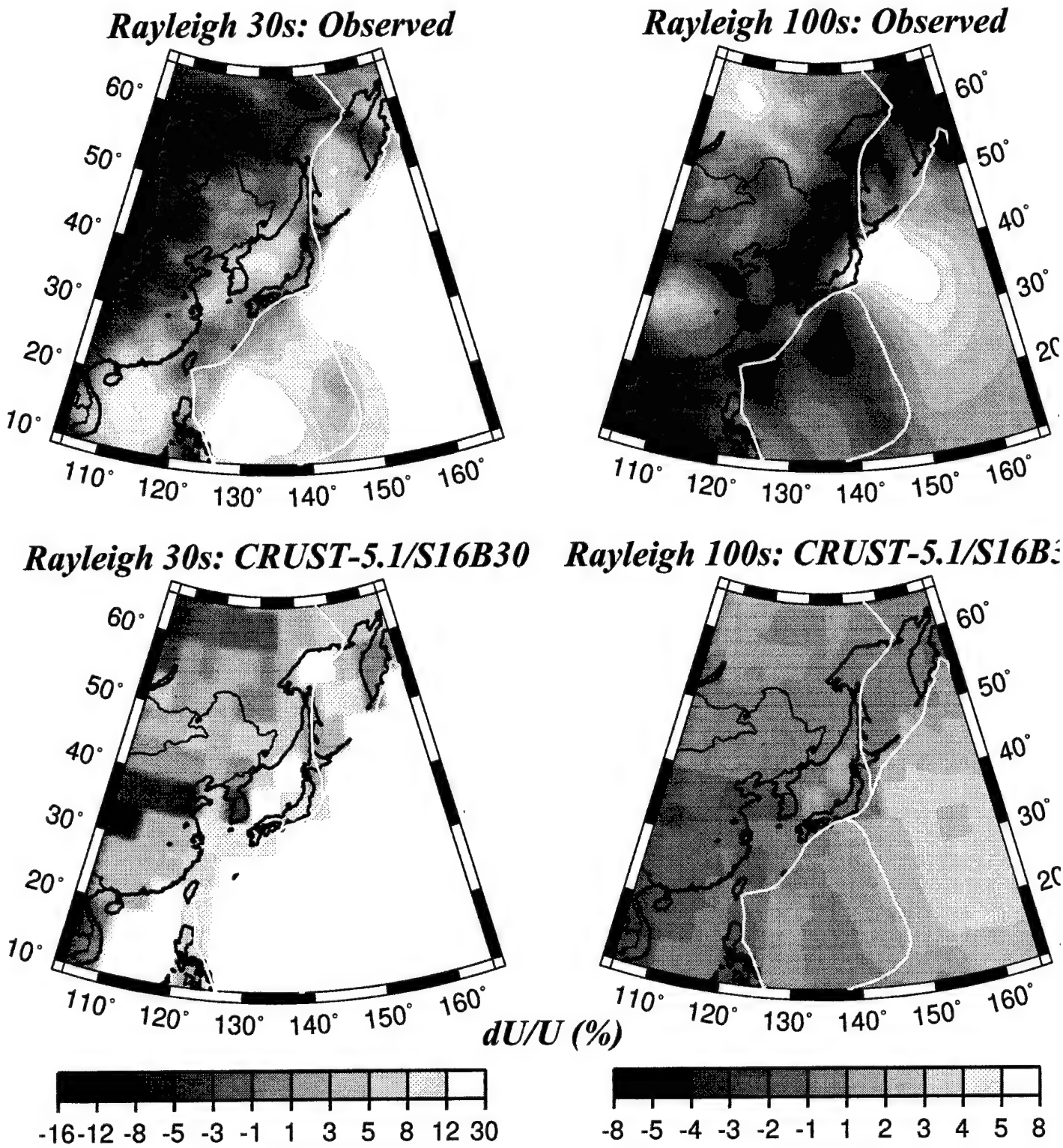


**Figure 22b.** Same as Fig. 22a, except these maps are for Rayleigh waves at 30 s and 100 s period across the Far East.

Several differences are apparent, however. First, the Tarim Basin, at about (40N, 85E), lies largely between grid nodes of CRUST-5.1, and is, therefore, somewhat muted in this model. Second, CRUST-5.1 displays two distinct sedimentary troughs associated with the Caspian Sea, one in the north and one in the south. Our 20 s Rayleigh and Love waves differ in the distribution of low velocities in the Caspian Sea with the Rayleigh wave showing low velocities across the entire sea and the Love wave having extremely low velocities only in the north. However, as Figure 9b shows, path coverage for 20 s Love waves is not very good in this region, and it is likely that our Love wave map is not right in the Southern Caspian. Levshin *et al.* (1994) present evidence for exceptionally strong off-great-circle propagation in this region which could be contributing to this effect. Third, the velocity anomalies predicted by CRUST-5.1 are generally much slower than we observe. Perhaps this is because we have damped the estimated models, but it is not unlikely that the shear velocities in the deeper parts of the sedimentary basins in CRUST-5.1 are too slow.

### 6.1b Ocean-Continent Variations

Inspection of the margins of the continent reveals information about the intrinsic resolution of the group velocity maps. Figure 22b shows a blow-up of the 30 s Rayleigh wave map in the Far East. The South China Sea, the Sea of Japan, and the Sea of Okhotsk are all imaged as relatively high velocities, whereas Kamchatka and the island arc comprising Japan, the Ryuku Islands, and Taiwan are clearly relatively low velocities. This observation is consistent with our earlier resolution analysis which resulted in claims of resolutions in this area of about 5 degrees. The distribution of anomalies on the 30 s Rayleigh wave group velocity map in the Far East is partially the effect of crustal thickness, the thicker crust of the island arc manifests itself as reduced group velocities, but the higher crustal velocities of the marginal seas also contribute. Much higher velocities follow to the east of the plate boundary and mark the transition to the much thinner and faster old oceanic crust.

These observations are similar to the predictions from the model CRUST-5.1/S16B30, also displayed in Figure 22b. There are several exceptions. (1) The observed group velocities on the continent are generally lower than in CRUST-5.1/S16B30. (2) The map predicted by

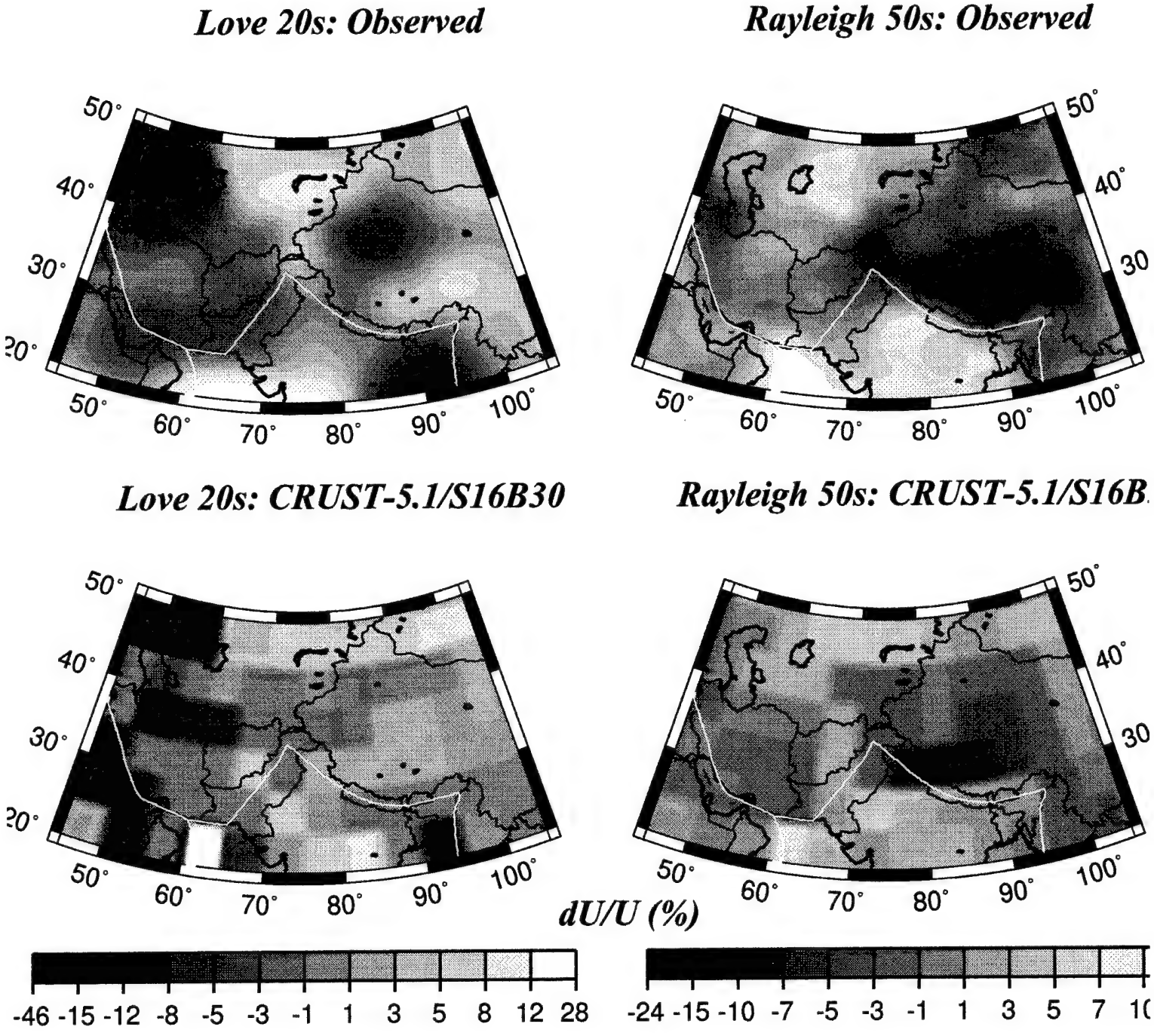


**Figure 22a.** Blow-ups in Central Asia of our group velocity maps at 20 s for Love waves and 50 s for Rayleigh waves compared with the same group velocity maps predicted by a model composed of the crustal model CRUST-5.1 and the mantle model S16B30.

the model under the marginal seas is much faster than observed, presumably due to shear velocities being too fast in the model or crustal thicknesses being somewhat too small in the model. (3) The observed map does not display the ability to resolve Korea from the Sea of Japan or the Yellow Sea that bound it. (4) However, our maps do show structural variations in the Philippine Plate that do not appear in CRUST-5.1/S16B30. The Kyushu-Palau Ridge runs more-or-less north-south in the center of the Philippine Plate. The West Mariana Basin is to the east of the ridge and shows up as relatively low velocities in most of the group velocity maps at the short period end of our study. This is probably partially due to sediment accumulated in the West Mariana Basin. However, this feature persists to much longer periods (e.g., 100 s Love wave in Fig. 18e) consistent with phase velocities reported in Trampert and Woodhouse (1996) and Ekstrom *et al.* (1996). Thus, it is likely that thicker crust exists on the east side of the Kyushu-Palau Ridge than on the west side.

### 6.1c Continental Flood Basalts

Massive basalt flows are known to exist in several regions across Eurasia, principally in northern Ethiopia, western India (Deccan Volcanic Province), and in Central Siberia. If unmodified by later sedimentation or thermal reworking, these regions should manifest themselves as high velocity anomalies on the 20 s Rayleigh and Love wave maps. The Central Siberian flows in the Tunguska Basin (Zonenshain *et al.*, 1990) have been reworked since they were initially produced in the late Paleozoic and they are also obscured by large sedimentary basins that surround them. Thus, it is not surprising that this feature does not appear on the estimated group velocity maps. On the other hand, the Ethiopian Flood Basalts (e.g., Mohr, 1983) and the Deccan Traps do display high velocity anomalies on the 20 s Love wave map. Unfortunately, they are both in regions poorly sampled in this study at short periods. In the case of the Deccan Traps, this may be attributed to 'leakage' of oceanic velocities onto the continent, but no such explanation is plausible for the Ethiopian anomaly. Thus, we believe that very high velocity anomalies on the short period maps in continental regions do reveal relatively young massive basalt flows.

The Ethiopian anomaly merges with another high velocity anomaly to the north near

the boundary between Egypt and the Sudan. This feature is not attributable to a basalt flow, but is the site of a small Archaean shield which is probably the source of the observed anomaly. These higher velocities near the Egyptian - Sudanese boundary are predicted by the model CRUST-5.1/S16B30.

### 6.1d Crustal Thickness

The effects of crustal thickness on the estimated group velocity maps are most striking in Central Asia where the Moho extend to depths greater than 70 km. Low velocity anomalies associated with Tibet, the Pamir and the Hindu Kush, the Altai Range in Mongolia, and the Zagros Mountains in Western Iran are clearly seen at 30 and 50 s on the Rayleigh wave maps in Figures 18a and 18b and on the 50 s Love wave map in Figure 18e. On the longer period Love maps, for example at 100 s and 125 s in Figure 18e and 18f, resolution in Western Iran is very poor as Figure 11d shows. This is the reason that, at these Love wave periods, low velocities associated with a depressed Moho are seen under Tibet, but not under the Zagros.

Figure 22a also presents a blow-up of the estimated 50 s Rayleigh wave group velocity map under the Near East and Central Asia and the group velocity map predicted by the model CRUST-5.1/S16B30 is shown for comparison. There is qualitative agreement, but the outlines of Tibet are much more clearly delineated on the observed map than can be produced by a relatively coarse gridded model. Tibet is not the only region of this map showing signs of a significantly depressed Moho. The Pamir, near the northern boundary of Pakistan and Afghanistan, also displays very low group velocities and, consequently, a significantly thickened crust. Low velocities extend to the northeast from the Pamir into the Altai Range of Mongolia in a characteristic pattern first reported by Wu and Levshin (1993), and also extend southwest of the Pamir approximately following the boundary between Pakistan and Afghanistan. Low velocity anomalies are also observed and predicted by CRUST-5.1/S16B30 underlying the Zagros. We note that crustal thickening due to the Ural mountains is not observed as low velocities on any of the relevant group velocity maps. Presumably the signature of these mountains is below the resolution of this study in North Central Asia.

## 6.2 Upper Mantle

As periods increase, the imprint of crustal structures on group velocity maps diminishes until, for Rayleigh wave maps at periods of 100 s and above, the signatures of upper mantle structures dominate the group velocity maps. For reasons discussed earlier in the report, we distrust large regions of the 200 s Rayleigh wave map and concentrate discussion here on the 100 s and 150 s maps shown in Figures 18b and 18c.

### 6.2a Archaean Shields/Continental Roots

Continental roots can be seen in various regions around Eurasia on the 100 s and 150 s group velocity maps. The largest features are the two Archaean shields underlying the Eastern European Platform and the Siberian Shield, separated by the Urals. These roots both exist and are apparent on the long period group velocity maps predicted by CRUST-5.1/S16B30, composing part of the mantle model S16B30. Several smaller shields or lithospheric blocks are also seen as high velocity anomalies, such as the Tarim block, the Indian Shield, and the East China Block. These features are too small to appear in global models such as S16B30.

### 6.2b Back Arc Spreading

After the high velocity anomalies which result from the continental roots underlying the Eastern European Platform and the Siberian Shield, the most striking feature on the long period maps may be the low velocity arc rimming the continent on its eastern edge. This feature, in a more poorly resolved form, appears in nearly all of the recent global mantle models and is probably attributable to the response of the mantle to back-arc spreading. This feature extends, essentially uninterrupted, from Kamchatka to Indochina, although the largest velocity anomalies appear to underlie Kamchatka, the back-arc west of Japan, and Indochina.

Figure 22b also presents a blow-up of the 100 s Rayleigh wave map in the Far East and

the map predicted by the model CRUST-5.1/S16B30. There is qualitatively agreement. The biggest differences appear to be resolution and amplitude which may be due to the damping necessary in the construction of global models. The amplitudes of the velocity anomalies in S16B30 are lower, and relatively small features, such as the East China Block, are missing in global models. As discussed above, the fact that crustal shear velocities in the marginal seas appear to be too large in CRUST-5.1 (e.g., Fig. 22b at left) results in the crustal part of the model continuing to imprint the 100 s Rayleigh wave map show in Figure 22b (at right) under the marginal seas. The observed 100 s Rayleigh wave does not clearly display the continued signature of crustal features in this region.

### 6.2c Plate Boundaries

Several significant features are apparent at plate boundaries on the long period Rayleigh wave maps. High velocity anomalies are associated with known subduction occurring in the Eastern Mediterranean, along the India-China border south of Tibet, and along the Pacific Plate boundary east of Japan. It is tempting to conclude that these anomalies are the signature of subduction in these regions or at least of a thickened lithosphere. These features are too small to be contained in the model S16B30.

There are three low velocity anomalies observed in the 100 s and 150 s Rayleigh wave maps that are worth mentioning. None of these anomalies underlies convergent plate boundaries, and the mantle anomalies are not likely to be the same as at convergent boundaries. The first is in Eastern Turkey under the Anatolian Fault which marks the collision zone between the Arabian and Eurasian Plates. The second is in the Laptev Sea associated with the southeastern edge of the Arctic spreading center. The third is under the Red Sea. Path coverage and expected resolution in the first of these regions are very good, but are less so in the other two regions.

Although the first two of these features are not apparent in the mantle model S16B30, the third is. In fact, low velocity anomalies underlying the Afar Triangle and extending north along the western edge of the Red Sea appear in the uppermost mantle in most of

the recent global mantle models. These anomalies have been interpreted as the head of the Afar Plume. The resolution and data coverage at long periods near the southern rim of our maps in East Africa are very poor, and we do not at this point assign significance to any geographical variations in the location of the 'Red Sea' low velocity anomaly among our group velocity maps or with those predicted by mantle models.

## 6.3 Misfit Compared with the Model CRUST-5.1/S16B30

As previously discussed in this section, there is good qualitative agreement between the observed group velocity maps and those predicted by the model CRUST-5.1/S16B30. Disagreements are mostly in amplitude and in certain features, particularly in the upper mantle, which are too small to appear in S16B30. We have concluded that: sedimentary shear velocities in CRUST-5.1 tend to be too small in deep basins, the crustal shear velocities in the marginal seas are too high in CRUST-5.1, crustal thicknesses in CRUST-5.1 across much of the continent are somewhat too small, upper mantle structures in S16B30 are too small in amplitude on average, and certain observed upper mantle features are spatially too small to be contained in S16B30. The question we ask here is, what is the effect of these observed differences on the fit to the group velocity observations?

This question is addressed by Figure 23 which presents the variance reduction and rms group velocity misfit between the observed group velocity curves and those predicted by our maps and the group velocity maps predicted by CRUST-5.1/S16B30. The variance reductions reported in this figure differ from those in Figure 20 in that here we take as the reference model, $U_0$, the group velocity curve predicted by PREM, whereas in Figure 20 we took the reference model to be the average velocity observed across the continent at each period. Thus, we get larger variance reductions here than in Figure 20. The rms group velocity misfits for the observed group velocity maps are the same in both figures, however.

Variance reductions to the observed group velocity measurements provided by CRUST-5.1/S16B30 are large and positive for both Rayleigh and Love waves across most of the band. Indeed, variance reductions are in excess of 80% for Rayleigh waves between 20

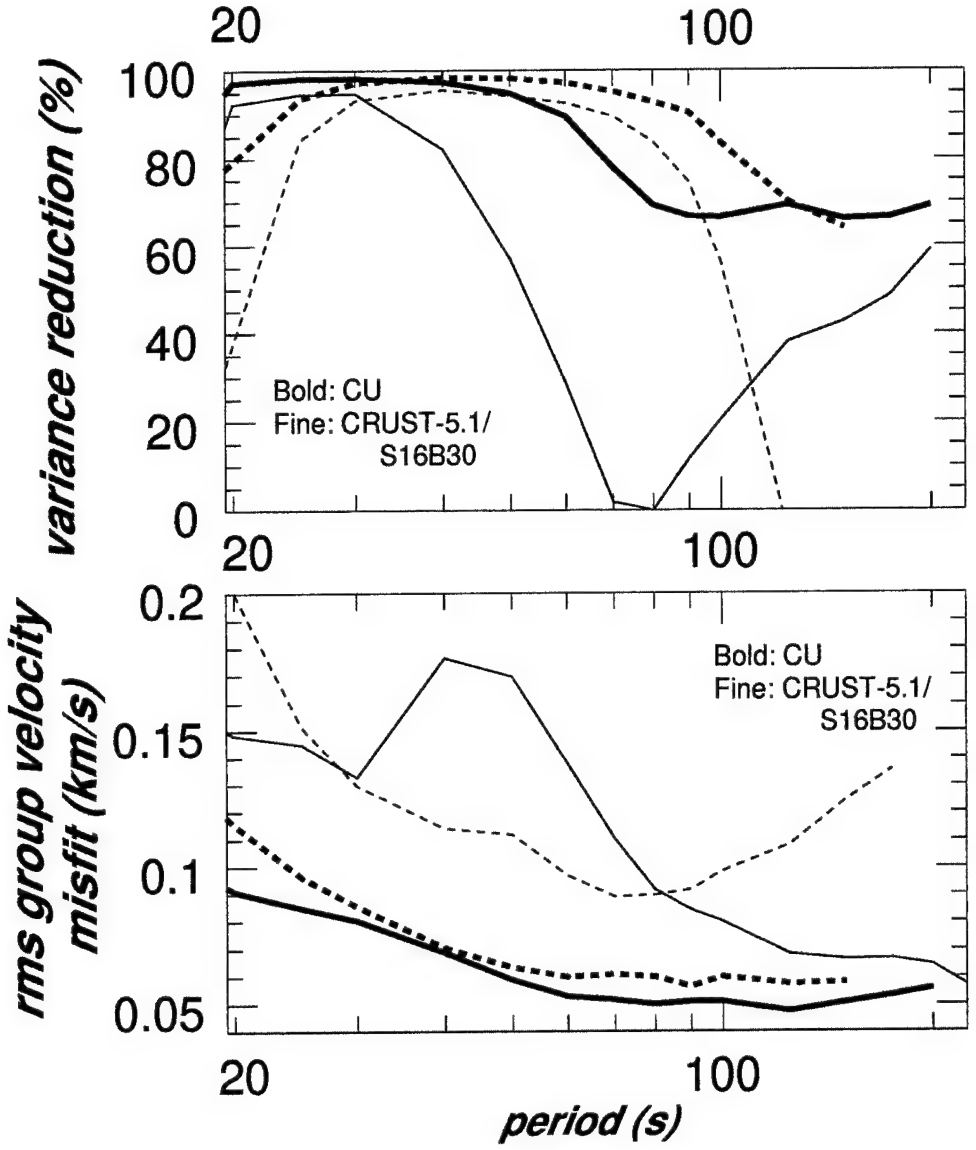


**Figure 23.** Two measures of misfit to our group velocity measurements for Rayleigh (solid lines) and Love (dashed lines) waves for two different sets of group velocity maps. Bold lines are for our group velocity maps and thin lines are for the group velocity maps predicted by the model composed of the crustal model CRUST-5.1 and the mantle model S16B30. (Top) Misfit is represented as variance reduction relative to the group velocity for PREM. Our variance reduction here differs from that reported in Fig. 20 since the reference values used in these figures differ. Here the reference is is the group velocity predicted by PREM and in Fig. 20 it is the average across our group velocity map. (Bottom) Misfit is RMS group velocity misfit [eq. (5)].

and 40 s period and for Love waves between 25 and 80 s. Both observed and predicted variance reductions decrease at longer periods because of a decrease in signal level. The principal exceptions are for Love waves at periods greater than about 80 s period and for Rayleigh waves from 50 - 100 s period. The degradation in misfit of CRUST-5.1/S16B30 to the Love waves is largely due to polarization anisotropy. CRUST-5.1/S16B30 is an isotropic model which cannot fit Rayleigh and Love waves well simultaneously. Rayleigh wave variance reductions for CRUST-5.1/S16B30 begin to decrease beyond about 30 s period and minimize between 70 and 80 s period. This is caused by the strong sensitivity of Rayleigh waves to crustal thickness in this period range and the fact that CRUST-5.1/S16B30 systematically underpredicts crustal thicknesses in Central Asia. The increase in absolute misfit for CRUST-5.1/S16B30 between 40 and 70 s period is due to the average group velocity across the continent in the model being in error, as shown in Figure 21. Thus, we attribute this increase in absolute misfit to errors in the average value of group velocity across the model. This is not reflected exactly in variance reduction since signal level increases in this period range which somewhat offsets the increased misfit.

The observed maps do, however, fit the group velocity measurements significantly better than the predictions from CRUST-5.1/S16B30. Recall that in Section 5 we estimate the observational error at about 0.025 km/s, so the estimated group velocity maps misfit the data at about the $2\sigma$ level and CRUST-5.1/S16B30 misfits at least at the $4\sigma$ level below about 80 s period for Rayleigh waves and greater than $4\sigma$ across the entire band for Love waves. This should not be surprising for three reasons. First, CRUST-5.1 is principally a $v_p$ model in which the $v_s$ variations have been approximated by use of a realistic Poisson's Ratio, and much of the crust in Eurasia is relatively unconstrained by seismological data at the disposal of Mooney *et al.*. Second, CRUST-5.1 is defined on a 5 degree grid in which velocities are assumed constant within each cell. Finally, the mantle part of the model, S16B30, displays much longer wavelengths and lower amplitudes than what is implied by the observed long period group velocity maps.

# 7. Conclusions

We have reported the results of a systematic study of broadband Rayleigh and Love wave dispersion across Eurasia. We believe, and argue here, that this study represents a significant improvement in the understanding of surface wave dispersion across this continent. As will be discussed further below, the results presented here are not complete. The methods described can continue to be applied across Eurasia to new and accumulating data in order to improve resolution and reliability further. The methods are already being applied successfully to other continents (e.g., Ritzwoller *et al.*, 1996c; Vdovin *et al.*, 1996) and can be developed further in the ways described below.

There are three main reasons why we believe that this study represents a significant improvement in the understanding of Eurasian surface wave dispersion. The first has to do with the data used. This study is broader band, displays denser and more uniform data coverage, and demonstrates higher resolution than previous studies that have been performed on this scale. Resolutions at most periods for the majority of the continent lie between 5 - 7.5 degrees. Second, the group velocity maps reveal the signatures of known geological and tectonic features never before revealed in surface wave studies on this scale. This both lends credence to the maps and spurs interest in their use to infer information about the features that are observed. Observations at short and intermediate periods ($\sim$20 - 80 s) are providing entirely new constraints on crustal structures and the long period observations ($\geq$100 s) are yielding higher resolution information about the deep lithosphere and upper mantle. Finally, group velocity maps provide a significant improvement in fit to the observed dispersion curves. This is particularly impressive when compared to misfits from existing mantle and crustal models.

Concerning the crust, observed group velocity anomalies include information about sedimentary velocities and thicknesses, crustal velocities, and Moho depth. The dispersion signatures of numerous sedimentary basins across the continent and off the coast are displayed clearly on the short period (20 - 30 s) group velocity maps (Tarim Basin, Ganges Fan and Delta, Persian Gulf, Tadjyk Depression, southern Indus River, Caspian Sea, Black Sea,

Eastern Mediterranean Sea, Western Siberian sedimentary complex, the Pri-Verkhoyansky Foredeep, Barents Sea Shelf). Although the effects of sedimentary basins on intermediate period surface wave velocities and polarizations have been reported before (e.g., Barents Sea Shelf: Levshin and Berteussen, 1979; Caspian: Levshin *et al.*, 1994), we are not aware of a similarly comprehensive study on a continental scale. Perhaps the most interesting crustal velocity variations are seen as high velocity anomalies on the short period maps for two continental regions of massive basalt flows (Ethiopian Flood Basalts, Deccan Traps). The significance of the observation of the surface wave signature of known massive basalt flows associated with the break-up of Gondwanaland is probably not greatest for its application to Eurasia, but lies in its potential application to other less well understood continents, in particular Antarctica (Ritzwoller *et al.*, 1996c). Perhaps the most striking feature on any of the group velocity maps is the low velocity anomalies that appear on both the Rayliegh (30 - 90 s) and Love (40 - 125 s) wave maps associated with the thickened crust of Central Asia, in particular Tibet. Such low velocity anomalies for Tibet have been presented before (e.g., Feng and Teng, 1983a; Wu and Levshin, 1994), but the present study provides a broader frequency band, better resolution, and larger spatial coverage than previous studies. It also reveals similar dispersion anomalies for other regions of thickened crust (e.g., Altai Range, the Hindu Kush and Pamir, Zagros Mountains) as well as variations in crustal thickness between continental and oceanic crust (e.g., the arc composed of Kamchatka, Kurile Islands, Japan, the Ryuku Islands, and Taiwan). The breadth of the frequency band over which the dispersion maps are produced holds the promise for resolving these crustal structures from one another and from upper mantle structures during structural inversion.

Concerning the lower lithosphere and upper mantle, observed group velocity anomalies include information about back-arc spreading, continental roots, the depth extent of the lithosphere, down-going slabs, and perhaps the upper reaches of a mantle plume. The observed long period Rayleigh wave maps (e.g., 100 s) provide a much sharper view of the linear low velocity anomaly that rims the continent in the Far East, which is apparently caused by the mantle's response to back-arc spreading, than global models (e.g., Su *et al.*, 1994; Masters *et al.*, 1996). Continental roots under shields have emerged in recent global

models (e.g., Trampert and Woodhouse, 1995; Masters *et al.*, 1996; Ekstrom *et al.*, 1996). The large Eurasian shields (Eastern European Platform, Siberian Shield, Indian Shield) are very clearly imaged on the long period maps presented here, as are other deep lithospheric blocks, such as the Tarim and the South China Blocks, which are too small to be seen in the global models. High velocity anomalies are also associated on the long period maps with descending slabs at the Pacific Plate margin, at the plate boundary between India, China, and Pakistan, and under the Aegean Sea. The 'Red Sea' low velocity anomaly, which appears clearly but more diffusely in many global models and has been hypothesized to result from the Afar Plume (Makris and Ginzburg, 1987; Hill *et al.*, 1992), is well seen on the long period maps presented here, centered on and just west of the Red Sea.

The group velocity maps we present here provide a great improvement in fit to the observed data relative to any laterally homogeneous model. Variance reductions relative to PREM are about 90% at the short period end and reduce to about 70% at the long period end of the study. To put this in context, comparisons are made with the variance reductions from a new high quality laterally inhomogeneous model, CRUST-5.1/S16B30 (Mooney *et al.*, 1996; Masters *et al.*, 1996). CRUST-5.1/S16B30 does a good job of fitting the observed group velocity curves and detailed comparisons between the observed group velocity maps and those predicted by CRUST-5.1/S16B30 demonstrate a very good qualitative agreement. Not surprisingly, however, the observed maps do significantly better in fitting the data and several characteristics of CRUST-5.1, in particular, appear to require future improvement. We believe that in CRUST-5.1 shear velocities are too low in the deep parts of sedimentary basins (presumably caused by inaccurately modeling the increase in shear velocities due to sedimentary compaction), the crustal shear velocities in the marginal seas are too high, and crustal thicknesses across much of the continent are somewhat too small particularly in Central Asia. Even noting these facts, CRUST-5.1/S16B30 represents a tremendous improvement over previous global models and is an excellent basis for future research. We have derived added confidence in the veracity of the observed group velocity maps from the fact that the observed and predicted maps agree well qualitatively but the observed maps provide a large improvement in fit to the data.

Although we have argued at some length that this study represents a significant step toward an understanding of Eurasian surface wave dispersion, there remain several shortcomings. First, corrections for source group time shifts at long periods have not yet been incorporated in the analysis. The nature and importance of this correction on tomographic studies is the subject of Levshin *et al.* (1997). Second, resolution and bias have not yet been optimized, for example, by modeling off-great-circle propagation, utilizing amplitude, polarization (e.g., Laske and Masters, 1996), and/or phase information, or making use of all of the available broadband data.

These shortcomings point the way for future research. First, resulting from the conclusions of Levshin *et al.* (1997), corrections for source group time shifts will be applied to the long period group velocity measurements. Second, phase velocity measurements have already been made along with the group velocities, and phase velocity maps will be constructed soon. Third, more waveform data will be analyzed and added to the tomographic inversion. Our studies in Central Asia have shown how important it is to utilize regional network and array data to improve resolution, particularly at short periods (Ritzwoller *et al.*, 1996b). The use of data from the new network in Saudi Arabia (Vernon *et al.*, 1996), new broadband stations installed by the Japanese in the Far East (e.g., POSEIDON), the NARS network in European Russia, the Ukraine, and Belorussia (Snieder and Paulssen, 1993), national regional networks such as the German Regional Seismic Network (e.g., Krueger and Stammler, 1996), past PASSCAL experiments (e.g., Tibetan Plateau, Pakistan, Lake Baikal), and broadband components of DoD arrays should help to improve resolutions in Europe, Central Asia, the Middle East and the Far East. Resolution in northern Asia can be improved if nearly meridional paths are analyzed. These paths can come from the analysis of data from recently installed North Eastern Siberian GSN stations (e.g., TIXI, BILL), from the Canadian National Seismic Network, and from the US National Seismic Network for events which take place across Eurasia. Finally, the estimated dispersion maps (group and phase) should be inverted for shear velocity models across Eurasia. These studies have begun for Central Asia (e.g., Ritzwoller *et al.*, 1996a).

# 8. Recommendations

It was shown here that the systematic study of the dispersion characteristics of broad-band Rayleigh and Love waves (20 - 250 s) across Eurasia can yield relatively uniform high resolution ( 550-800 km resolution) dispersion maps. These maps can be used to construct accurate and detailed shear velocity models of the crust and lithosphere across the continent. Such models should prove to be extremely useful in improving regional location capabilities, and the technical means of incorporating such regional information into a more general 'Knowledge Base' need to be developed.

This sort of study can be built upon to improve the accuracy and resolution of regional models in the following ways:

(1) Focused dispersion studies of intermediate period surface waves, such as our companion study in Central Asia, should be applied in other well instrumented, seismically active areas of strategic interest, such as the Middle East and the Far East.

(2) Dispersion map inversion methods should be generalized to model more realistic ray paths incorporating lateral refractions through the imaged structures (in an iterative way).

(3) Body wave studies (e.g, Pn, Pnl, and receiver function) can be used to complement the dispersion information by enhancing resolution in certain regions of the model.

**Acknowledgements**

Many people and organizations contributed to this study. Most of the data were acquired from the IRIS-DMC and the GEOSCOPE Data Center. We are grateful to a number of individuals at regional and global data collection centers who really control the quality of the data used in this study. These include the groups at UCSD (IRIS/IDA, Jon Berger, Peter Davis; KNET, Frank Vernon), Albuquerque Seismic Laboratory (IRIS/GSN, Robert Woodward), LDEO (KAZNET, W.Y. Kim), and MEDNET (A. Morelli). We would like to thank John Woodhouse and Robert Hermann for providing eigenfunction codes. Gabi Laske, Walter Mooney, Stuart Johnson, and Guy Masters provided the crustal model CRUST-5.1 and the mantle model S16B30. Our analysts Ludmila Ratnikova, Steven Smith, David

Tremblay, Christian Lee, Mark James, and Oleg Vdovin made all of the measurements that form the backbone of this research. Dan Quinlan and Danny Harvey provided a great deal of software and data management advise and support over the years. Much of the database software was written with Datascope (Quinlan, 1994). A.A. Egorkin and M.P. Barmin played central roles in the development of software used in several aspects this study, in particular in developing the UNIX version of FTAN and in code used in the resolution analysis. We would like to thank T.B. Yanovskaya and P.G. Ditmar for supplying their group velocity tomography code. All maps were generated with the Generic Mapping Tools (GMT) data processing and display software package (Wessel and Smith, 1991, 1995).

This research was supported by AFOSR contract F49620-95-1-0139 and partly by AFTAC contract F19628-95-C-0099, and NATO linkage grant N950775 between the University of Colorado, Boulder and the Institute of Earthquake Prediction Theory and Mathematical Geophysics, Russian Academy of Sciences, Moscow.

# References


Backus, G. and J.F. Gilbert, Resolving power of gross earth data, *Geophys. J. R. astr. Soc.*, **16**, 169 - 205, 1968.

Backus, G. and J.F. Gilbert, Uniqueness in the inversion of inaccurate gross earth data, *Phil. Trans. R. Soc. A.*, **266**, 123 - 192, 1970.

Bird, P. and M.N. Toksoz, Strong attenuation of Rayleigh waves in Tibet, *Nature*, **266**, 161 - 163, 1977.

Bourjot, L. and B. Romanowicz, Crust and upper mantle tomography in Tibet using surface waves, *Geophys. Res. Let.*, **19**, 1992.

Brandon, C. and B. Romanowicz, A 'no-lid' zone in the Central Chang-Thang platform of Tibet: Evidence from pure path phase velocity measurements of long period Rayleigh waves, *J. Geophys. Res.*, **91**, 6547 - 6564, 1986.

Byerly, P., The dispersion of seismic waves of the Love type and the thickness of the surface layer of the earth under the Pacific, *Beitr. Geophys.*, **26**, 27 - 33, 1930.

Calcagnile, G., and G. F. Panza, Crust and upper mantle structure under the Baltic Shield and Barents Sea from the dispersion of Rayleigh waves, *Tectonophysics*, **47**, 59-71, 1978.

Calcagnile, G., G. F. Panza, and L. Knopoff, Upper mantle structure of North-Central Italy from Rayleigh waves phase velocities, *Tectonophysics*, **56**, 51-63, 1979.

Calcagnile, G., and G. F. Panza, Crustal and upper mantle structure beneath the Apennines region as inferred from the study of Rayleigh waves, *J. Geophys.*, **45**, 319-327, 1979.

Calcagnile, G.,and G. F. Panza, Upper mantle structure of the Apulian plate from Rayleigh waves, *Pageoph*, **118**, 823-830, 1980.

Calcagnile, G., U. Mascia, V. del Gaudio, and G. F. Panza, Deep structure of southeastern Europe from the dispersion of Rayleigh waves, *Tectonophysics*, **110**, 93-111, 1985.

Calcagnile, G., and G. F. Panza, Crustal and upper mantle structure of the Mediterranean area

derived from surface-wave data, *Phys. Earth Planet. Int.*, **60**, 163-168, 1990.

Cara, M., Filtering of dispersed wave trains, *Geophys. J. R. astr. Soc.*, **33**, 65 - 80, 1973.

Chen, W.-P. and P. Molnar, Short-period Rayleigh wave dispersion across the Tibetan Plateau, *Bull. Seism. soc. Amer.*, **65**, 1051 - 1057, 1975.

Chun, K.Y. and T. Yoshii, Crustal structure of the Tibetan Plateau: a surface wave study, *Bull. Seism. soc. Amer.*, **67**, 735 - 750, 1977.

Curtis, A. and R. Snieder, Surface Wave phase velocities and shear velocity structure beneath Eurasia, to be submitted to *J. Geophys. Res.*, 1997.

Curtis, A. and J. Woodhouse, Crust and upper mantle shear velocity structure beneath the Tibetan plateau and surrounding regions from inter-event surface wave phase velocity inversion, submitted to *Geophys. J. Int.*, 1996.

Dahlmann, O. and H. Israelson, *Monitoring Underground Nuclear Explosions*, Elsevier, Amsterdam, 1977.

Das, T. and G. Nolet, Crustal thickness using high frequency Rayleigh waves, *Geophys. Res. Lett.*, **22**, 539 - 542, 1995.

Ditmar, P.G., and Yanovskaya, T.B., A generalization of the Backus-Gilbert method for estimation of lateral variations of surface wave velocity, *Izv. AN SSSR, Fizika Zemli (Solid Earth)*, **6**, 30 - 60, 1987. (Russian original).

Dost, B., Upper mantle structure under western Europe from fundamental and higher mode surface waves using the NARS array, *Geophys. J. Int.*, **100**, 131-152, 1990.

Dziewonski, A.M., On regional differences in dispersion of mantle waves, *Geophys. J.*, **22**, 289 - 325, 1971.

Dziewonski, A. M. and D. L. Anderson, Preliminary Reference Earth Model, *Phys. Earth Planet. Int.*, **25**, 297-356, 1981.

Dziewonski, A. M., Bloch, S., and M. Landisman, 1969. A technique for the analysis of transient

seismic signals, *Bull. seism. Soc. Am.*, **59**, 427 - 444, 1969.

Dziewonski, A.M., T.-A. Chou, and J.H. Woodhouse, Determination of earthquake source parameters from waveform data for studies of global and regional seismicity, *J. Geophys. Res.*, **86**, 2825 - 2852, 1981.

Ekstrom, G., J. Tromp, and E.W.F. Larson, Measurements and global models of surface wave propagation, submitted to *J. Geophys. Res.*, 1996.

Ewing, W.M., W.S. Jardetsky, and F. Press, *Elastic Waves in Layered Media*, McGraw-Hill Book Company, Inc., New York, 1957.

Feng, C.C. and T. Teng, Three-dimensional crust and upper mantle structure of the Eurasian continent, *J. Geophys. Res.*,**88**, 2261 - 2272, 1983a.

Feng, C.C. and T. Teng, An error analysis of FTAN, *Bull. Seism. Soc. Am.*, **73**, 143 - 156, 1983b.

Feng, R., J.S. Zhu, Y. Y. Ding, G.Y. Chen, Z. Q. He, S. B. Yang, H. N. Zhou, and K. Z. Sun, Crustal structure in China from surface waves, in: *Chinese Geophysics*, Am. Geophys. Union, **2**, 273-289, 1983.

Griot, D.A., J.P. Montagner, and P. Tapponier, Surface wave phase velocity tomography and azimuthal anisotropy in Central Asia, submitted to *J. Geophys. Res.*, 1997.

Golitzin, B.B., On dispersion and attenuation of surface seismic waves, *Izvestia of the Russian Academy of Sciences*, **2**, 1912. (in Russian)

Herrin, E, and T. Goforth, Phase matched filters: application to the study of Rayleigh waves, *Bull. Seism. Soc. Am.*, **67**, 1259, 1977.

Gutenberg, B., Dispersion und extinktion von seismischen oberflachenwellen und der aufbau der obersten erdschechten, *Phys. Z.*, **25**, 377 - 381, 1924.

Gutenberg, B., Uber gruppengeschwindigkeit bei erbebebwellen, *Phys. Z.*, **27**, 111 - 114, 1926.

Gutenberg, B. and C.F. Richter, On seismic waves, *Beitr. Geophys.*, **47**, 73 - 131, 1936.

Hill, R.I., I.H. Campbell, G.R. Davies, and R.W. Griffiths, Mantle plumes and continental tectonics, *Science*, **256**, 186 - 193, 1992.

Jeffreys, H., The effect on Love waves of heterogeneity in the lower mantle, *Mon. Not. R. astr. Soc. Geophys. Suppl.*, **2**, 101 - 111, 1928.

Jeffreys, H., The surface waves of earthquakes, *Mon. Not. R. astr. Soc. Geophys. Suppl.*, **3**, 253 - 261, 1935.

Jobert, N., B. Journet, G. Jobert, A. Hirn, and S.-K. Zhong, Deep structure of southern Tibet inferred from the dispersion of Rayleigh waves through a long-period seismic network, *Nature*, **313**, 386 - 388, 1985.

Kim, W-Y., V. V. Kazakov, A. G. Vanchugov, and D. W. Simpson, Broadband and array observations at low noise sites in Kazakhstan: Opportunities for seismic monitoring of a Comprehensive Test Ban Treaty. In *Monitoring a Comprehensive Test Ban Treaty*, (editors E. S.Husebye), 1995.

Knopoff, L., Observation and inversion of surface wave dispersion, *Tectonophysics*, **13**, 497 - 519, 1972.

Knopoff, L., The thickness of the lithosphere from dispersion of surface waves, *Geophys. J. R. astr. Soc.*, **74**, 55 - 81, 1983.

Knopoff, L and F.-S. Chang, Upper mantle structure under the Tibetan Plateau, in *Geological and Ecological Studies of the Qinghai-Xizang Plateau*, **1**, 627 - 632, ed. Liu Dong-Sheng, Gordon and Breach, New York, 1981.

Knopoff, L and A.A. Fouda, Upper mantle structure under the Arabian Peninsula, *Tectonophys.*, **26**, 121 - 134, 1975.

Knopoff, L. and F.A. Schwab, Apparent initial phase of a source of Rayleigh waves, *J. Geophys. Res.*, **73**, 755 - 760, 1968.

Kozhevnikov, V. M., and M. P. Barmin, Dispersion curves of Rayleigh wave group velocities for several regions of the Asian continent. *Izv. AN SSSR, Fizika Zemli (Solid Earth)*, no. 9,

16-25, 1989.

Kozhevnikov, V. M., D. E. Lokshtanov, and M. P. Barmin, Shear-velocity structure of the lithosphere for nine large tectonic regions of the Asian continent. *Izv. AN SSSR, Fizika Zemli (Solid Earth)*, no. 1, 61-70, 1992.

Krueger, F. and K. Stammler, The German Regional Seismic Network (GRSN) used as mid- and long-period array, *Eur. Geophys. Soc. News.*, **58**, 57, 1996.

Lander, A.V., Levshin, A.L., Ratnikova, L.I., Yakobson, A.N., Peculiarities of the deep structure of Northern Eurasia from seismic surface wave data. *Proceedings of the Acad. Sci. USSR*, **285**, No. 4, 845 - 848, 1985. (Russian original)

Landisman, M., A. Dziewonski, and Y. Sato, Recent improvements in the analysis of surface wave observations, *Geophys. J. R. astron. Soc.*, **17**, 369 - 403, 1969.

Laske, G., Global observations of off-great-circle propagation of long-period surface waves, *J. Geophys. Res.*, **90**, 605 - 621, 1995.

Laske, G. and G. Masters, Constraints on global phase velocity maps from long-period polarization data, *J. Geophys. Res.*, **101**, 16,059 - 16,075, 1996.

Lerner-Lam, A. L. and T. H. Jordan, Earth structure from fundamental and higher-mode waveform analysis, *Geophys. J. R. Astron. Soc.*, **75**, 759-797, 1983.

Levshin, A. L., Pisarenko, V. F., and G. A. Pogrebinsky, On a frequency-time analysis of oscillations, *Ann. Geophys.*, **28**, 211 - 218, 1972.

Levshin, A. and K. A. Berteussen, Anomalous propagation of surface waves in the Barents Sea as inferred from NORSAR recordings, *Geophys. J. R. Astr. Soc.*, 56, 97-118, 1979.

Levshin, A. L., T. B. Yanovskaya, A. V. Lander, B. G. Bukchin, M. P. Barmin, L. I. Ratnikova, and E. N. Its, *Seismic surface waves in a laterally inhomogeneous Earth*, (ed. V. I. Keilis-Borok), Kluwer Publ., Dordrecht, 1989.

Levshin, A. L., L. Ratnikova, and J. Berger, Peculiarities of surface wave propagation across Central Eurasia, *Bull. seism. Soc. Am.*, **82**, 2464 - 2493, 1992.

Levshin, A. L., M. H. Ritzwoller, and L. I. Ratnikova, The nature and cause of polarization anomalies of surface waves crossing northern and central Eurasia, *Geophys. J. Int.*, **117**, 577 - 590, 1994.

Levshin, A.L. and M. H. Ritzwoller, Characteristics of surface waves generated by events on and near the Chinese nuclear test site, *Geophys. J. Int.*, **123**, 131-149, 1995.

Levshin, A.L., M.H. Ritzwoller, and S.S. Smith, Group velocity variations across Eurasia, *Proceedings of the 18th Seismic Research Symposium on Monitoring a CTBT*, 70 - 79, 1996.

Levshin, A.L., M.H. Ritzwoller, and J.S. Resovsky, The effect of source phase on group travel times and group velocity maps, to be submitted to *Geophys. J. Int.*, Spring, 1997.

Li, X.D. and B. Romanowicz, Global mantle shear velocity model developed using nonlinear asymptotic coupling theory, *J. Geophys. Res.*, in press, 1996.

Lieberman, R. C., and P. W. Pomeroy, Relative excitation of surface waves by earthquakes and underground explosions. *J. Geophys. Res.*, **74**, 1575-1590, 1969.

Lomax, A., and R. Snieder, The contrast in the upper mantle shear-wave velocity between the East European Platform and tectonic Europe obtained with genetic algorithm inversion of Rayleigh-wave group velocity dispersion, *Geophys. J. Int.*, **123**, 169-182, 1995.

Love, A.E.H., *Some Problems in Geodynamics*, Cambridge University Press, 1911. (Reprinted 1967, Dover, New York.)

Lyon-Caen, H., Comparison of the upper mantle shear wave velocity structure of the Indian Shield and the Tibetan Plateau and tectonic implications, *Geophys. J. R. astron. Soc.*, **86**, 727 - 749, 1986.

Makris, J. and A. Ginzburg, The Afar depression: transition between continental rifting and sea floor spreading, *Tectonophysics*, **141**, 199 - 214, 1987.

Mantovani, E., G. Nolet, and G. F. Panza, Lateral heterogeneity in the crust of the Italian region from regionalized Rayleigh-wave group velocities, *Annales Geophysicae*, **3**, 519-530, 1985.

Masters, G., S. Johnson, G. Laske, and H. Bolton, A shear-velocity model of the mantle, *Phil. Trans. R. Soc. Lond. A*, **354**, 1385-1411, 1996.

Mindevalli, O.Y., and B. J. Mitchell, Crustal structure and possible anisotropy in Turkey from seismic surface wave dispersion, *Geophys. J. Int.*, **98**, 93-106, 1989.

Mohr, P., Ethiopian flood basalt province, *Nature*, **303**, 577 - 584, 1983.

Montagner, J.P. and H.C. Nataf, A simple method for inverting the azimuthal anisotropy of surface waves, *J. Geophys. Res.*, **91**, 511 - 520, 1986.

Montagner, J.P. and T. Tanimoto, Global anisotropy in the upper mantle inferred from the regionalization of phase velocities, *J. Geophys. Res.*, **95**, 4794 - 4819, 1990.

Montagner, J.P. and T. Tanimoto, Global upper mantle tomography of seismic velocities and anisotropies, *J. Geophys. Res.*, **96**, 20337 - 20351, 1991.

Mooney, W.D., G. Laske, and G. Masters, CRUST 5.1: A global crustal model at 5 degrees by 5 degrees, submitted to *J. Geophys. Res.*, 1996.

Mueller, S and C. Sprecher, Upper mantle structure along a profile through the eastern Alps from Rayleigh wave dispersion, in *Alps, Apennines, Hellenides*, ed. H. Closs, *Int. Geodyn. Comm. sci. Rep.*, **38**, 40 - 44, 1978.

Neuenhofer, H., F. Mariller, and G. F. Panza, Crust and upper mantle structure in the Bohemian Massif from the dispersion of Rayleigh waves, *Gerlands Beitr. Geophysik*, **90**, 514-520, 1981.

Nishimura, C.E. and D.W. Forsyth, Rayleigh wave phase velocities in the Pacific with implications for azimuthal anisotropy and lateral heterogeneities, *Geophys. J. Int.*, **94**, 479 - 501, 1988.

Nolet, G., The upper mantle under Western Europe inferred from the dispersion of Rayleigh wave modes, *J. Geophysics*, **43**, 265-276, 1977.

Nolet, G., Wave form tomography, in: *Seismic Tomography with Applications in Global Seismology and Exploration Geophysics*, G. Nolet, ed., Reidel Publ. Co., Dordrecht, 301-322,

1987.

Oliver, J., A summary of observed surface wave dispersion, *Bull. Seism. Soc. Am.*, **52**, 81 - 86, 1962.

Panza, G.F., H. Neuenhofer, and G. Calcagnile, Contribution to phase velocity investigation of Rayleigh waves in Middle Europe. *Pageoph*, **116**, 1299-1306, 1978.

Panza, G. F., S. Mueller, and G. Calcagnile, The gross features of the lithosphere-asthenosphere system in Europe from seismic surface waves and body waves, *Pure Appl. Geophysics*, **118**, 1209-1213, 1980.

Patton, H., Crustal and upper mantle structure of the Eurasian continent from the phase velocity and Q of surface waves. *J. Rev. Geophys. Space Phys.*, **18**, 605-625, 1980.

Pavlis G., H. Al-Shukri, H. Mahdi, and D. Repin, JSP arrays and networks in Central Asia, *IRIS Newsletter*, **XIII**, **2**, 10-12, 1994.

Pedersen, H. A., M. Camillo, and N. Balling, Changes in the lithospheric structure across the Sorgenfrei-Tornquist Zone inferred from dispersion of Rayleigh waves, *Earth Planetary Sci. Lett.*, **128**, 37-46, 1994.

Pines, I., T.-L. Teng, and R. Rosenthal, A surface wave dispersion study of the crustal and upper mantle structure of China, *J. Geophys. Res.*, **85**, 3829 - 3844, 1980.

Press, F, Determination of crustal structure from phase velocity of Rayleigh waves, I. Southern California, *Bull. geol. Soc. Am.*, **67**, 1647 - 1658, 1956.

Press, F., M. Ewing, and J. Oliver, Crustal structure and surface wave dispersion in Africa, *Bull. seism. Soc. Am.*, **46**, 97 - 103, 1956.

Quinlan, D.M., Datascope: A relational database system for scientists, *EOS Trans. Am. Geophys. Union.*, **75**, F431, 1994.

Ritzwoller, M.H. and E.M. Lavely, Three-dimensional seismic models of the Earth's mantle, *Revs. of Geophys.*, **33**, 1-66, 1995.

Ritzwoller, M.H., A.L. Levshin, S.S. Smith, and C.S. Lee, Making accurate continental broadband surface wave measurements, *Proceedings of the 17th Seismic Research Symposium on Monitoring a CTBT*, 482-490, 1995.

Ritzwoller, M.H., A.L. Levshin, and L.I. Ratnikova, Surface wave tomography across Tibet, *EOS Trans. Am. Geophys. Un.*, **77**, F675, 1996a.

Ritzwoller, M.H., A.L. Levshin, L.I. Ratnikova, and D.M. Tremblay, High resolution group velocity variations across Central Asia, *Proceedings of the 18th Seismic Research Symposium on Monitoring a CTBT*, 98 - 107, 1996b.

Ritzwoller, M.H., A.L. Levshin, D.M. Tremblay, and M.B. James, Broadband surface wave dispersion across the Antarctic Plate, *EOS Trans. Am. Geophys. Un.*, **77**, F477, 1996c.

Romanowicz, B.A., Constraints on the structure of the Tibet Plateau from pure-path phase velocities of Love and Rayleigh waves, *J. Geophys. Res.*, **87**, 6865 - 6883, 1982.

Romanowicz, B., M. Cara, J. F. Fels and D. Rouland, GEOSCOPE: a French initiative in long period, three component, global seismic networks, *EOS, Trans. Am. Geophys. Un.*, **65**, 753-754, 1984.

Russell, D. W., R. B. Herrman, and H. Hwang, 1988. Application of frequency-variable filters to surface wave amplitude analysis, *Bull. seism. Soc. Am.*, **78**, 339 - 354.

Snieder, R. Global inversions using normal modes and long-period surface waves, in *Seismic Tomography: Theory and Practice*, ed. H.M. Iyer and K. Hirahara, 23 - 63, Chapman and Hall, New York, 1993a.

Snieder, R., Large scale waveform inversion of surface waves for lateral heterogeneity: 2. Application to surface wave in Europe and Mediterranean, *J. Geophys. Res.*, **93**, 12067-12080, 1993b.

Snieder, R. and H. Paulssen, Future deployment of the NARS array, *Proceedings of the Europrobe Symposium, Jablonna 1991*, ed. D.G. Gee and M. Beckholmen, C Warsawa, 129-132, 1993.

Stange, S., and W. Friederich, Surface wave dispersion and upper mantle structure beneath Southern Germany from joined inversion of network recorded teleseismic events, *Geophys. Res. Lett.*, **20**, 2375-2378, 1993.

Stevens, J.L. and S.M. Day, The physical basis for $m_b : M_s$ and variable frequency magnitude methods for earthquake/explosion discrimination, *J. Geophys. Res.*, **90**, 3009 - 3020, 1985.

Stoneley, R., The effect of the ocean on Rayleigh waves, *Mon. Not. R. astr. Soc. Geophys. Suppl.*, **1**, 349 - 356, 1926.

Stoneley, R., Dispersion of waves in a double surficial layer, *Mon. Not. R. astr. Soc. Geophys. Suppl.*, **2**, 527 - 531, 1928.

Su, W., R. L. Woodward, and A.M. Dziewonski, Degree 12 model of shear velocity heterogeneity in the mantle, *J. Geophys. Res.*, **99**, 6945 - 6980, 1994.

Tanimoto, T. and D. L. Anderson, Lateral heterogeneity and azimuthal anisotropy of the upper mantle: Love and Rayleigh waves 100–250s, *J. Geophys. Res.*, **90**, 1842-1858, 1985.

Taylor, S. R., A review of broadband regional discrimination studies of NTS explosions and Western U.S. earthquakes, in Monitoring a Comprehensive Test Ban Treaty, ed. E. S. Husebye and A. M. Dainty, NATO ASI Series, Kluwer Acad. Publ., 1996.

Trampert, J. and J. Woodhouse, Global phase velocity maps of Love and Rayleigh waves between 40 and 150 seconds, *Geophys. J. Int.*, **122**, 675 - 690, 1995.

Trampert, J. and J. Woodhouse, Global azimuthal anisotropy, *Eur. Geophys. Soc. Newslet.*, **58**, 57, 1996.

Vaccari, F., and G. F. Panza, Vp/Vs estimation in south-western Europe from P-wave tomography and surface wave tomography analysis, it Phys. Earth Planet. Int, **78**, 229-237, 1993.

Vdovin, O., J.A. Rial, M.H. Ritzwoller, and A.L. Levshin, Surface wave inversion of the South American Lithosphere (SISAL), *EOS Trans. Am. Geophys. Un.*, **77**, F464, 1996.

Vernon, F., The Kyrghyz Seismic Network, *IRIS Newsletter*, **XIII**, 7-8, 1994.

Vernon, F., Mellors, R.J., J. Berger, A.M. Al-Amri, J. Zollweg, Initial results from the deployment of broadband seismometers in the Saudi Arabian Shield, *Proceedings of the 18th Seismic Research Symposium on Monitoring a CTBT*, 108 - 117, 1996.

Wessel, P., and W.H. F. Smith, New version of the Generic Mapping Tools released, *EOS Trans. AGU*, **76**, 329, 1995.

Wessel, P., and W.H. F. Smith, 1991, Free software helps map and display data, *EOS Trans. AGU*, **72**, 441, 1991.

White, R. and D. McKenzie, Magmatism at rift zones: The generation of volcanic continental margins and flood basalts, *J. Geophys. Res.*, **94**, 7685 - 7729, 1989.

Wier, S., Surface wave dispersion and Earth structure in South-Eastern China, *Geophys. J. Roy. Astr. Soc.*, **69**, 33-47, 1982.

Wu, F.T. and A. Levshin, Surface wave group velocity tomography of East Asia, *Phys. Earth Planet. Int.*, **84**, 59 - 77, 1994.

Yanovskaya, T.B., and P.G. Ditmar, Smoothness criteria in surface wave tomography. *Geophys. J. Int.*, **102**, 63-72, 1990.

Yanovskaya, T. B., G. F. Panza, P. G. Ditmar, P. Suhadolc, and S. Mueller, Structural heterogeneity and anisotropy based on 2-D phase velocity patterns of Rayleigh waves in Western Europe, *Atti Acad. Naz. Lincei*, **1**, 127-135, 1990.

Zeng, Y., T.-L. Teng, and K. Aki, Suface wave mapping of the crust and upper mantle in the Arctic Region, *Bull. Seism. Soc. Am.*, **79**, 1520 - 1541, 1989.

Zhang, Y.-S., Three-dimensional velocity structure beneath East Asia and its tectonic implication, submitted to *Mantle Dynamics and Plate Interactions in East Asia, AGU/GSA Geodynamics Series*, 1996.

Zhang, Y.S. and T. Tanimoto, High resolution global upper mantle structure and plate tectonics, *J. Geophys. Res.*, **98**, 9793 - 9823, 1993.

Zonenshain, L. P., M. I. Kuzmin, and L. M. Natapov, *Geology of the USSR: A plate-tectonic*

*synthesis*, B. M. Page ed., AGU Geodynamics Series, **21**, Washington, D. C., 1990.

# Figures

1. Rayleigh wave phase (bold dashed lines) velocity and group (bold solid lines) velocity sensitivity kernels to shear velocity and compressional velocity at three periods: 20s, 50s, and 200 s. These kernels are computed for PREM.

2. Station and event locations. The locations of the stations used in this study are marked with triangles in (a) and event locations are marked with circles in (b).

3. FTAN. Example of a frequency-time analysis for the vertical, radial, and transverse components recorded at the GSN station at Kevo, Finland for an event in the Kurile Islands (10/9/94, $M_s = 7.0$, $\Delta = 58.5$ degrees). (a) The analyst-defined filter removes potentially interfering signals such as body waves, other surface waves, overtones, and coda. Group velocity curves are estimated automatically on the filtered images. (b) Rayleigh and Love wave group velocity measurements (solid lines) are compared with the predictions from PREM (dashed lines). (c) Comparison of the raw (thin solid) with the filtered (bold dashed) waveforms reveals the effect of the filtering displayed in (a).

4. The number of dispersion measurements before (bold lines) and after (thin lines) the cluster analysis. Rayleigh waves are solid lines and Love waves are dotted lines. The cluster analysis reduces the size of the data set by combining redundant measurements and discarding outliers.

5. Cluster analysis. (a) Example of a cluster of measured group velocity curves. Estimated Rayleigh wave group velocity curves from a set of five events in the Philippines measured at Eskdalemuir (ESK), Scotland are compared with one another (solid lines) and the group velocity curve predicted from PREM (dashed line). (1989 349, $M_s = 7.4$; 1990 39, $M_s = 6.6$; 1991 49, $M_s = 6.6$; 1991 317, $M_s = 6.4$; 1992 138, $M_s = 7.1$) (b) The total number of clusters in the data set plotted as a function of period and wave type (Rayleigh: solid line, Love: dashed line.) (c) The average path length in km versus period (Rayleigh: solid line, Love: dashed line.) (d) The average of the standard deviation of the group velocity curves composing all of the clusters. We assign

these values as uncertainties to all measured group velocity curves which are not part of some cluster.

6. Two measures of misfit as a function of the damping parameter $\lambda$ in equation (1) for the 40 s Rayleigh wave. Three values of the damping parameter are highlighted as crosses on the trade-off curves: one severely underdamped ($\lambda \sim 0.2$), one slightly underdamped ($\lambda \sim 1$), and one highly overdamped ($\lambda \sim 100$). The group velocity maps constructed with these three values of $\lambda$ are shown in Figure 7. The application of the a posteriori smoothing filter to the group velocity map from the slightly underdamped inversion degrades fit to the data by a small amount, as is indicated with the closed circle. (Top) Variance reduction relative to the average group velocity across the slightly underdamped map. (Bottom) Rms velocity difference between the observed group velocities and those predicted from the group velocity maps.

7. Group velocity maps constructed with the three damping parameters which are indicated with crosses in Figure 6: (top left) highly underdamped ($\lambda \sim 0.2$), (top right) slightly underdamped ($\lambda \sim 1$), and (bottom left) highly overdamped ($\lambda \sim 100$). The application of the a posteriori smoothing filter (full-width at the $e^{-1}$ point of 2.5 degrees) to the map at top right produces the smoothed map at bottom right.

8. Plots of several one-dimensional slices of the two-dimensional Gaussian smoothing filters with full-widths at the $e^{-1}$ points of 2.5, 3.75, 5, and 6.25 degrees. The horizontal dashed line denotes $e^{-1}$.

9a. Path density for Rayleigh waves at the six indicated periods. Path density is defined as the number of rays intersecting a 2 degree square cell ($\sim 50,000$ km$^2$). Regions of group velocity maps with path densities below about 15 rays per cell should be suspect.

9b. Same as Figure 9a, but for Love waves at the indicated periods.

10a. Checker-board test for the 40 s Rayleigh wave with cells of three different sizes: (top) 3 degrees, (middle) 5 degrees, (bottom) 7.5 degrees. There are regions in which 3 degree cells are resolved, but if cells are smaller than 5 degrees most are not well resolved.

Resolutions of 5 degrees are observed across most of Eurasia, with the notable exception of North Central Siberia, where cells are not resolved below about 7.5 degrees in size.

10b. Plots of the resolution index ($\mathcal{R}_i$, eqn. (6)) for the 40 s Rayleigh wave with the same cell sizes as in Figure 10a. Light grey cells are considered resolved, increasingly darker cells denote poorer resolution. The same sort of information is included in these figures as in Figure 10a, but in this form it is more readily and quickly interpreted, although this resolution criterion is somewhat liberal.

11a. Resolution index ($\mathcal{R}_i$, eqn. (6)) plotted for intermediate period Rayleigh waves at the indicated periods and with the specified cell sizes. Three grey-scale values are presented, the lightest indicates good resolution, increasingly dark cells reveal poorer resolutions.

11b. Same as Figure 11a, but for the long period Rayleigh waves at the indicated periods.

11c. Same as Figure 11a, but for intermediate period Love waves at the indicated periods.

11b. Same as Figure 11a, but for the long period Love waves at the indicated periods.

12. Estimated average resolution across the Eurasian continent. The value of resolution is chosen such that most of the continent appears to be resolved in 'Resolution index' plots, such as those shown in Figure 11. Some regions of the continent will display better or worse resolutions.

13. Bias analysis in which there are only two non-zero 7.5 degree square input cells, one in Cental Asia (a region of very good resolution) and one in North Central Siberia (a region with poor resolution). Synthetic data used are the same as in Figure 7 for the 40 s Rayleigh wave. (Top) The estimated tomographic map is shown which demonstrates the southern shift of the North Central Siberian cell (by about one-half the cell width) and the high fidelity of the Central Asian cell. (Bottom) The input locations and shapes of the cells are shown. Both input cells have a velocity variation of 10%. The rest of the continent is homogeneous with no velocity variation.

14. Histograms displaying the azimuthal distribution of the unique paths that pierce the two cells shown in Figure 13, (top) North Central Siberia and (bottom) Central Asia. Both regions demonstrate a shortage of nearly meridional (north-south) paths. Azimuthal distribution alone cannot account for the differences in resolution between these two regions.

15. Histograms displaying the length distribution of the unique paths that pierce the two cells shown in Figure 13, (top) North Central Siberia and (bottom) Central Asia. (A degree is approximately 111 km.) The reduced resolution in North Central Siberia results from the lack of short paths combined with the the absence of nearly meridional paths (Fig. 14).

16. Mislocation bias. Results of a synthetic experiment in which approximately 15 events in two source regions (the Kurile Islands and the Hindu Kush) are shifted in the same direction by 10 km to determine the effect of systematic errors in source locations on the tomographic images. All events in the Kuriles are mislocated to the northwest and in the Hindu Kush to the north. Three Rayleigh wave periods (20 s, 50 s, 150 s) are shown for the Kurile Islands events and one period (20 s) for the Hindu Kush events. Bias is displayed in percent relative to the average group velocity across the map. Event locations are marked by small white dots.

17. Average group velocity curve across the entire region of study (latitude: 10N - 80N, longitude: 10E - 170E).

18a. Estimated group velocity maps across Eurasia for the 20 s and 30 s Rayleigh waves.

18b. Same as Figure 18a, except for the 50 s and 100 s Rayleigh waves.

18c. Same as Figure 18a, except for the 150 s and 200 s Rayleigh waves.

18d. Same as Figure 18a, except for the 20 s and 30 s Love waves.

18e. Same as Figure 18a, except for the 50 s and 200 s Love waves.

18f. Same as Figure 18a, except for the 125 s and 150 s Love waves.

19. Group velocity curves constructed by combining values at the locations specified in the map at top from the estimated group velocity maps. The left column presents Rayleigh waves and the right Love waves. The curves are segregated by structural setting into three groups: sedimentary basins (1-Tarim Basin, 2-N. Caspian Sea, 3-W. Siberian Sedimentary Complex, 4-Lena River Sedimentary Complex), mountain ranges and continental plateaus (5-Tibet, 6-Altai Mountains, 7-Zagros Mountains), and shields (8-E. European Platform, 9-Siberian Shield). The group velocity curve for PREM is shown as the dashed line on each graph. The jerkiness in the curves results from small inconsistencies between the group velocity maps at different periods. The observed curves are much smoother (e.g., Fig. 3).

20. Two measures of misfit to our group velocity measurements for Rayleigh (solid lines) and Love (dashed lines) waves of our estimated group velocity maps. (Top) Misfit is represented as variance reduction relative to the average across each map [eq. (4)]. (Bottom) Misfit is the RMS group velocity misfit [eq. (5)].

21. Average group velocity across the studies region (lat: 10N - 80N, lon: 10E - 170E) for our estimated group velocity maps (CU: solid lines), PREM (PREM: long dashed line), and the group maps predicted by a model composed of the crustal model CRUST-5.1 and the mantle model S16B30 (CRUST-5.1/S16B30: short dashed line).

22a. Blow-ups in Central Asia of our group velocity maps at 20 s for Love waves and 50 s for Rayleigh waves compared with the same group velocity maps predicted by a model composed of the crustal model CRUST-5.1 and the mantle model S16B30.

22b. Same as Fig. 22a, except these maps are for Rayleigh waves at 30 s and 100 s period across the Far East.

23. Two measures of misfit to our group velocity measurements for Rayleigh (solid lines) and Love (dashed lines) waves for two different sets of group velocity maps. Bold lines are for our group velocity maps and thin lines are for the group velocity maps predicted by the model composed of the crustal model CRUST-5.1 and the mantle model S16B30. (Top) Misfit is represented as variance reduction relative to the group

velocity from PREM. Our variance reduction here differs from that reported in Fig. 20 since the reference values used in these figures differ. Here the reference is the group velocity predicted by PREM and in Fig. 20 it is the average across our group velocity map. (Bottom) Misfit is the RMS group velocity misfit [eq. (5)].